

**UNDERSTANDING THE ROLE OF CENTROSOME AMPLIFICATION IN  
HEALTH AND DISEASE**

by

Michelle Stephanie Levine

A dissertation submitted to Johns Hopkins University in conformity with the  
requirements for the degree of Doctor of Philosophy

Baltimore, Maryland

January 2019

© Michelle S. Levine 2019

All rights reserved

# Abstract

Centrioles are microtubule-based structures that are important for forming the mitotic spindle and nucleating cilia. Cycling cells contain exactly two centrosomes, each consisting of two centrioles at their core, in order to form a bipolar spindle in mitosis for proper chromosome segregation. Abnormalities in centriole number are commonly observed in human cancers, and it has long been debated whether increases in centriole number occur as a passenger event in malignant cellular transformation, or whether extra centrioles contribute to tumorigenesis. In the first part of my thesis work, I sought to tackle this question using a mouse model in which extra centrioles can be created at will across a range of different tissues. Using this model, I demonstrate that centriole amplification can play a causative role in tumorigenesis.

In the second part of my thesis work, I examined how centrioles are normally amplified in terminally differentiated multiciliated epithelial cells. Multiciliated cells line the epithelial surfaces of the brain ventricles, respiratory tract, and oviducts and require extra

centrioles for their proper function. One centriole nucleates each cilium, and the cell must create hundreds of centrioles to have as many motile cilia to produce fluid flow. The process of multiciliogenesis has long been thought to require the deuterosome, a specialized structure upon which multiple new centrioles can form simultaneously. I used a mouse model to test the requirement of deuterosomes for centriole amplification and showed that, surprisingly, this structure is dispensable for multiciliogenesis.

Lastly, my work sought to determine whether centriole amplification plays a contributing role in kidney cystogenesis. Autosomal Dominant Polycystic Kidney Disease (ADPKD) affects about 1 in 500 people and manifests as large kidneys with fluid-filled cysts. Although the two genes involved in ADPKD were identified over three decades ago, the molecular mechanism underlying ADPKD is not well understood. It is known that defects in cilia number, length, or function can cause cystogenesis and centriole amplification has been observed in the cyst of ADPKD patients. Therefore, I tested whether extra centrioles could contribute to kidney cystogenesis, and found that they could not. In summary, by studying centriole biogenesis in different cellular contexts *in vivo*, we now have better understanding of the role of centriole amplification in health and disease.

Primary Reader: Andrew Holland, Ph.D.

Secondary Reader: Andrew Ewald, Ph.D.

# Acknowledgments

First and foremost, I would like to thank my thesis advisor, Dr. Andrew Holland. I could write an entire dissertation's worth of praise for his mentorship. He is truly a world-class, dedicated, and passionate scientist. His ability to absorb information and put different pieces together to design the thoughtful experiments that should be done to best answer a scientific question is unparalleled. In addition, he always encourages the highest quality work from all of us and for us to be critical of our own data, both of which are required to be a top-notch scientist. Furthermore, although I was one of his first graduate students and he did not have a "track record" of mentorship, there was never any question that he would be an excellent mentor and advocate for his students—it was clear from day 1 of my rotation and has held true throughout my time in his lab. I have grown so much both personally and professionally because of him. This growth not only spans the ability to think critically about experiments and data, but also the ability to communicate clearly and present new ideas logically. In addition to the wonderful scientific environment he has built, he has also created a lab environment that makes it a pleasure to come in every

day, as although everyone works very hard and very long hours, there is never a shortage of conversation and laughter in the day.

Next, I'd like to thank my labmates. I have been fortunate to be surrounded by generous, intelligent, and fun scientists throughout graduate school. More specifically, I'd like to thank Kevin Clutario, a technician in the lab when I joined, who had been taking care of the mouse lines and graciously handed them over and taught me animal husbandry when I joined the lab. I'd also specifically like to thank my labmates/classmates Bram Lambrus and Tyler Moyer. Together we joined the Holland lab and spent more time together than we did apart in the first couple of years. I learned so much from both of them on what it means to be a thoughtful person and scientist. I know that I wouldn't have grown as much if I had not had them as my peers from the start. As my baymate, Bram Lambrus was an especially helpful "science consultant," with whom I always felt comfortable asking questions and bouncing ideas off of without feeling stupid. I could not have asked for a better person with whom to spend the past five and a half years in close proximity. All other labmates have been a pleasure to work with, and have been a great support as well. Andrew also gave me the opportunity to work with undergraduates and rotation students in my time here, and I've had the pleasure of mentoring 7 junior scientists, which is an experience I have learned and grown from as well.

I also feel very fortunate to have trained at Johns Hopkins. It is such a collaborative, supportive environment, especially in the Molecular Biology and Genetics department. I have felt comfortable turning to various labs in the department for help with mouse work throughout my thesis. PIs and lab members alike have been equally helpful. I'd like to especially thank Dr. Jeremy Nathans, and Drs. Yanshu Wang and Amir Rattner, two staff scientists in Dr. Nathans' lab. Dr. Nathans was so generous with allowing me to use his lab's equipment. He also made himself available when I wanted to meet with him about career advice and was very patient and helpful. Dr. Wang was exceedingly generous with her time and was an excellent and patient teacher. She taught me how to use different pieces of equipment and to perform various mouse dissection techniques. She spent hours of her time with me before we even knew each other well. My thesis work would have progressed much more slowly and been much more difficult to do if it had not been for Dr. Wang. Dr. Rattner looked after the confocal microscope, which I used constantly throughout my thesis work, and would always make sure that it was in working order and that I was doing well. Drs. Greider and Armanios were especially helpful during the beginning of my thesis work when we had joint lab meetings, in which they would ask probing questions. I'd also like to thank my thesis committee members: Drs. Stephen Desiderio, Andrew Ewald, and Rong Li. Their input throughout my thesis work, both

about my work, about career and internship options, and about writing this dissertation were exceedingly helpful. I am grateful for their support.

I cannot say enough about the emotional and scientific support I've received from my friends from Hopkins. It has been a pleasure going through this process with them by my side. They have been wonderful whether it be bouncing ideas off of them, venting to them, or enjoying spending time with them away from lab. My college friends have also been huge cheerleaders and "proud parents" of mine through this process as well, and I am so grateful for their constant support and friendship.

Finally, I would like to thank my parents. In addition to being wonderful role models, the loudest cheerleaders and proudest parents, they have always encouraged me to do what I love. They have also always put my happiness first. I cannot thank them enough.



# Table of Contents

Acknowledgments .....	v
Table of Contents .....	ix
List of Figures .....	xi
<b>Introduction.....</b>	<b>1</b>
1.1 The functions of centrosomes in proliferating cells .....	1
1.2 Centrosome amplification can cause mitotic errors and aneuploidy.....	2
1.3 Centrosome amplification and tumorigenesis.....	4
1.4 The role of centrioles and deuterosomes in multiciliated cells.....	6
1.5 The role of centrosomes and cilia in kidney cystogenesis.....	9
<b>Centrosome amplification is sufficient to promote spontaneous tumorigenesis in mammals .....</b>	<b>13</b>
2.1 Plk4 overexpression drives centrosome amplification <i>in vitro</i> .....	13
2.2 Elevated Plk4 expression promotes formation of supernumerary centrosomes in tissues .....	16
2.3 Centrosome amplification impairs epidermal architecture.....	18
2.4 Centrosome amplification causes aneuploidy <i>in vivo</i> .....	19
2.5 Centrosome amplification increases the initiation of intestinal tumors.....	20
2.6 Centrosome amplification drives spontaneous tumorigenesis .....	21
2.7 Centrosome amplification promotes the development of aneuploid tumors .....	23
<b>Deuterosomes are dispensable for multiciliogenesis.....</b>	<b>48</b>
3.1 Creation of a <i>Deup1</i> <sup>-/-</sup> mouse .....	48
3.2 <i>Deup1</i> <sup>-/-</sup> mice lack deuterosomes.....	50
3.3 Deuterosomes are dispensable for multiciliogenesis.....	50
3.4 <i>Cep63</i> does not compensate for <i>Deup1</i> loss.....	52
<b>The Role of Extra Centrioles in Kidney Cystogenesis .....</b>	<b>66</b>
4.1 A mouse model to create extra centrosomes in the kidney .....	66
4.2 Plk4 overexpression induces centrosome amplification but does not alter cilia number.....	67
4.3 Extra centrosomes are not sufficient to promote kidney cystogenesis .....	68
<b>Discussion.....</b>	<b>76</b>
5.1 Centrosome amplification is sufficient to promote tumorigenesis .....	76

5.2 Deuterosomes are dispensable for multiciliogenesis.....	80
5.3 Extra centrioles do not play a role in kidney cystogenesis.....	82
<b>Materials and Methods .....</b>	<b>85</b>
<b>References.....</b>	<b>110</b>
<b>Curriculum Vitae .....</b>	<b>120</b>

# List of Figures

Figure 1. Centriole biogenesis in cycling and multiciliated cells .....	11
Figure 2. A modest increase in Plk4 promotes centrosome amplification and aneuploidy <i>in vitro</i> .....	26
Figure 3. Centrosome amplification does not promote DNA damage or cytokinesis failure .....	29
Figure 4. Increased Plk4 levels promote chronic centrosome amplification in multiple tissues.....	32
Figure 5. There is no Plk4 overexpression or centrosome amplification in the brain of doxycycline-treated Plk4 <sup>Dox</sup> mice .....	34
Figure 6. Centrosome amplification leads to progressive hair loss.....	36
Figure 7. Centrosome amplification drives aneuploidy <i>in vivo</i> .....	38
Figure 8. Centrosome amplification leads to aneuploidy in the spleen of aged mice	40
Figure 9. Centrosome amplification promotes tumor initiation.....	42
Figure 10. Centrosome amplification promotes spontaneous tumorigenesis.....	44
Figure 11. Transient Plk4 overexpression triggers spontaneous tumor development .....	46
Figure 12. <i>Deup1</i> knockout mice do not express <i>Deup1</i> mRNA or DEUP1 protein....	53
Figure 13. DEUP1 antibodies can recognize protein produced from full-length and exons 8-12 of <i>Deup1</i> . .....	55
Figure 14. <i>Deup1</i> knockout mice do not contain deuterosomes.....	57
Figure 15. Deuterosomes are not required for proper centriole number. ....	58
Figure 16. Deuterosomes are not required for multiciliogenesis <i>in vivo</i> .....	60
Figure 17. Live-imaging of differentiating <i>Deup1</i> <sup>-/-</sup> ependymal cells reveals deuterosome-independent centriole amplification.....	61
Figure 18. Cep63 does not compensate for <i>Deup1</i> loss. ....	62
Figure 19. Cep63 knockout animals and <i>Deup1</i> ; Cep63 double-knockout animals do not exhibit defects in multiciliogenesis <i>in vitro</i> or <i>in vivo</i> . ....	64
Figure 20. Centrosome amplification does not alter cilia number, cell death or proliferation in mouse kidneys.....	70
Figure 21. Centrosome amplification in adult animals does not affect kidney histology or size.....	72
Figure 22. Centrosome amplification is not sufficient to promote cystogenesis.....	73

Figure 23. Centrosome amplification does not cooperate with injury to promote kidney cystogenesis ..... 74

# Chapter 1

## Introduction

### 1.1 The functions of centrosomes in proliferating cells

Centrosomes are the microtubule nucleation hubs of animal cells. At their core exists a pair of centrioles, or microtubule-based structures, that aid with the recruitment and organization of hundreds of proteins that form the pericentriolar material (PCM).

Pericentriolar proteins anchor the minus ends of microtubules. This stabilization endows centrosomes with the ability to be microtubule nucleation centers (Conduit et al. 2015).

In interphase, centrosomes are responsible for organizing the microtubule cytoskeleton for maintenance of cellular architecture. In mitosis, each centrosome helps build the bipolar spindle apparatus by nucleating spindle microtubules. These microtubules attach to chromosomes via a protein structure known as a kinetochore, to allow the sister chromatids can be equally distributed into each daughter cell (Figure 1A). Since each

daughter cell inherits one centrosome, a cell must duplicate its centrosome before entry into the next mitosis. This duplication begins at the start of S-phase and is controlled by the master regulator, Polo-like Kinase 4 (Plk4) (Bettencourt-Dias et al. 2005; Habedanck et al. 2005). Plk4 is a dose-dependent regulator of centriole number: modest overexpression of Plk4 causes extra centrosomes to form, known as centrosome amplification, whereas knockdown of Plk4 leads to centrosome duplication failure (Holland et al. 2010a). Control of the activity and abundance of Plk4 is tightly regulated so that centriole biogenesis occurs with precise spatiotemporal and numerical control (Holland et al. 2010b; Holland et al. 2012b; Moyer et al. 2015). The correct number of centrosomes is key to cellular homeostasis, as the incorrect number can lead to chromosome missegregation and aneuploidy, which is discussed in the next section.

## **1.2 Centrosome amplification can cause mitotic errors and aneuploidy**

Supernumerary centrosomes are a common feature of human cancers and can arise through several different pathways including a cell division failure, cell fusion and centrosome overduplication (Chan 2011a; Nigg and Holland 2018). The presence of extra centrosomes leads to the formation of a multipolar mitotic spindle, which if not corrected prior to anaphase, results in the segregation of chromosomes into more than two daughter

cells. Live-cell imaging has revealed that the progeny of multi-polar divisions are frequently inviable, since daughter cells are unlikely to inherit a full complement of chromosomes (Ganem et al. 2009). The best-characterized mechanism for dealing with this burden is the clustering of extra centrosomes to form a pseudo-bipolar spindle (Quintyne et al. 2005; Basto et al. 2008; Kwon et al. 2008; Leber et al. 2010).

Efficient centrosome clustering is required for the survival of cancer cells with extra centrosomes (Kwon et al. 2008). While the coalescence of centrosomes in a multi-polar spindle provides a pathway to avoid lethal divisions, it also promotes the formation of incorrect kinetochore-microtubule attachments where a single kinetochore becomes bound to microtubules anchored at both spindle poles (Figure 1B). These attachments can go unrecognized by the spindle assembly checkpoint, leading to lagging anaphase chromosomes (Ganem et al. 2009; Silkworth et al. 2009). These tardy chromosomes can be missegregated to produce aneuploid daughter cells (Cimini et al. 2001; Cimini et al. 2003). More frequently, however, lagging chromosomes are segregated to the correct daughter cell but fail to reach the main chromosome mass prior to nuclear envelope reassembly and are partitioned into a micronucleus (Thompson and Compton 2011). DNA trapped within micronuclei undergoes extensive DNA damage that can lead to chromosome rearrangements (Zhang et al. 2015). Centrosome amplification is thus likely

to be a major source of genetic instability in human tumors. This provides an explanation for the association of centrosome amplification with aneuploidy and CIN.

### **1.3 Centrosome amplification and tumorigenesis**

Faithful control of centrosome number is deregulated in a wide range of solid and blood-borne cancers, leading to the acquisition of extra copies of centrosomes, a feature known as centrosome amplification (Chan 2011b). Supernumerary centrosomes are observed early in the development of many tumors and often correlate with advanced tumor grade and poor clinical outcome (Nigg 2006; Nigg and Raff 2009; Godinho and Pellman 2014). In cultured cells, centrosome amplification causes mitotic errors that can lead to chromosome missegregation (Ganem et al. 2009; Silkworth et al. 2009) and chromosomal rearrangements (Janssen et al. 2011; Crasta et al. 2012; Ganem and Pellman 2012). Moreover, extra centrosomes can promote invasive phenotypes in a 3D culture model (Godinho et al. 2014). These observations suggest that centrosome amplification could promote the initial stages of tumor development, but definitive evidence for this proposal is still lacking.

To examine the consequences of centrosome amplification *in vivo*, considerable attention has been focused on Plk4, a key regulator of centrosome duplication (Bettencourt-Dias et



al. 2005; Habedanck et al. 2005). Overexpression of this kinase increases centrosome number in the absence of direct effects on cellular ploidy or oncogenes and tumor suppressor genes and provides an excellent experimental tool to study the long-term consequence of having cells with excess centrosomes. However, studies in animal models have so far provided contradictory views on the specific contribution of centrosome amplification to tumor development. Experiments in flies have shown that larval brain and wing disk tissues with supernumerary centrosomes are able to initiate tumors in transplantation assays (Basto et al. 2008; Castellanos et al. 2008; Sabino et al. 2015). In mammals, however, centrosome amplification in embryonic neural progenitors results in aneuploidy, cell death and microcephaly, but does not promote tumorigenesis (Marthiens et al. 2013). In addition, increasing centrosome number in the skin of mice failed to promote formation of spontaneous, or carcinogen-induced, skin tumors (Kulukian et al. 2015; Vitre et al. 2015). By contrast, centrosome amplification—either globally or in the skin—accelerates the onset of tumors caused by loss of p53 (Coelho et al. 2015; Sercin et al. 2016). Thus, while centrosome amplification can modify tumor outcome in a p53-null background, the interpretation is complicated by the fact that loss of p53 is associated with increased numbers of centrosomes in some contexts (Fukasawa et al. 1996). Furthermore, it remains unclear if centrosome amplification can trigger tumor formation in the absence of direct effects on the p53 tumor suppressor pathway. Therefore, our lab

developed a doxycycline-inducible mouse model in which the levels of Plk4 can be increased to promote widespread and chronic centrosome amplification *in vivo*. This model allowed us to rigorously assess the long-term consequences of having cells with too many centrosomes and their contribution to tumor initiation.

## **1.4 The role of centrioles and deuterosomes in multiciliated cells**

Cilia are microtubule-based organelles that project from the surface of cells. Most cells elaborate a single non-motile primary cilium that serves a critical role in sensing mechanical and chemical stimuli. However, specialized multiciliated cells (MCCs) exist in the respiratory tract, brain, and oviducts that contain hundreds of motile cilia that beat in a coordinated manner to drive fluid flow across epithelial surfaces. Defects in motile cilia formation or beating in mice lead to fluid buildup in the brain (hydrocephaly), increased respiratory tract infections, and, in some cases, infertility (Song et al. 2014; Funk et al. 2015; Nemajerova et al. 2016; Terre et al. 2016; Siller et al. 2017). Furthermore, mutations in multiciliated cell differentiation factors lead to hydrocephaly and respiratory symptoms in human patients (Boon et al. 2014; Wallmeier et al. 2014).

A centriole, or basal body, forms the base of each cilium and serves as a template for the cilium axoneme. In cycling cells, centriole formation is tightly controlled so that a single new procentriole forms adjacent to each of the two parent centrioles (Nigg and Raff 2009; Levine and Holland 2018). However, MCCs deviate from this centriolar pathway in that these post-mitotic cells produce hundreds of centrioles to serve as the foundation for producing as many motile cilia (Figure 1C). It has long been appreciated that the production of new centrioles in MCCs utilizes a unique structure, known as a deuterosome (Sorokin 1968; Brenner 1969; Anderson and Brenner 1971). Soon after differentiation begins, tens of deuterosomes form, starting as electron-dense foci of ~200 nm in diameter and maturing to form ~350 nm toroidal structures (Zhao et al. 2013). Deuterosomes can be nucleated by the daughter centriole (Al Jord et al. 2014) or form spontaneously in the cytoplasm of MCCs (Zhao et al. 2018). Once produced, deuterosomes recruit several proteins required for centriole duplication and form 6-8 new procentrioles on their surfaces (Zhao et al. 2013). After deuterosome production, multiple procentrioles also form around the two parental centrioles via the centriolar pathway. These procentrioles grow in length before disengaging simultaneously from the deuterosomes and parental centrioles. Finally, the centrioles are trafficked to the apical plasma membrane where they dock and serve as basal bodies to nucleate motile cilia.

While deuterosomes were identified > 50 years ago, their molecular makeup had long remained elusive. Most of the proteins required for centriole amplification in MCCs function in both procentriole and deuterosome-dependent centriole amplification. Recently, however, Deup1 (gene name: *CCDC67*) was identified as a specific component required for the formation of the deuterosome (Figure 1B). *DEUPI* arose from a gene duplication event of the centriolar gene, *CEP63*. This event occurred post-lobe finned fish, and tracks with the increase in motile cilia number per cell observed in higher eukaryotes. For example, zebrafish do not encode a Deup1 orthologue and average ~ 20 cilia per kidney epithelial cell (Liu et al. 2007). By comparison, mammalian tracheal epithelial cells contain upwards of 300 motile cilia per cell. Given that deuterosomes have not been found in organisms lacking Deup1, the current evidence suggests that Deup1 evolved to enable the formation of the deuterosome and allow the generation of increased numbers of cilia per cell in higher eukaryotes. In accord with this proposal, Deup1 knockdown by shRNA prevents the formation of deuterosomes and reduces centriole amplification in mouse tracheal epithelial cells (Zhao et al. 2013). Indeed, it has been estimated the deuterosome-dependent centriole amplification pathway contributed ~95% of the procentrioles needed for mammalian MCCs (Sorokin 1968).

Although deuterosomes are formed uniquely in epithelial cells that undergo massive centriole amplification, the requirement of the deuterosome for centriole amplification *in vivo* has not been explored. In this thesis, I interrogate the *in vivo* function of the deuterosome using a *Deup1*<sup>-/-</sup> mouse model.

## **1.5 The role of centrosomes and cilia in kidney cystogenesis**

Autosomal Dominant Polycystic Kidney Disease (ADPKD) is a genetic disease that affects about 1 in 500 people and is characterized by the progressive development of fluid-filled cysts in the kidneys that can eventually cause end stage renal failure (Ong et al. 2015). Currently, there are very few therapeutic options for these patients, and they often require lifelong dialysis or kidney transplantation. Mutations in one of two genes—PKD1 and PKD2—have been identified as causative of ADPKD. These genes encode polycystin 1 (PC1) and polycystin 2 (PC2), which are transmembrane proteins localized on primary cilia that act as a complex to help regulate calcium influx and signaling (Zhou and Li 2015). Despite the identification of these causative genes over 30 years ago, the molecular mechanism behind ADPKD is still unknown.

One theory of cystogenesis is that defective primary cilia on renal tubule epithelial cells affects cell signaling, which leads to increased proliferation. This aberrant proliferation

can create polycystic kidneys, as evidenced by mouse models of defective cilia length, number, or composition (Park et al. 2015). Other pieces of evidence to support this proposal are that extra centrioles, which nucleate cilia, and altered cilia formation have been observed in kidneys of ADPKD patients (Battini et al. 2008; Park et al. 2015). Furthermore, extra centrioles have been proposed to increase cilia number and perturb signaling in cultured cells (Mahjoub and Stearns 2012). In this thesis, we test whether extra centrioles are sufficient to promote kidney cystogenesis *in vivo*.

**Figure 1. Centriole biogenesis in cycling and multiciliated cells**

(A) After mitosis, each daughter cell inherits one centrosome consisting of two centrioles.

New centriole production occurs on the side of pre-existing centrioles in S-phase of the cell cycle, so that cells contain two centrosomes each with two centrioles upon entry into

mitosis. (B) Extra centrosomes are clustered and create a pseudo-bipolar spindle, which

causes increased merotelic attachments. The incorrectly attached chromosome can lag in the middle of the dividing cell and have one of four fates: the resulting cells can be

diploid, they can be diploid with a micronucleus forming around the lagging chromosome,

they can both be aneuploid or they can be aneuploid with a micronucleus. Therefore,

extra centrosomes can frequently cause mitotic errors and aneuploidy.

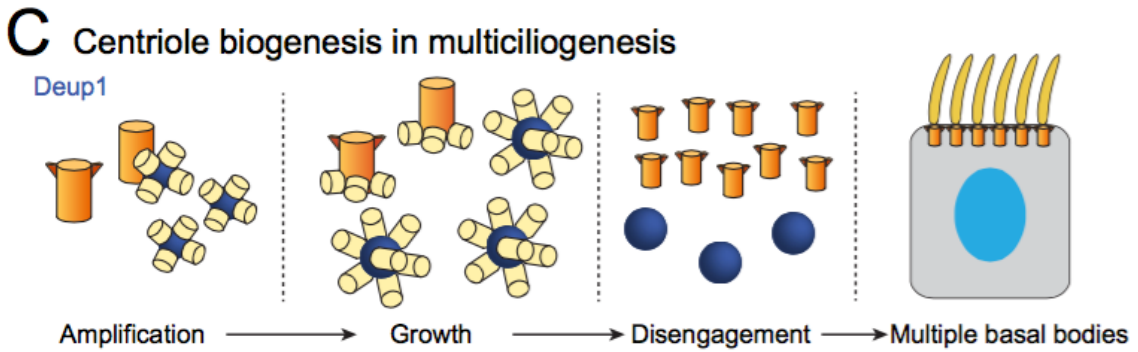
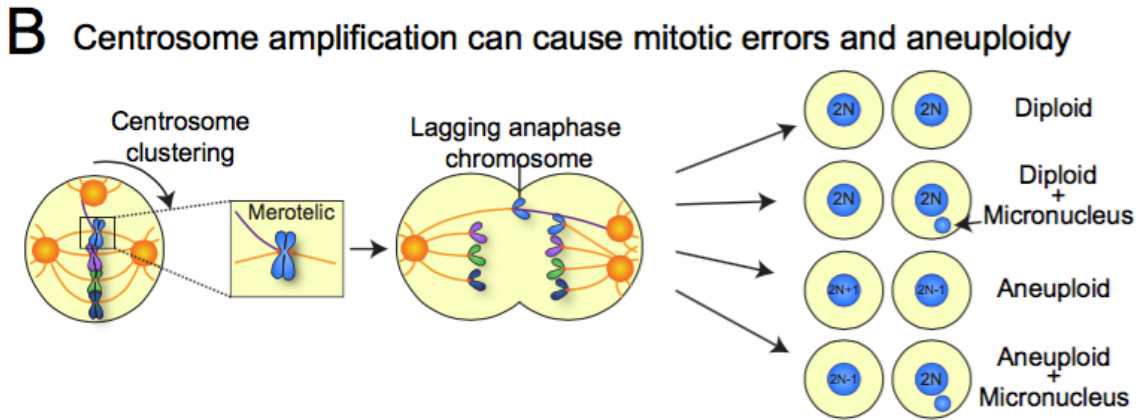
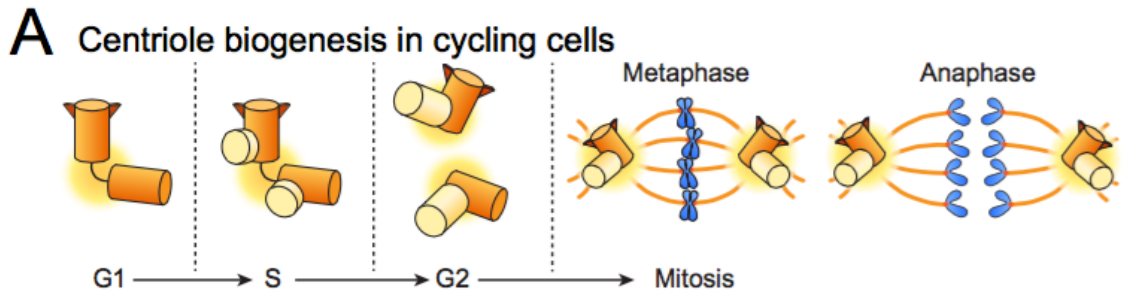
(C) Centriole biogenesis in multiciliated cells occurs on structures known as

deuterosomes. The deuterosome forms off the side of the daughter centriole or in the

cytoplasm and acts as a hub for procentriole creation and growth. Each cell produces tens

of deuterosomes on which 6-8 centrioles can amplify, so that hundreds of centrioles can

grow, disengage, and migrate to the apical cell surface to nucleate axonemes of cilia.





## Chapter 2

# Centrosome amplification is sufficient to promote spontaneous tumorigenesis in mammals

**Modified from:** Levine MS, Bakker B, Boeckx B, Moyett J, Lu J, Vitre B, Spierings DC, Lansdorp PM, Cleveland DW, Lambrechts D, Foijer F, Holland AJ. Dev Cell. 2017 Feb 6;40(3):313-322.e5. doi: 10.1016/j.devcel.2016.12.022. Epub 2017 Jan 26.

**Data generated by Michelle Levine:** All figures, except Figures 7B-7C, 10D-10G, and 11G-I

### 2.1 Plk4 overexpression drives centrosome amplification *in vitro*

To drive centrosome amplification in a temporally-controlled manner *in vivo*, we developed a mouse model in which increased synthesis of Plk4 can be induced by

addition of doxycycline. We integrated a single-copy Plk4-EYFP transgene, driven by a doxycycline-regulatable promoter, downstream of the *Col1a1* locus in ES cells. Targeted ES cells were then used to produce the Plk4-EYFP transgenic mice, which were crossed with mice expressing the reverse tetracycline transactivator (rtTA) to allow doxycycline-inducible expression of Plk4-EYFP (Figure 2A). Mice and cells that harbor homozygous copies of the Plk4-EYFP and rtTA transgenes (Plk4-EYFP<sup>hom</sup>; rtTA<sup>hom</sup>) are referred to hereafter as Plk4<sup>Dox</sup>.

To characterize the effect of Plk4 overexpression *in vitro*, we derived primary mouse embryonic fibroblasts (MEFs) from control and Plk4<sup>Dox</sup> embryos. In doxycycline-treated Plk4<sup>Dox</sup> MEFs, Plk4 mRNA levels rose ~6-fold (Figure 3A) and the level of Plk4 protein at the centrosome increased ~2-fold (Figure 2B and Figure 3B and 3C). This modest elevation in the level of Plk4 induced substantial centrosome amplification; after 3 and 5 days the number of cells with increased centrosome amplification rose to 69% and 79%, respectively (Figure 2C and 2D and Figure 3D). As expected, centrosome amplification was not observed in doxycycline-treated MEFs that carried either the Plk4-EYFP or rtTA transgene alone (Figure 3E).

Cells that enter mitosis with centrosome amplification can either undergo multipolar

divisions or cluster their centrosomes prior to division (Ring et al. 1982; Quintyne et al. 2005; Basto et al. 2008). Examination of mitotic figures revealed that Plk4<sup>Dox</sup> MEFs avoided lethal multipolar divisions by clustering extra centrosomes into pseudo-bipolar spindles with high efficiency (Figure 2E). Consistent with previous reports (Ganem et al. 2009; Silkworth et al. 2009), centrosome clustering significantly increased the frequency of mitotic errors (Figure 2F). Although aneuploidy increased in primary MEFs with repeated passages in culture (Hao and Greider 2004; Weaver et al. 2007), cells with supernumerary centrosomes were more aneuploid than wildtype MEFs at both time points (as determined with fluorescence *in situ* hybridization for chromosome 15 or 16) (Figure 2G and 2H). Importantly, supernumerary centrosomes did not lead to an increase in DNA damage or tetraploidization (Figure 3F-I).

Previously, we showed that centrosome amplification elicits a durable p53-dependent proliferative arrest in non-transformed human cells (Holland et al. 2012a). Consistently, supernumerary centrosomes prevented the proliferation of primary MEFs (Figure 2I), and knocking out p53 alleviated this block (Figure 2J). The fraction of cells with 5 or more centrosomes declined in Plk4<sup>Dox</sup> MEFs after 5 days of doxycycline treatment, but continued to increase in cells lacking p53 (Figure 3D and Figure 3J-K). This suggests that cells with high levels of centrosome amplification are outcompeted in a p53-dependent

manner *in vitro*. Together, our data demonstrate that modest overexpression of Plk4 *in vitro* drives centrosome amplification, mitotic errors and a p53-dependent cell cycle arrest.

## **2.2 Elevated Plk4 expression promotes formation of supernumerary centrosomes in tissues**

To determine the effect of Plk4 overexpression on centrosome number *in vivo*, we treated Plk4<sup>Dox</sup> and control animals with doxycycline for 1 or 8 months and sacrificed animals to analyze centrosome number in tissues. With the exception of the brain (see below), there was an increase in Plk4 mRNA levels in all tissues analyzed in Plk4<sup>Dox</sup> mice (Figure 3A and Figure 4A). In line with the prior results in MEFs, we observed a modest (<2-fold) increase in Plk4 protein levels at the centrosome in the thymus of Plk4<sup>Dox</sup> mice (Figure 4B). Consistent with increased Plk4, we observed a chronic increase in centrosome number in the skin, spleen, intestine, thymus, liver, pancreas and stomach of Plk4-overexpressing mice (Figure 3B-C and Figure 4C). In almost every case where an increase in centrosome number was observed, cells contained at most three extra centrosomes (Figure 3D and 3E and Figure 4D). By contrast, there was no increase in

centrosome amplification in the lung and kidney, despite the 11 and 338-fold increase in Plk4 mRNA levels in these tissues, respectively (Figure 4A and 4C).

To determine whether the lack of centrosome amplification in the lung and kidney was caused by the death of cells with extra centrosomes, we assessed the expression of active caspase 3 and used TUNEL staining in tissues from Plk4<sup>Dox</sup> animals that were treated for 1 month with doxycycline. There was no significant increase in active caspase 3 or TUNEL staining in any of the tissues examined, suggesting that cells with extra centrosomes are not eliminated by cell death (Figure 3F and 3G). Plk4 overexpression does not promote centrosome amplification in quiescent cells (data not shown), suggesting that differences in proliferation rates could contribute to tissue specific differences in centrosome amplification in response to Plk4 overexpression.

Concordantly, analysis of Ki67 staining in tissues revealed high rates of proliferation in the skin, intestine, spleen and thymus, where robust centrosome amplification was observed, and low turnover rates in the lung and kidney, where there was no increase in centrosome number (Figure 3B, 3H and 4C). Nevertheless, the liver, pancreas and stomach showed a significant increase in centrosome amplification despite a very small fraction of proliferating cells (Figure 3H and 4C). This suggests additional tissue-specific factors likely influence the relationship between Plk4 overexpression and centrosome

amplification. Surprisingly, increased centrosome numbers correlated with hyperproliferation of cells in the thymus and decreased proliferation in the kidney (Figure 3H). These differences in cell proliferation highlight tissue specific differences in the response to centrosome amplification and may arise from alterations in growth signaling as a result of changes in centrosome or cilia number (Arquint et al. 2014).

Overexpression of Plk4 in the brain of mice has been reported to cause microcephaly and behavioral defects (Marthiens et al. 2013; Coelho et al. 2015). However, transgenes integrated downstream of the *Col1a1* locus are not expressed in major cells types of the brain (Hochedlinger et al. 2005) (Figure 4E). Consistently, there was no increase in Plk4 RNA levels or centrosome amplification in the brain of doxycycline-treated Plk4<sup>Dox</sup> mice (Figure 5A and 5C). Moreover, Plk4-overexpressing animals did not show behavioral deficits or alterations in brain size (Data not shown and Figure 6A).

### **2.3 Centrosome amplification impairs epidermal architecture**

A striking feature in mice overexpressing Plk4 was progressive hair loss that continued throughout the life of the animal and led to almost complete balding in one-year-old mice (Figure 6B). Consistent with previous reports in mice exhibiting centrosome amplification in the skin (Coelho et al. 2015; Sercin et al. 2016), mice overexpressing

Plk4 exhibited a thickened epidermis and disrupted hair follicle morphology. Systematic histological examination of other tissues from Plk4-overexpressing mice revealed no major pathology (Figure 6C and 6D). We conclude that, with the notable exception of the skin, centrosome amplification is tolerated in many tissues *in vivo*.

## **2.4 Centrosome amplification causes aneuploidy *in vivo***

To evaluate whether centrosome amplification leads to aneuploidy *in vivo*, we assessed chromosome number in splenocytes from mice treated with doxycycline for 1 or 8 months. Centrosome amplification increased the fraction of aneuploid splenocytes at both time points (Figure 7A and Figure 8A and 8B), but did not promote cytokinesis failure or polyploidization (Figure 8C). To investigate whether extra centrosomes lead to the accumulation of aneuploid cells in aged mice, we isolated epidermal cells from 12-21 month old mice and determined their karyotype by low coverage genomic copy number analysis in single-cells. Analysis of 99 cells from 3 mice with centrosome amplification revealed 23 of the cells to be aneuploid (average of 23%), whereas 0 aneuploid cells were identified in the 78 single cells sequenced from two control animals (Figure 7B-C). In summary, supernumerary centrosomes promote chromosome segregation errors and aneuploidy, in the absence of polyploidization, in tissues.

## 2.5 Centrosome amplification increases the initiation of intestinal tumors

To test whether centrosome amplification is able to influence tumorigenesis, we first used a mouse model of intestinal neoplasia (Moser et al. 1990; Su et al. 1992). Mice that express a single truncated allele of the adenomatous polyposis coli (APC) tumor suppressor ( $APC^{Min}$ ) develop early onset adenomatous intestinal tumors with complete penetrance. To evaluate the effect of Plk4 overexpression on centrosome number in  $APC^{Min/+}$  cells, we derived MEFs from  $APC^{Min/+};Plk4^{Dox}$  embryos. Doxycycline addition drove increased levels of Plk4 expression leading to sustained centrosome amplification, with 55% and 89% of  $APC^{Min/+};Plk4^{Dox}$  cells containing extra centrosomes at day 3 and day 14 after doxycycline addition, respectively (Figure 8D and Figure 9A). As expected, extra centrosomes increased the frequency of chromosome segregation errors and micronuclei formation in  $APC^{Min/+};Plk4^{Dox}$  MEFs and led to a cell cycle arrest *in vitro* (Figure 8E and 9B-C).

Next, we examined the size and number of tumors formed in the intestine of  $APC^{Min/+}$  and  $APC^{Min/+};Plk4^{Dox}$  animals. Once again, centrosome number was significantly increased in both the normal intestine and in intestinal tumors from doxycycline-treated  $APC^{Min/+};Plk4^{Dox}$  mice (Figure 9D-F). Importantly, tumor number was significantly



increased in mice with centrosome amplification (average of 69 tumors in APC<sup>Min/+</sup> animals compared to 129 tumors in APC<sup>Min/+</sup>;Plk4<sup>Dox</sup> mice; Figure 9G and 9I). However, tumor size remained unchanged (Figure 9H and 9I). Consistent with prior reports (Luongo et al. 1994), we observed that intestinal APC<sup>Min/+</sup> and APC<sup>Min/+</sup>;Plk4<sup>Dox</sup> tumors showed a reduced abundance of the wildtype allele of APC (Figure 8F). These data demonstrate that, in this context, centrosome amplification promotes the initiation, but not progression, of intestinal tumors.

## **2.6 Centrosome amplification drives spontaneous tumorigenesis**

Despite the fact that centrosome amplification is a common feature of many cancer cells, it remains untested whether chronic centrosome amplification is sufficient to initiate tumorigenesis in mammals. To address this question, we aged cohorts of Plk4Dox and control mice that were fed doxycycline starting from 1-2 months of age. Strikingly, Plk4Dox mice succumbed to the development of spontaneous tumors starting at 36 weeks (median tumor-free survival of 55 weeks) (Figure 10A). Specifically, Plk4-overexpressing mice developed lymphomas, squamous cell carcinomas and sarcomas, whilst spontaneous tumors were not observed in Plk4-EYFP, rtTA or wild-type mice

treated with doxycycline (Figure 10A and 10C). In contrast to lymphomas that developed in mice lacking p53, tumors from Plk4-overexpressing mice exhibited high levels of centrosome amplification (average of 44% amplification in lymphomas and squamous cell carcinomas in Plk4Dox mice) (Figure 10B). The vast majority of the tumor cells exhibiting centrosome amplification contained just one or two extra centrosomes (Figure 11A). Two of the lymphomas that developed in mice with centrosome amplification exhibited acute tumor lysis syndrome, a feature that was not observed in lymphomas that developed in p53-null animals (Figure 11B).

p53 has been shown to suppress the proliferation of cells with extra centrosomes in cell culture (Holland et al. 2012a). To examine whether spontaneous tumors that develop in mice with centrosome amplification exhibit inactivation of the p53 pathway, we analyzed the expression level of p53 target genes in thymic lymphomas that developed in p53<sup>-/-</sup> and Plk4Dox mice. As expected, p53<sup>-/-</sup> tumors had low expression of p53 and p53 transcriptional target genes (FAS, BCL2, BAX and PUMA) (Figure 11C). By contrast, thymic lymphomas that developed in Plk4Dox animals had a wide variation in the level of p53 expression. Despite the variation in p53 levels, the thymic tumors from Plk4Dox mice showed an overall reduction in the expression of p53 target genes, indicating the p53 pathway is at least partly comprised in spontaneous tumors that develop as a result of

centrosome amplification (Figure 11C). Together, these data suggest that the p53 pathway acts as a barrier to the continued growth of cells with supernumerary centrosomes in vivo.

Since chronic increases in Plk4 could have consequences independent of centrosome amplification, we also tested whether a transient increase in Plk4 levels could trigger spontaneous tumor development. Remarkably, treatment with doxycycline for one month led to an increase in centrosome number in the spleen, intestine, liver and pancreas of 16-18 month old Plk4Dox mice (Figure 11D). Centrosome amplification can therefore persist in some tissues for long periods of time after transient Plk4 overexpression. Consistent with the observations in chronically-treated mice, Plk4Dox animals treated with doxycycline for one month also developed lymphomas, squamous cell carcinomas and sarcomas (Figure 11E). Moreover, tumors from these animals displayed high levels of centrosome amplification (Figure 11F). Together, these data establish a direct causal relationship between increased Plk4 levels, centrosome amplification and spontaneous tumor development.

## **2.7 Centrosome amplification promotes the development of aneuploid tumors**

In human tumors, centrosome amplification strongly correlates with genomic instability. To evaluate the degree of aneuploidy and genome instability in tumors caused by centrosome amplification, we performed whole genome sequencing of tumor DNA isolated from three spontaneous T-cell lymphomas, two B-cell lymphomas, five squamous cell *carcinomas* and one sarcoma from doxycycline-treated Plk4<sup>Dox</sup> mice. All tumors showed evidence of aneuploidy, and each tumor type showed evidence of clonal selection for recurring chromosomal abnormalities. In particular, gains of chromosome 2, 5 and 17 were observed in squamous cell carcinomas, while T and B cell lymphomas showed recurrent gains of chromosome 14 and 15 (Figure 10D-H and Figure 11G-I). Notably, chromosome 15 carries the Myc proto-oncogene and is frequently gained in murine blood cancers (Bakker et al. 2016). To examine the extent of tumor heterogeneity, we performed whole genome sequencing of single cells isolated from a thymic and a splenic lymphoma that developed in two mice chronically overexpressing Plk4. In the T-cell lymphoma, 12 aneuploid cells were sequenced and many showed gains of chromosomes 1, 11, 15 as well as segments of chromosomes 4 and 10. 32 aneuploid cells were sequenced in the splenic lymphoma, with most cells having gains of chromosomes 14, 15 and 17 (Figure 10G and 10H). Importantly, while both of the tumor samples contained recurrent chromosomal alterations, these tumors also exhibited karyotypic diversity, with some cells in each tumor exhibiting different gains and losses of whole

chromosomes. These data suggest ongoing chromosome segregation errors in tumors with extra centrosomes.

**Figure 2. A modest increase in Plk4 promotes centrosome amplification and aneuploidy *in vitro***

(A) System used for doxycycline-inducible expression of Plk4.

(B) Quantification of the level of centrosomal Plk4 in Plk4<sup>Dox</sup> MEFs. N = 3, >150 centrosomes per experiment.

(C) Quantification of the level of centrosome amplification in Plk4<sup>Dox</sup> MEFs. N = 3, >150 cells per experiment.

(D) Immunofluorescent images of centrosomes in Plk4<sup>Dox</sup> MEFs.

(E) Quantification of anaphase phenotypes in Plk4<sup>Dox</sup> MEFs. N = 3, >150 cells per experiment.

(F) Quantification of anaphase lagging chromosomes in Plk4<sup>Dox</sup> MEFs. N = 3, >150 cells per experiment.

(G) Quantification of the fraction of cells having <2 or >2 copies of chromosome 15 or 16. N = 3, >150 cells per experiment.

(H) Immunofluorescent images of FISH performed on Plk4<sup>Dox</sup> MEFs using probes against chromosome 15 and 16. Arrowheads mark each copy of Chr15 or Chr16.

(I) Graph showing the fold increase in cell number for Plk4<sup>Dox</sup> MEFs. N = 3, performed in triplicate.

(J) Graph showing the fold increase in cell number for Plk4<sup>Dox</sup> MEFs expressing SpCas9 and an sgRNA against p53. N = 3, performed in triplicate.

All data represent the means  $\pm$ SEM. \* $P$  < 0.05, \*\* $P$  < 0.01 and \*\*\* $P$  < 0.001; two-tailed

Student's  $t$ -test. Scale bars represent 10  $\mu$ m.

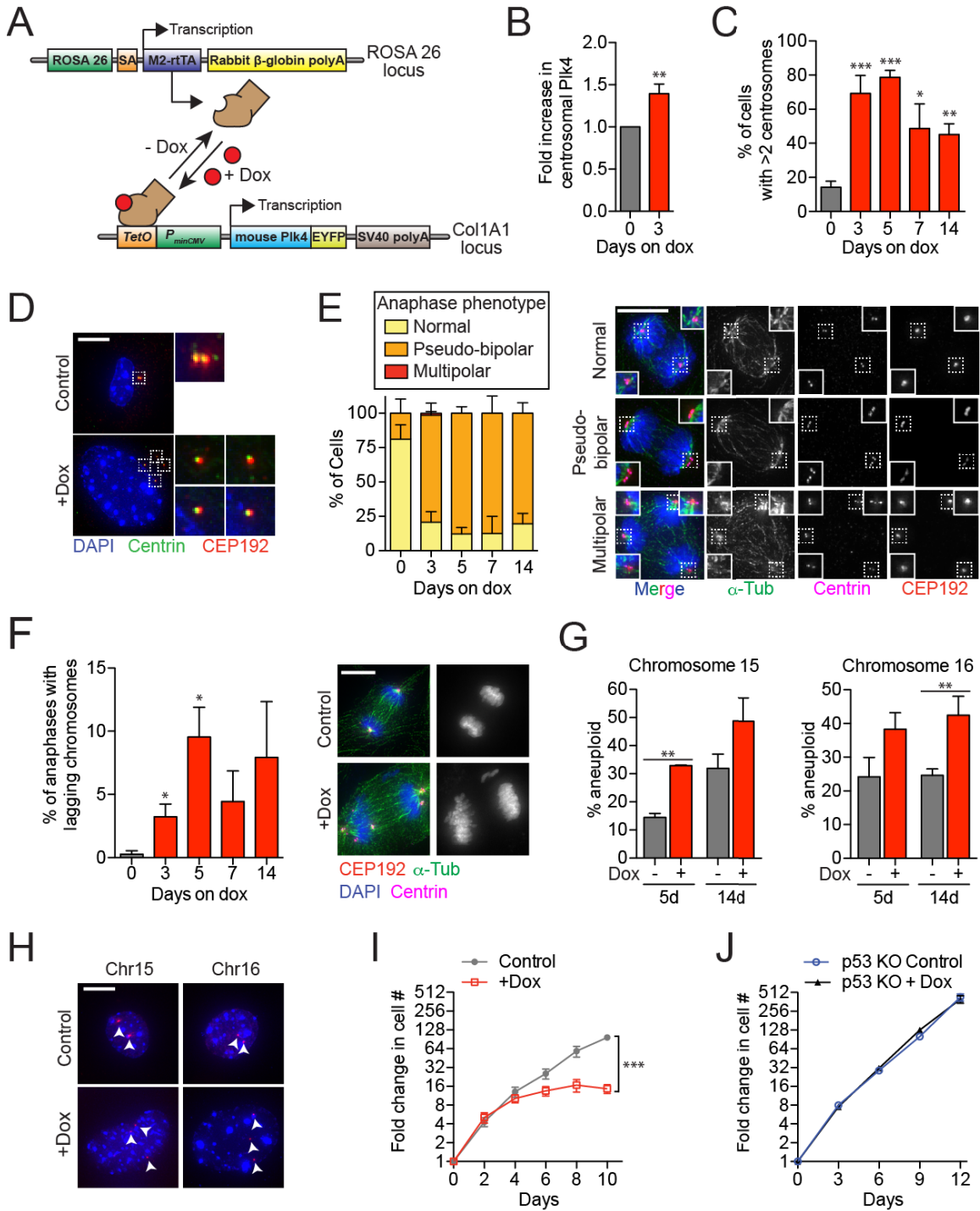




**Figure 3. Centrosome amplification does not promote DNA damage or cytokinesis failure**

(A) Quantification of the level of Plk4 mRNA in Plk4<sup>Dox</sup> MEFs at different times after doxycycline treatment. Data are means  $\pm$ SEM (N = 3, performed in triplicate).

(B) Quantification of the level of centrosomal Plk4 at different times after doxycycline treatment. Data are means  $\pm$ SEM from two different Plk4 antibodies (Plk4 ab #1 and #3) (N = 3, >150 centrosomes per experiment).

(C) Representative immunofluorescent images of centrosomal Plk4 in Plk4<sup>Dox</sup> MEFs.

(D) Quantification of centrosome number in Plk4<sup>Dox</sup> MEFs at different times after doxycycline treatment. Data are means  $\pm$ SEM (N = 3, >150 cells per experiment).

(E) Quantification of the level of centrosome amplification in Plk4-EYFP, rtTA and Plk4<sup>Dox</sup> MEFs at two days after doxycycline addition. Data are means  $\pm$ SEM (N = 3, >150 cells per experiment).

(F) Quantification of DNA damage foci in Plk4<sup>Dox</sup> MEFs at different times after doxycycline treatment. Doxorubicin treatment (Doxo.) is shown as a control. Data are means  $\pm$ SEM (N = 3, >150 cells per experiment).

(G) Quantification of the fraction of binuclear Plk4<sup>Dox</sup> MEFs at different times after doxycycline treatment. Data are means  $\pm$ SEM (N = 3, >135 cells per experiment).

(H) Quantification of the fraction of Plk4<sup>Dox</sup> MEFs with >4N DNA content at different times after doxycycline treatment. Data are means  $\pm$ SEM (N = 3, 10,000 cells per experiment).

(I) Representative flow cytometry profiles show cell cycle analysis in Plk4<sup>Dox</sup> MEFs.

(J) Quantification of the level of centrosome amplification in Plk4<sup>Dox</sup>; p53<sup>-/-</sup> MEFs at different times after doxycycline addition. Data are means  $\pm$ SEM (N = 3, >150 cells per experiment).

(K) Quantification of centrosome number in Plk4<sup>Dox</sup>; p53<sup>-/-</sup> MEFs at different times after doxycycline treatment. Data are means  $\pm$ SEM (N = 3, >150 cells per experiment).

\* $P < 0.05$ , \*\* $P < 0.01$ , \*\*\* $P < 0.005$  and NS (not significant) indicates  $P > 0.05$ ; two-tailed Student's  $t$ -test.

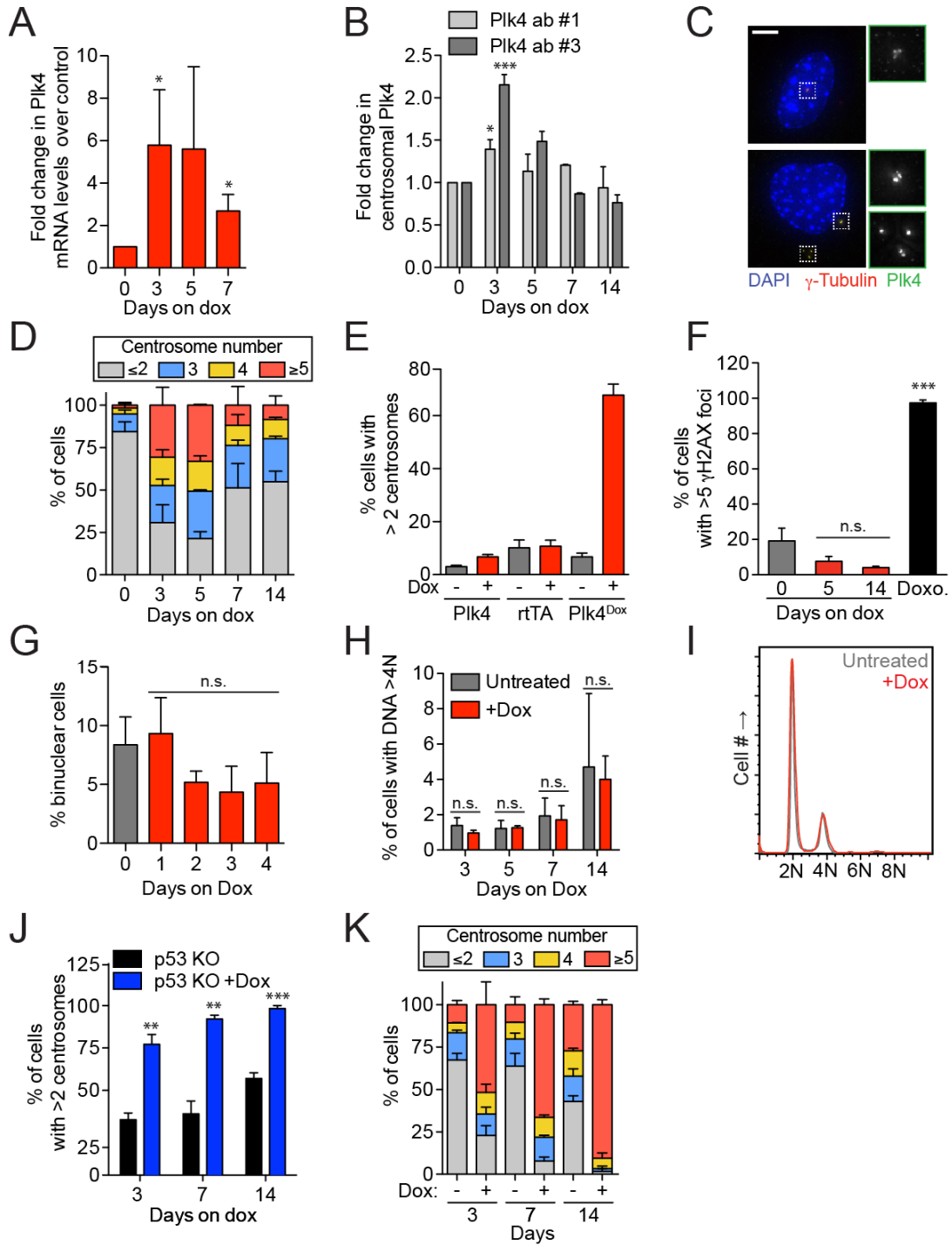


**Figure 4. Increased Plk4 levels promote chronic centrosome amplification in multiple tissues**

(A) Fold increase in Plk4 mRNA in tissues from Plk4<sup>Dox</sup> mice treated with doxycycline for 1 month. N = 3, performed in triplicate.

(B and C) Quantification of the level of centrosome amplification in tissues from Plk4<sup>Dox</sup> mice treated with doxycycline for 1 or 8 month. N ≥ 4.

(D) Quantification of centrosome number in tissues from Plk4<sup>Dox</sup> mice treated with doxycycline for 8 months. N = 4.

(E) Representative images of centrosomes in tissues from doxycycline treated Plk4<sup>Dox</sup> or control animals.

(F-H) Quantification of the fraction of cleaved caspase 3, TUNEL, or Ki67 positive cells in tissues from Plk4<sup>Dox</sup> mice treated with doxycycline for 1 month. Data are means ±SEM (N = ≥4).

All data represent the means ±SEM. \**P* < 0.05, \*\**P* < 0.01 and \*\*\**P* < 0.001; two-tailed

Student's *t*-test. Scale bars represent 10 μm.

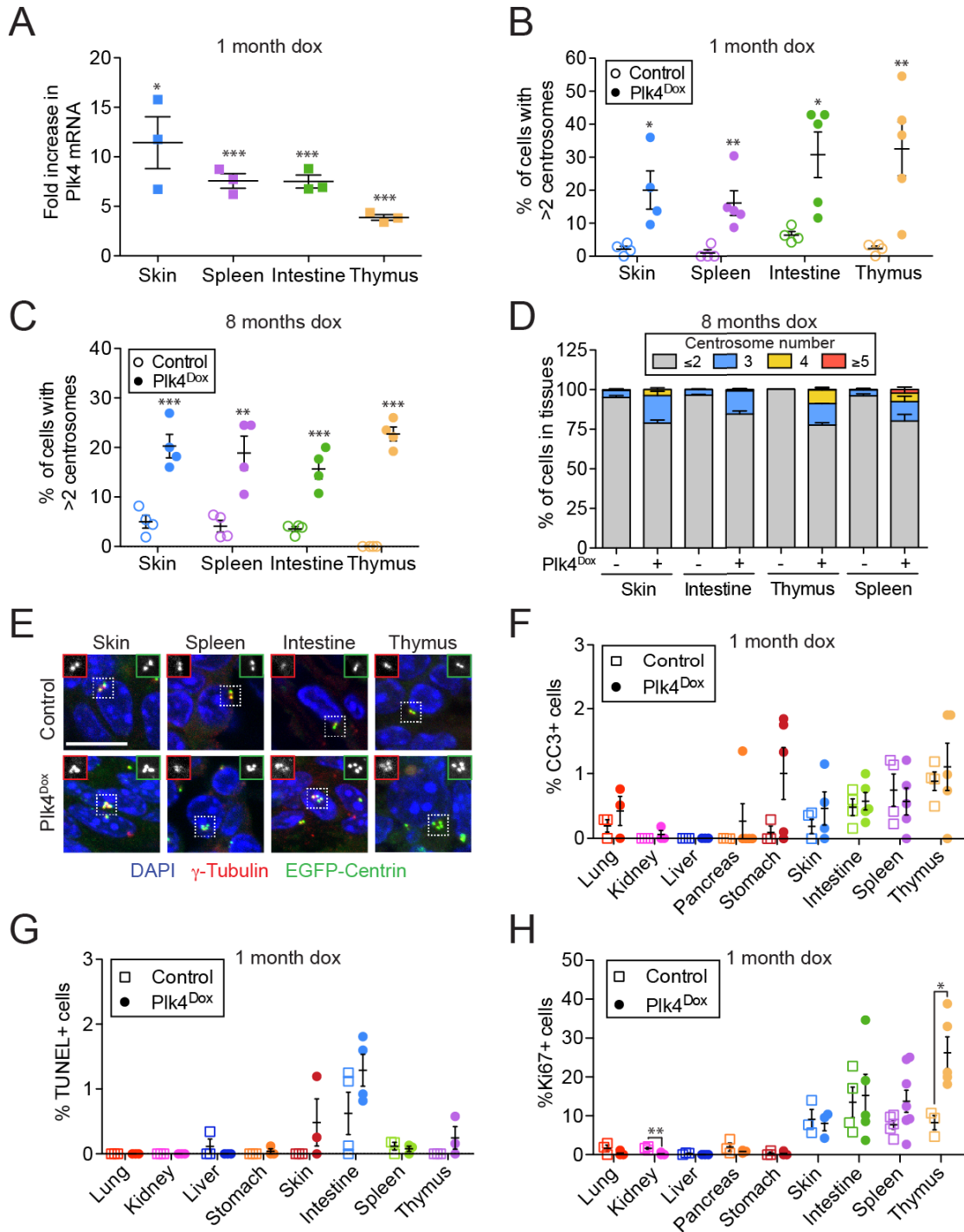


**Figure 5. There is no Plk4 overexpression or centrosome amplification in the brain of doxycycline-treated Plk4<sup>Dox</sup> mice**

(A) Graph showing the fold increase in Plk4 mRNA in tissues from Plk4<sup>Dox</sup> mice treated with doxycycline for 1 month. Data are means  $\pm$ SEM (N = 3, performed in triplicate).

(B) Quantification of the level of centrosomal Plk4 in tissues from Plk4<sup>Dox</sup> mice treated with doxycycline for 1 month. Representative immunofluorescent images show centrosomal Plk4 in tissue sections. Data are means  $\pm$ SEM (N = 3). Scale bar represents 10  $\mu$ m.

(C) Quantification of the level of centrosome amplification in tissues from Plk4<sup>Dox</sup> mice treated with doxycycline for 8 months. Data are means  $\pm$ SEM (N = 4).

(D) Quantification of centrosome number in tissues from Plk4<sup>Dox</sup> mice treated with doxycycline for 1 month. Data are means  $\pm$ SEM (N =  $\geq$ 4).

(E) Images of tissue sections taken from Histone H2B-mCherry;rtTA mice treated with doxycycline for 1 month. The Histone H2B-mCherry expression construct was integrated at the same location as the Plk4-EYFP transgene. This reporter showed widespread doxycycline-inducible expression, but was undetectable in the brain. Scale bar represents 200  $\mu$ m.

\* $P < 0.05$ , \*\* $P < 0.01$ , \*\*\* $P < 0.005$  and NS (not significant) indicates  $P > 0.05$ ; two-tailed Student's  $t$ -test.

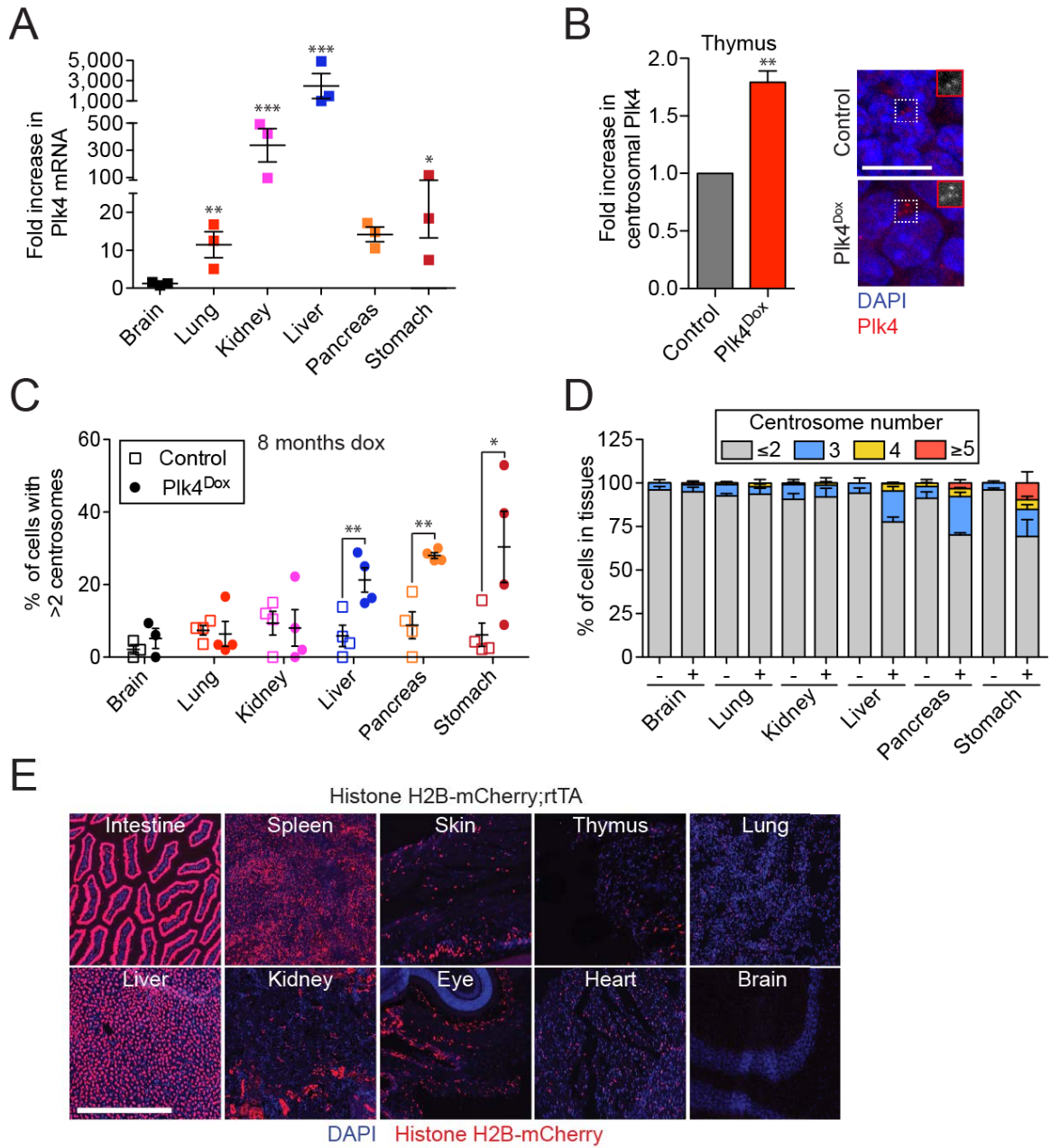


**Figure 6. Centrosome amplification leads to progressive hair loss.**

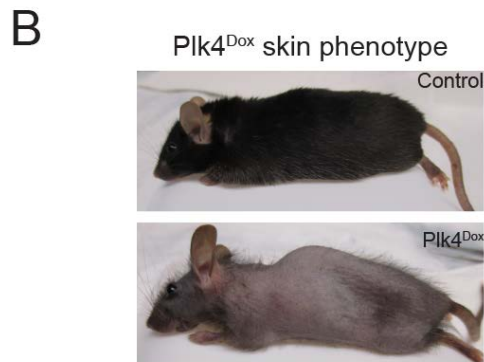
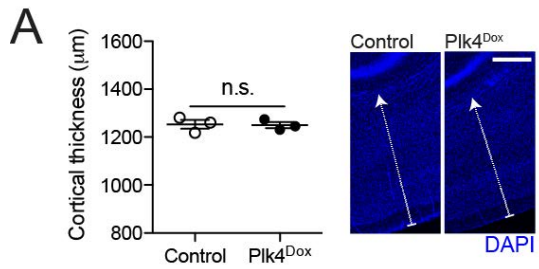
(A) Quantification of cortex thickness measured in four-month old control or Plk4<sup>Dox</sup> animals treated with doxycycline for 3 months (N = 3). Images show the cerebral cortex in control and Plk4<sup>Dox</sup> mice. Scale bar represents 200  $\mu$ m.

(B) Images show hair loss in eight-month old Plk4<sup>Dox</sup> animals fed doxycycline chronically from one week of age.

(C) Pathology report from eight-month old Plk4<sup>Dox</sup> animals fed doxycycline chronically from one week of age. Tissues analyzed by a veterinary pathologist (N = 4 for control and Plk4<sup>Dox</sup> mice).

(D) Images show hematoxylin and eosin stained tissue sections from eight-month old control and Plk4<sup>Dox</sup> mice fed doxycycline chronically from one week of age. Scale bars represent 200  $\mu$ m.





**C**

Tissues	Pathology
Skin	Small, widely-spaced follicles; sparse hair; hyperkeratosis
Liver	Normal
Lungs	Normal
Kidney	Normal
Pancreas	Normal
Stomach	Normal
Intestine	Normal
Spleen	Modestly elevated white pulp
Bone Marrow	Normal
Thymus	Normal
Lymph Nodes	Modestly reactive
Heart	Normal
Reproductive System	Normal

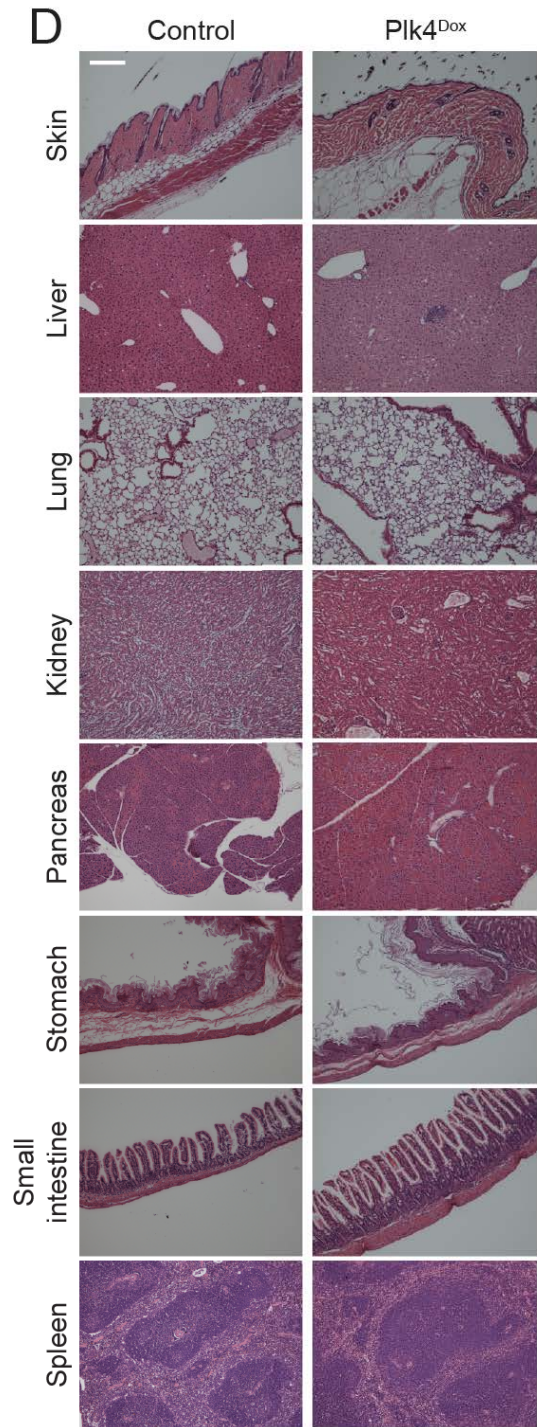


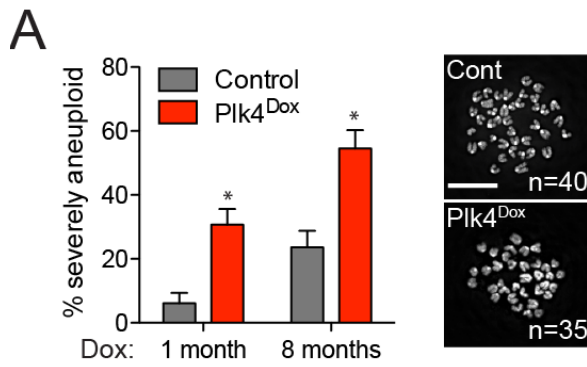
**Figure 7. Centrosome amplification drives aneuploidy in vivo**

(A) Proportion of severely aneuploid ( $4N \pm > 2$  chromosomes) splenocytes from control and Plk4<sup>Dox</sup> mice treated with doxycycline for 1 or 8 months. N = 3, > 120 cells per experiment.

(B) Table shows the fraction of aneuploid cells determined by single cell sequencing of epidermal cells from doxycycline-treated control or Plk4<sup>Dox</sup> mice.

(C) Genome-wide copy number plots of aneuploid single cells sequenced from the epidermis of 3 Plk4<sup>Dox</sup> mice treated with doxycycline for 12-18.5 months. Individual cells are represented in rows with copy number states indicated in colors.

All data represent the means  $\pm$ SEM. \* $P < 0.05$ ; two-tailed Student's *t*-test. Scale bars represent 10  $\mu$ m.



**B**

	Animal # (Sex)	Months on Dox	Aneuploid epidermal cells
Control	116 (M)	14.5	0% (0/37)
	810 (M)	21	0% (0/41)
Plk4 <sup>Dox</sup>	631 (F)	18.5	12% (3/25)
	635 (F)	16	19% (6/32)
	639 (M)	12	33% (14/42)

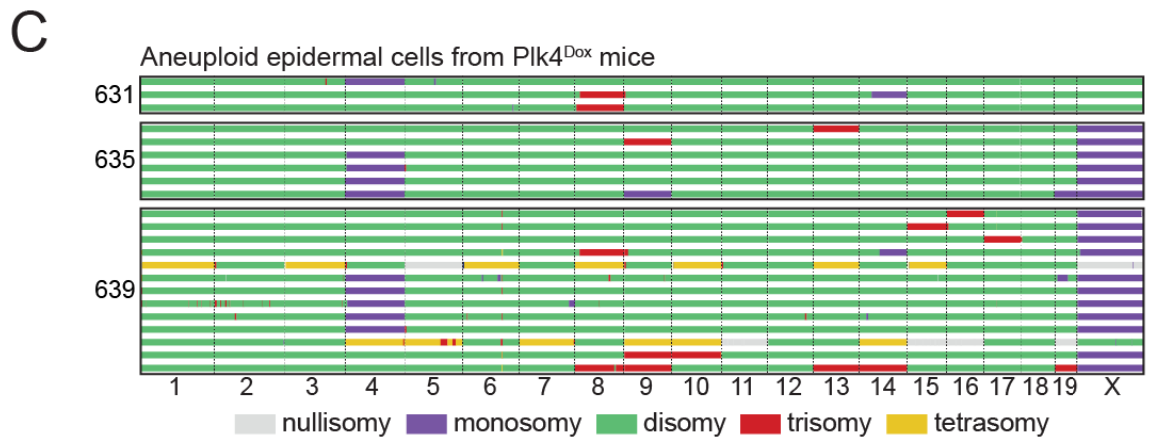


**Figure 8. Centrosome amplification leads to aneuploidy in the spleen of aged mice**

(A and B) Fraction of splenocytes with the indicated number of chromosomes. Cells were derived from control and Plk4<sup>Dox</sup> mice treated with doxycycline for either 1 or 8 months.

Data are means  $\pm$ SEM (N = 3, 50 cells per experiment).

(C) Quantification of the fraction of Plk4<sup>Dox</sup> or control splenocytes with >4N DNA content at different times after doxycycline treatment. Data are means  $\pm$ SEM (N = 3, 10,000 cells per experiment). Representative flow cytometry profiles show cell cycle analysis in Plk4<sup>Dox</sup> and control splenocytes.

(D) Quantification of the level of Plk4 mRNA in APC<sup>Min/+</sup>; Plk4<sup>Dox</sup> MEFs at different times after doxycycline treatment. Data are means  $\pm$ SEM (N = 3, performed in triplicate).

(E) Graph showing the fold increase in cell number for APC<sup>Min/+</sup>; Plk4<sup>Dox</sup> MEFs grown in the presence and absence of doxycycline. Data are means  $\pm$ SEM (N = 5, in triplicate).

(F) Graph showing the APC<sup>+</sup> to APC<sup>Min</sup> PCR ratios generated from intestinal adenomas (Polyp) and normal intestine (Int.) from APC<sup>Min/+</sup> and APC<sup>Min/+</sup>; Plk4<sup>Dox</sup> mice. The mean APC<sup>+</sup>/APC<sup>Min</sup> value for adenomas from APC<sup>Min</sup> and APC<sup>Min</sup>;Plk4<sup>Dox</sup> mice is reduced compared to normal tissue from these animals, indicating partial loss of the APC<sup>+</sup> allele.

Data are means  $\pm$ SEM (N =  $\geq$ 2, performed in duplicate).

\*\* $P < 0.01$ , \*\*\* $P < 0.001$  and n.s. (not significant) indicates  $P > 0.05$ ; two-tailed

Student's *t*-test.

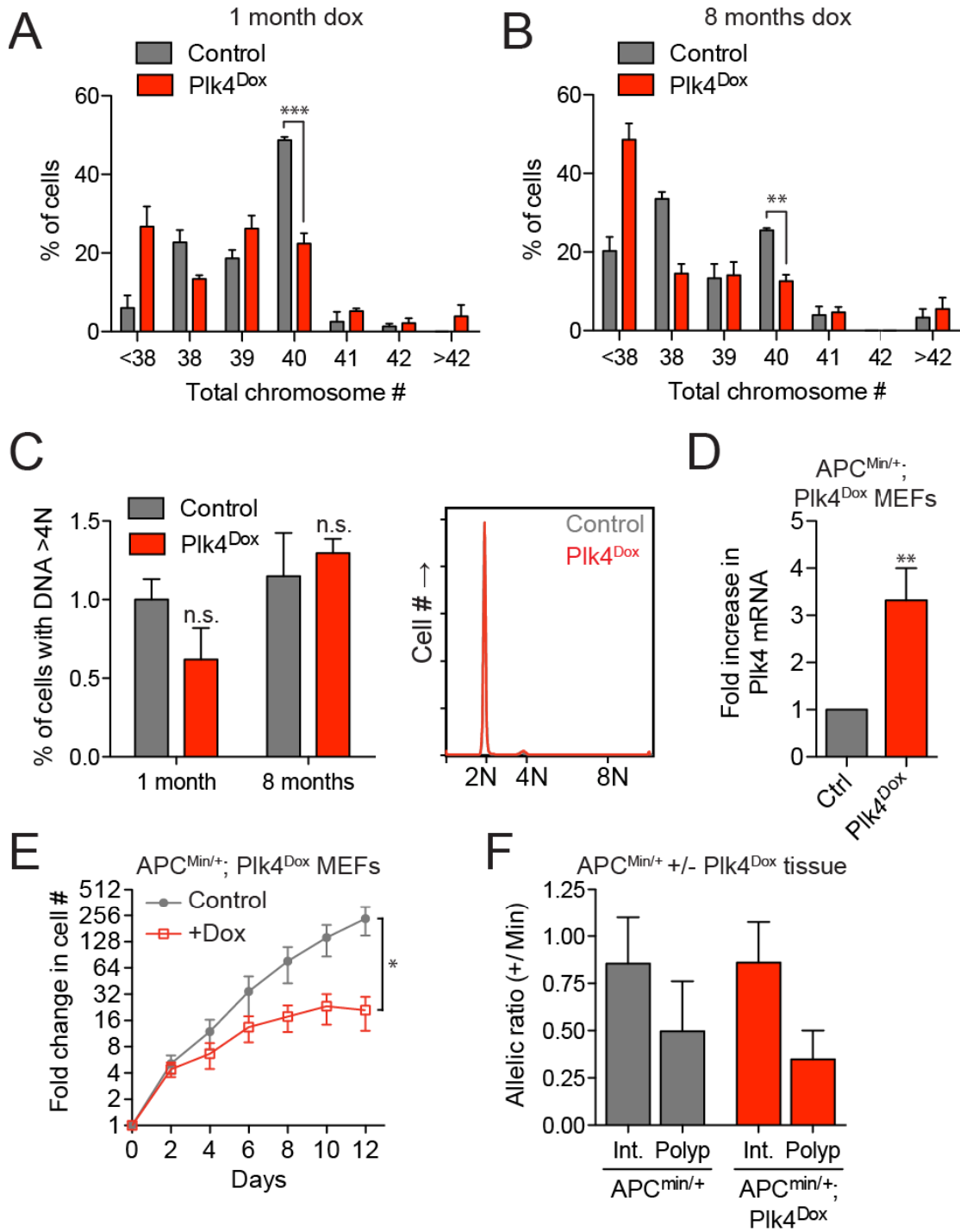


**Figure 9. Centrosome amplification promotes tumor initiation**

(A) Quantification of the level of centrosome amplification in APC<sup>Min/+</sup>; Plk4<sup>Dox</sup> MEFs.

N = 3, >150 cells per experiment.

(B) Quantification of anaphase lagging chromosomes in APC<sup>Min/+</sup>; Plk4<sup>Dox</sup> MEFs. N = 3, >84 cells per experiment. Scale bar represents 10  $\mu$ m.

(C) Frequency of micronuclei observed in APC<sup>Min/+</sup>; Plk4<sup>Dox</sup> MEFs. N = 3, >50 cells per experiment.

(D and E) APC<sup>Min</sup> and APC<sup>Min/+</sup>; Plk4<sup>Dox</sup> mice were treated with doxycycline from 10 days of age and sacrificed at 90 days old. Quantification shows the level of centrosome amplification in the intestines or intestinal polyps of APC<sup>Min</sup> and APC<sup>Min/+</sup>; Plk4<sup>Dox</sup> mice. N = 3, >150 cells per experiment.

(F) (Left) Immunofluorescence staining of an intestinal polyp and (Right) a magnified view of centrosomes in this tumor. Scale bars represent 200  $\mu$ m (left) and 10 $\mu$ m (right).

(G and H) Quantification of tumor number (G) or size (H) in 90 day old APC<sup>Min</sup> and APC<sup>Min/+</sup>; Plk4<sup>Dox</sup> mice.

(I) Images show intestinal polyps in an APC<sup>Min</sup> and APC<sup>Min/+</sup>; Plk4<sup>Dox</sup> mouse.

All data represent the means  $\pm$ SEM. \* $P < 0.05$ , \*\* $P < 0.01$ , \*\*\* $P < 0.001$  and NS (not significant) indicates  $P > 0.05$ ; two-tailed Student's  $t$ -test.

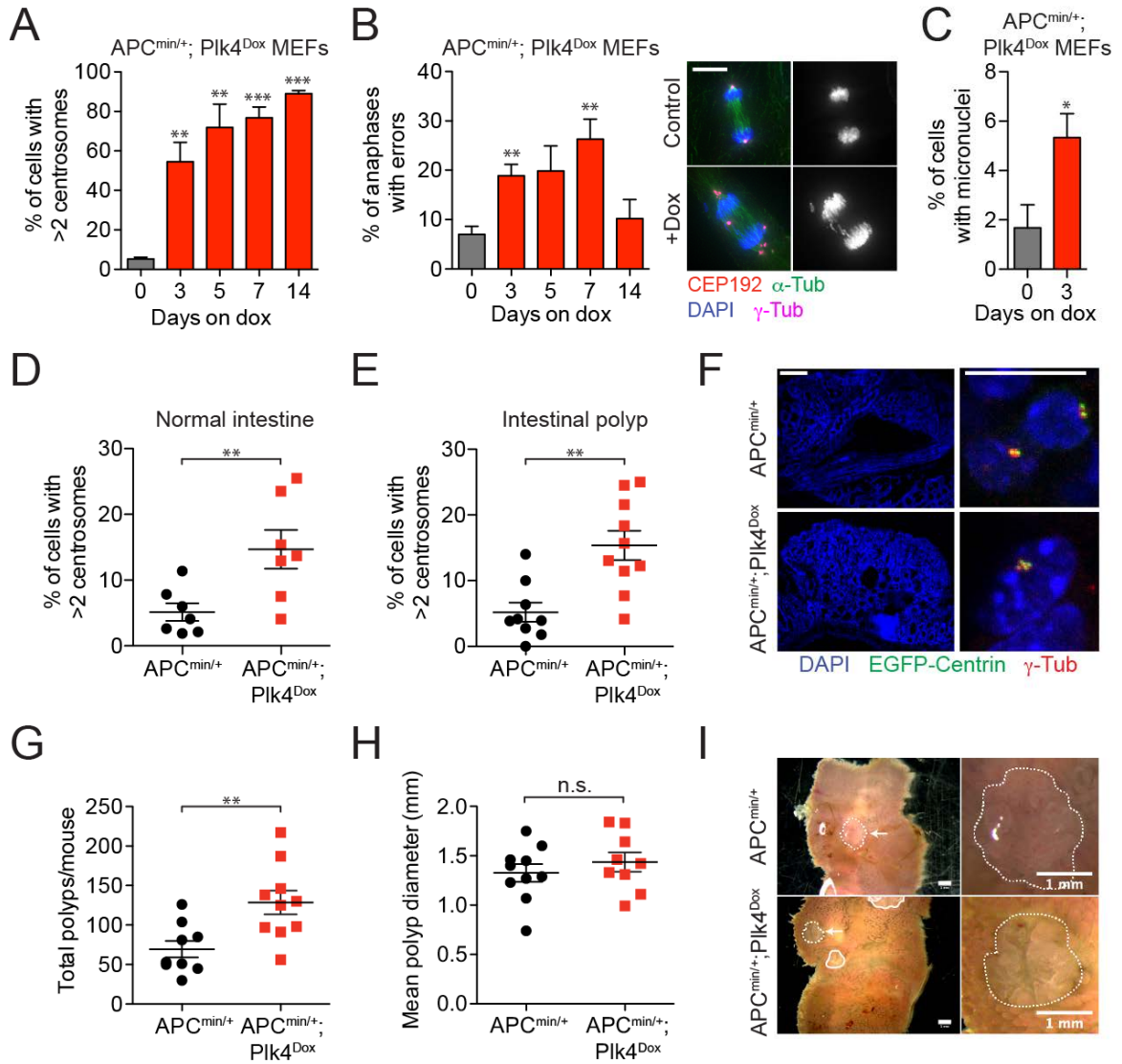


**Figure 10. Centrosome amplification promotes spontaneous tumorigenesis**

(A) Kaplan-Meier survival analysis of Plk4<sup>Dox</sup> and control (C57BL/6J) mice chronically fed doxycycline from 1-2 months of age. *P* value was calculated using the Log-rank test.

(B) Quantification of the level of centrosome amplification in tumors from Plk4<sup>Dox</sup> and p53<sup>-/-</sup> mice. Horizontal lines represent the mean and bars represent  $\pm$ SEM.

(C) Representative examples of the different tumor types that develop in doxycycline-treated Plk4<sup>Dox</sup> mice.

(D and E) GISTIC analysis of low-coverage whole-genome sequencing of Squamous Cell Carcinomas (SCCs) and lymphomas from doxycycline-treated Plk4<sup>Dox</sup> mice shows gains of specific chromosomes. Scale represents *Q* values.

(F) Low-coverage whole-genome sequencing (WGS) plots for a Sarcoma and a Squamous Cell Carcinoma derived from Plk4<sup>Dox</sup> mice.

(G) (Top) WGS plots from a T-Cell Lymphoma derived from doxycycline-treated Plk4<sup>Dox</sup> mice. (Bottom) Genome-wide copy number plots of aneuploid single cells sequenced from the same T-cell lymphoma. 12/39 sequenced cells showed evidence of aneuploidy. Individual cells are represented in rows with copy number indicated in colors.

(H) (Top) WGS plots from a B-Cell Lymphoma derived from doxycycline-treated Plk4<sup>Dox</sup> mice. (Bottom) Genome-wide copy number plots of aneuploid single cells from the same B-cell lymphoma. 32/47 sequenced cells showed evidence of aneuploidy.



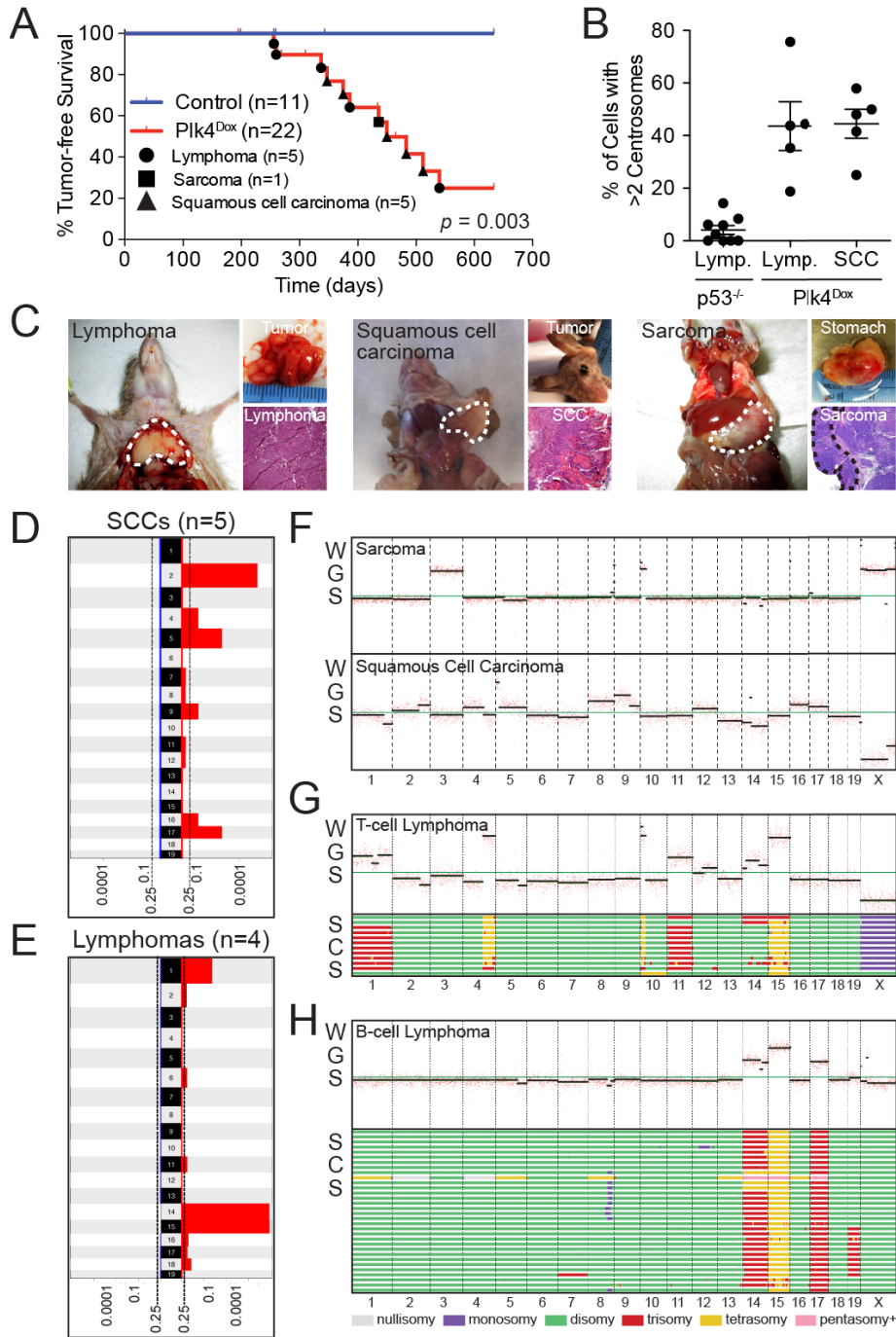


## Figure 11. Transient Plk4 overexpression triggers spontaneous tumor development

(A) Quantification of centrosome number in tumors that arise in Plk4<sup>Dox</sup> mice chronically fed doxycycline. Data are means  $\pm$ SEM. (N =  $\geq$ 4).

(B) Quantification of the fraction of cleaved caspase 3 positive cells in tumors from Plk4<sup>Dox</sup> and p53<sup>-/-</sup> mice. Data are means  $\pm$ SEM. (N =  $\leq$ 4, with each data point representing a single tumor).

(C) Graph showing the expression level of p53 target genes in tumors formed in Plk4<sup>Dox</sup> and p53<sup>-/-</sup> mice.

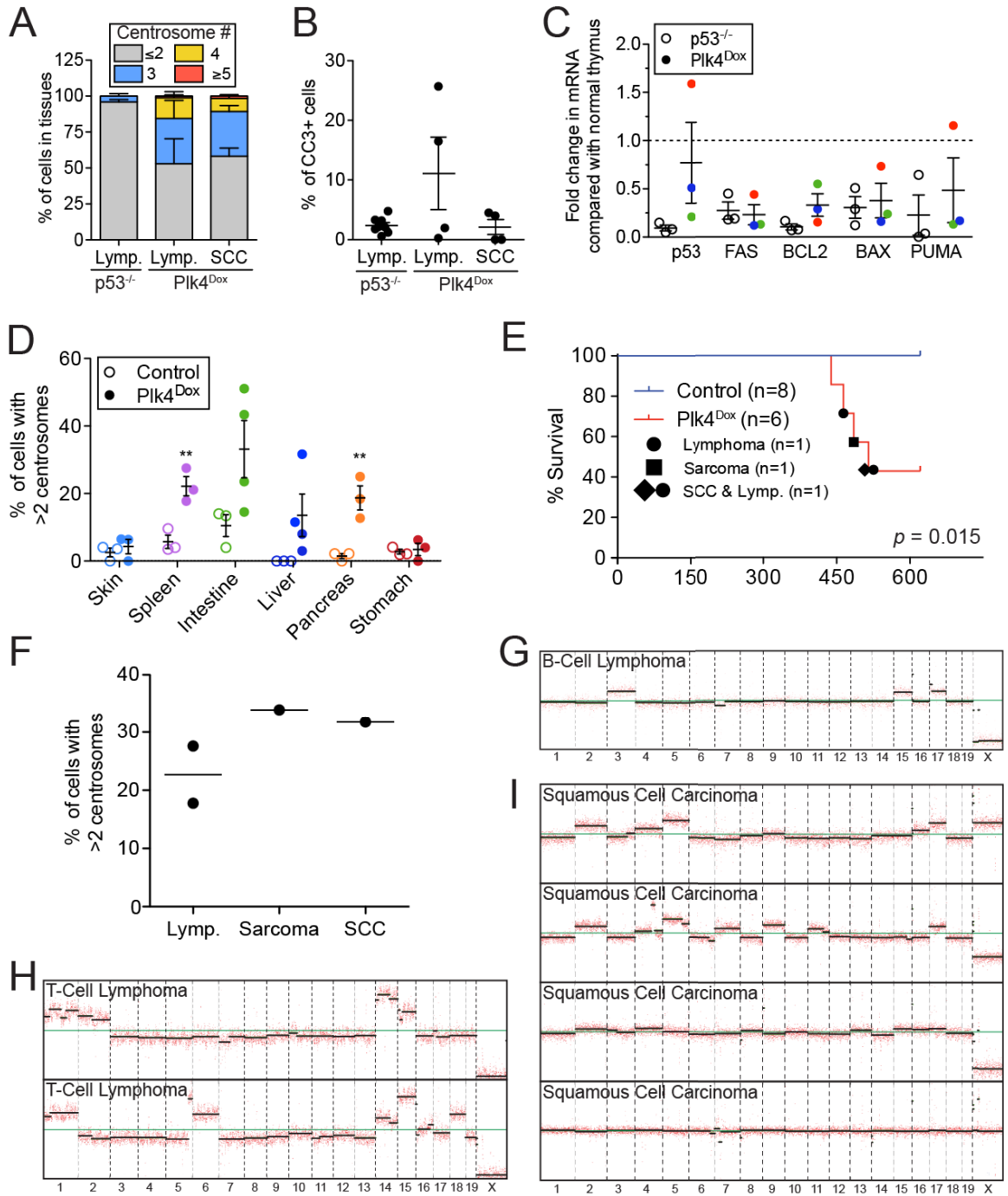
(D) Quantification of the level of centrosome amplification in tissues from 16-18 month old Plk4<sup>Dox</sup> mice treated with doxycycline for 1 month. Data are means  $\pm$ SEM (N =  $\geq$ 3).

(E) Kaplan-Meier survival analysis of Plk4<sup>Dox</sup> and control (C57BL/6J) mice fed dox at 1 month of age for one month. *P* value was calculated using the Log-rank test.

(F) Quantification of the level of centrosome amplification in tumors from Plk4<sup>Dox</sup> mice fed doxycycline for one month. Each point represents a single tumor and horizontal lines represent the mean.

(G) Low-coverage whole-genome sequencing (WGS) plots for a B-cell Lymphoma derived from Plk4<sup>Dox</sup> mice fed doxycycline for one month.

(H-I) Low-coverage whole-genome sequencing plots of two T-Cell Lymphomas and four Squamous Cell Carcinomas (SCC) from Plk4<sup>Dox</sup> mice chronically treated with dox.



## Chapter 3

# Deuterosomes are dispensable for multiciliogenesis

**In preparation:** Levine, MS,\* Mercey, O\*, Meunier, A and Holland, AJ.

**Data generated by Michelle Levine:** All, except data shown in Figure 14 and Figure 17 (generated by Olivier Mercey, Meunier laboratory, Ecole Normale Supérieure)

### 3.1 Creation of a *Deup1*<sup>-/-</sup> mouse

To examine the role of the deuterosome in multiciliogenesis, a *Deup1* knockout mouse was created by replacing exons 2-7 of the *Deup1* gene with a LacZ reporter followed by a polyA sequence (Figure 12A). To observe the process of multiciliogenesis *ex vivo*, we utilized two different cell culture systems: mouse tracheal epithelial cells (mTECs) and ependymal cells. Cells are isolated from the adult trachea or newborn mouse brains and grown to confluence then serum-starved, and in the case of mTECs, exposed to an air-

liquid interface (ALI), which induces differentiation (You and Brody 2013; Delgehyr et al. 2015). These systems mimic the *in vivo* process that occurs late in embryonic development in the trachea and in the brains of developing mouse pups (Stockinger and Cireli 1965; Spassky et al. 2005). To evaluate whether *Deup1* expression was abolished, *Deup1* mRNA expression levels were measured by qPCR. In the brain, tracheal epithelial cells, and testis, *Deup1* mRNA levels were reduced by > 40 fold in the *Deup1* knockout compared to control mice (Figure 12B, 12C and Figure 13A). Furthermore, at ALI d3 we observed several *Deup1* foci form in control cells, but no signal was detectable in the *Deup1*<sup>-/-</sup> mTECs (Figure 13B).

As expected, full-length DEUP1 protein was undetectable in multiciliating *Deup1*<sup>-/-</sup> mouse tracheal epithelial cells and ependymal cells via immunoblot (Figure 12D). It is plausible that a DEUP1 protein fragment could be expressed from an in-frame ATG present near the start of exon 8 in our *Deup1*<sup>-/-</sup> animals. To confirm that the absence of detectable protein was not due to an inability of our antibody to detect this DEUP1 protein fragment, we created DLD-1 cell lines that could inducibly express either full-length DEUP1 or HEK293FT cells that overexpress full-length DEUP1 or exons 8-12 of DEUP1 fused to a C-terminal Myc tag. Our DEUP1 antibody detected both full-length *Deup1* and the DEUP1 exons 8-12 protein fragment (Figure 13C-D). Given that neither

protein species were detectable in lysates from *Deup1*<sup>-/-</sup> mouse tracheal epithelial cells, we conclude that *Deup1*<sup>-/-</sup> mice are complete knockouts for the DEUP1 protein.

### **3.2 *Deup1*<sup>-/-</sup> mice lack deuterosomes**

To determine whether *Deup1*<sup>-/-</sup> MCCs lacked deuterosomes, we used serial transmission electron microscopy (sTEM) through the volume of wild-type and *Deup1*<sup>-/-</sup> ependymal cells. While deuterosomes were clearly observed in the control ependymal cells, *Deup1*<sup>-/-</sup> ependymal cells did not contain deuterosomes (Figure 14A and 14B). These data confirm the previous findings that DEUP1 is the main structural component of the deuterosome (Zhao et al., 2013).

### **3.3 Deuterosomes are dispensable for multiciliogenesis**

To establish the requirement of deuterosomes for centriole amplification in MCCs, we examined centriole number in MCCs from *Deup1*<sup>-/-</sup> mice compared with controls. Ependymal cells from control mice create on average 250 ±71.58 centrioles and similarly *Deup1*<sup>-/-</sup> ependymal cells create 250 ±82 centrioles (Figure 15A and 15B). Furthermore, control mTECs create a mean of 82 ±14 centrioles, while *Deup1*<sup>-/-</sup> create 75 ±16 centrioles (Figure 15C and 15D). To confirm these findings *in vivo*, we quantified centrioles in multiciliated ependymal cells in the brains of mice. Consistent with our

results *in vitro*, there was no difference in the number of centrioles generated in ependymal cells in the brain of control and *Deup1*<sup>-/-</sup> mice (Figure 15E and 15F). Furthermore, scanning electron microscopy of mouse trachea revealed no obvious differences in cilia number or morphology in *Deup1*<sup>-/-</sup> animals compared with control (Figure 16). Together, these data show that deuterosomes are not required for generating the correct number of basal bodies in multiciliated cells.

To characterize how centriole amplification occurs in the absence of deuterosomes, we followed differentiating ependymal cells using live cell imaging. In normal centriole amplification in MCCs, centrioles can be observed amplifying in large clusters indicating nucleation from deuterosome structures as well as procentriole formation from being born off the sides of the preexisting centrioles (data not shown). Using transgenic mice expressing a GFP-tagged version of the centriole protein Centrin 2, we observed that centrioles are amplifying as singlets and doublets (Figure 17). In addition, at disengagement, many more procentrioles detach from the preexisting centriolar space than would allow, based on the circumference of the preexisting centrioles. This suggests that procentrioles are created on and in proximity to the preexisting centrioles (Figure 17). These observations as well as the sTEM data (Figure 14) suggest that centrioles are

created on, and in proximity to, the parental centrioles in a differentiating cell without deuterosomes.

### **3.4 Cep63 does not compensate for Deup1 loss**

*Deup1* and *Cep63* are paralogs that are 37% identical at the amino acid level (Zhao et al. 2013). It is therefore possible that the loss of DEUP1 is compensated for, in part, by CEP63. To address this, we obtained *Cep63<sup>TT</sup>* mice that have the *Cep63* gene disrupted with a gene-trap insertion (Brown et al. 2013; Marjanovic et al. 2015). As expected, *Cep63<sup>TT</sup>* mice showed a > 20 fold reduction in *Cep63* mRNA levels in both mouse testes and mTECs (Figure 19A and 19B). Loss of *Cep63* expression by itself did not alter centriole or cilia number in mTECs or ependymal cells in culture or *in vivo* (Figure 18A-F). Furthermore, knockout of both *Cep63* and *Deup1* did not reduce centriole numbers in these cells, indicating that *Cep63* does not compensate for *Deup1* loss (Figure 18A-F and Figure 19C). In addition, *Deup1<sup>-/-</sup>* mTECs did not show increased levels of *Cep63* further confirming that *Cep63* does not compensate for *Deup1* loss (Figure 19D).



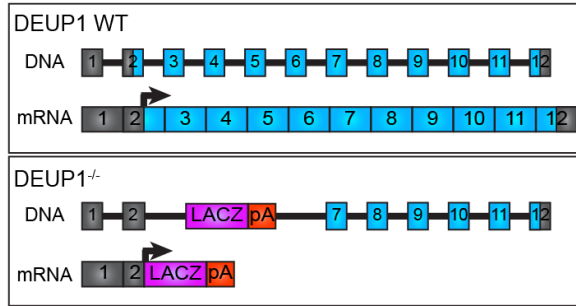
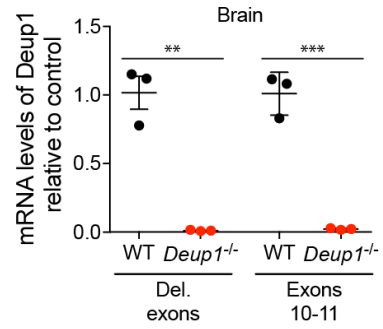
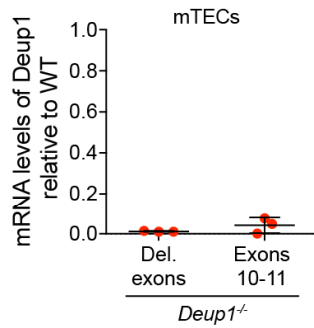
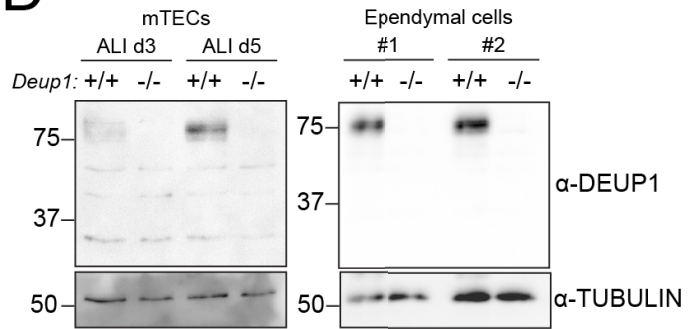
**Figure 12. *Deup1* knockout mice do not express *Deup1* mRNA or DEUP1 protein.**

(A) Schematic representation of the *Deup1* gene and mRNA structures (top) and the portion deleted in the *Deup1*<sup>-/-</sup> mouse (bottom).

(B) qPCR analysis of *Deup1* mRNA levels in control and *Deup1*<sup>-/-</sup> post-natal day 5 brain tissue using two different primer sets corresponding to the *Deup1* transcript. Deleted (Del.) exons denote primers designed to amplify exons 2-3, and act as a negative control.

(C) qPCR analysis of *Deup1*<sup>-/-</sup> mouse tracheal epithelial cells (mTECs). Control mTEC levels of *Deup1* were normalized to 1, and the values shown are relative to control.

(D) Western blot of lysates from mTECs differentiated at air-liquid interface (ALI) for 3 and 5 days, and two different ependymal cell cultures differentiated for 8 days. An antibody raised against full-length *Deup1* was used to determine expression of *Deup1* in knockouts (-/-) compared to controls (+/+).  $\alpha$ -Tubulin was used as a normalization control.

**A****B****C****D**

**Figure 13. DEUP1 antibodies can recognize protein produced from full-length and exons 8-12 of *Deup1*.**

(A) qPCR analysis of *Deup1* gene expression in control and *Deup1*<sup>-/-</sup> mouse testes using 3 different primer sets.

(B) Immunofluorescent images of control and *Deup1*<sup>-/-</sup> mTECs at ALI d3 showing multiciliating cells that lack *Deup1* signal in knockouts compared with multiple *Deup1* foci in controls.

(C) An isogenic DLD-1 cell line was created with an integrated copy of *mus musculus* *Deup1* cDNA with a C-terminal myc tag under the control of a doxycycline (dox)-inducible promoter. Immunoblot of protein lysates using an antibody recognizing *Deup1* or myc. Arrow denotes band of interest. Astrisk denotes endogenous myc in these cell lines.

(D) Immunoblot of HEK293 cells expressing either full-length (F.L.) or exons 8-12 (Ex 8-12) of DEUP1 with or without the proteasome inhibitor, MG132. Membranes were probed with antibodies against *Deup1* or Myc.  $\alpha$ -tubulin was used as a loading control.

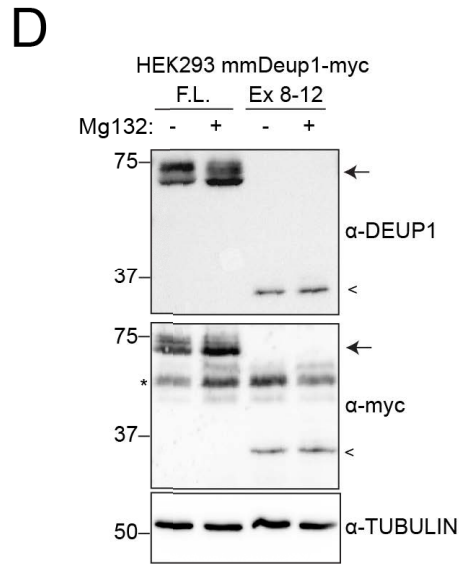
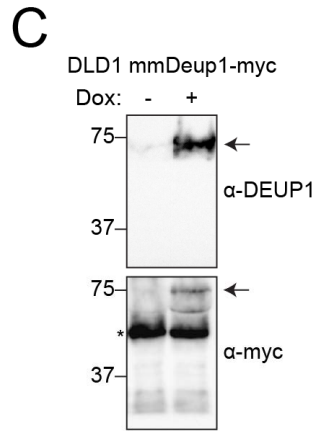
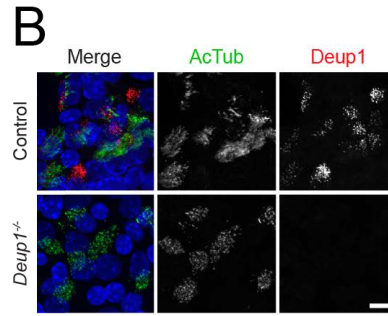
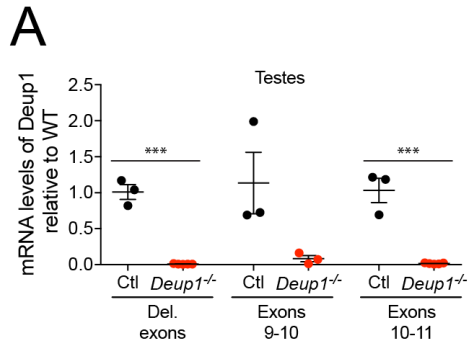


**Figure 14. *Deup1* knockout mice do not contain deuterosomes.**

(A) Serial transmission electron microscopy through the volume of a *Deup1* knockout cell reveals that centriole amplification occurs in the absence of deuterosomes, and instead occurs on or proximal to the preexisting centrioles.

(B) Schematic representing the location of the procentrioles relative to the preexisting centrioles (green and orange).

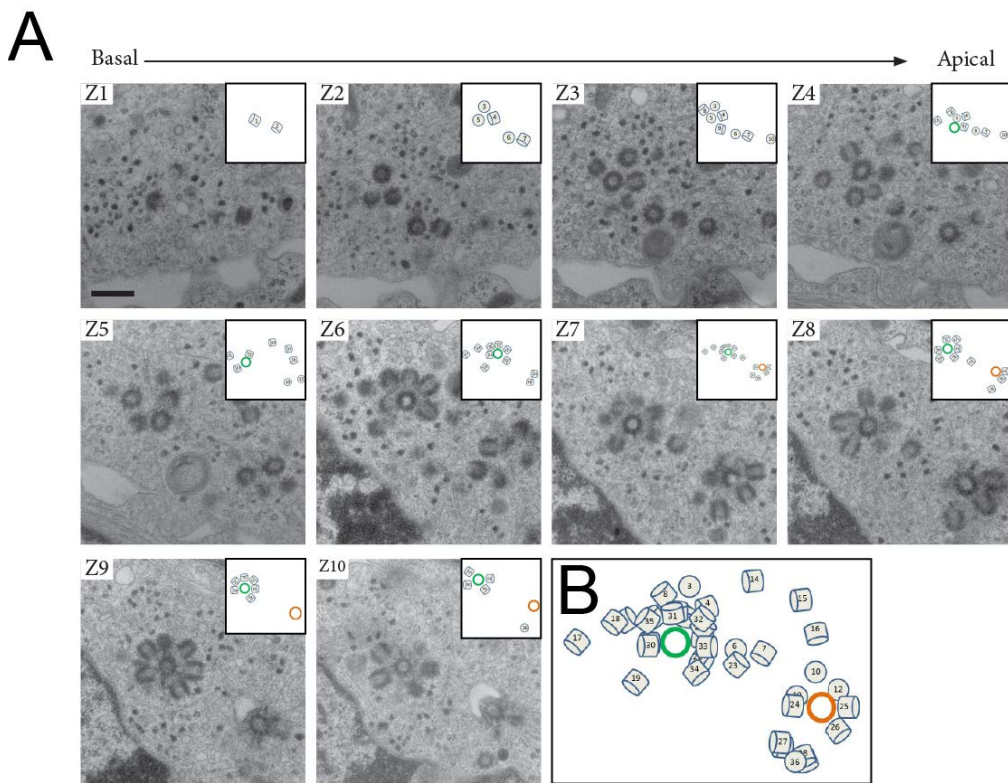


**Figure 15. Deuterosomes are not required for proper centriole number.**

(A) Quantification of basal body number in control or Deup1<sup>-/-</sup> ependymal cells. n=3 mice/genotype; >40 cells/mouse

(B) Representative images of mature centrioles using an antibody against Cep164 in control or Deup1<sup>-/-</sup> ependymal cells.

(C) Quantification of basal body number in control or Deup1<sup>-/-</sup> mouse tracheal epithelial cells (mTECs). n=3 mice/genotype; >40 cells/mouse

(D) Representative images of centrioles using an antibody against Cep164.

(E) Quantification of centriole number in brain sections of control or Deup1<sup>-/-</sup> mice. n=3 mice/genotype; >40 cells/mouse.

(F) Representative images of ependymal cells in brain sections from control or Deup1<sup>-/-</sup> mice. DAPI marks the nuclei, ZO-1 is a tight junction marker and Cep164 stains mature centrioles.

Scale bar represents 10µm. n.s.=not statistically significant (p>0.05)

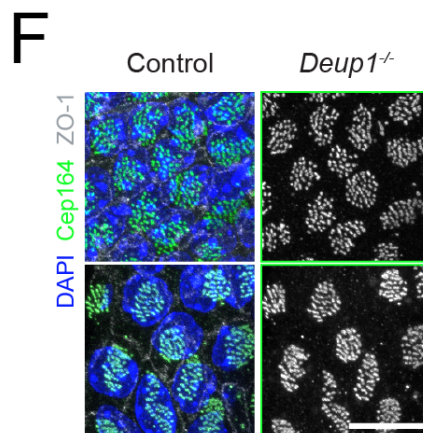
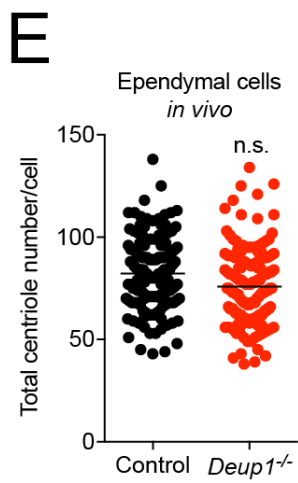
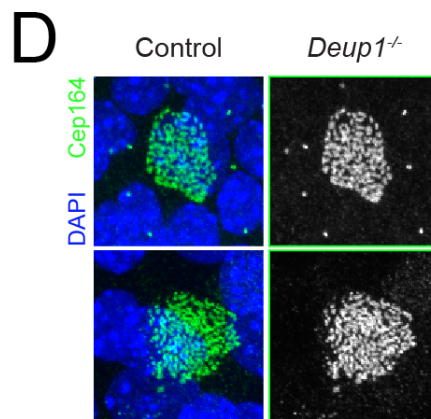
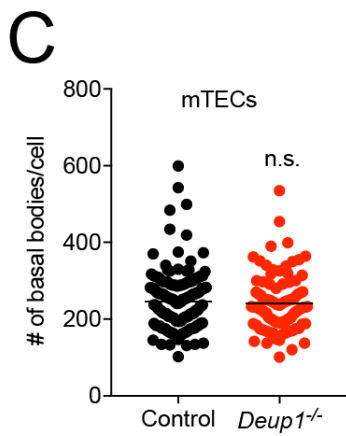
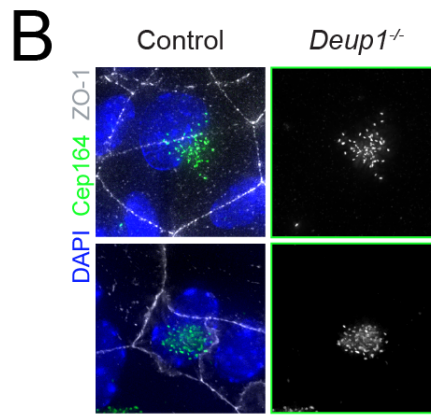
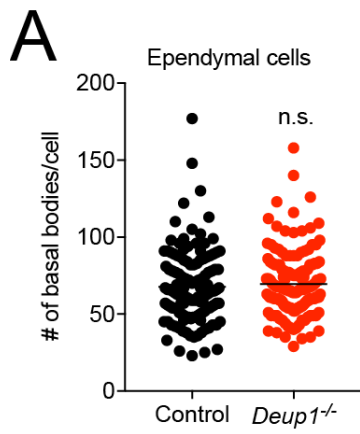


**Figure 16. Deuterosomes are not required for multiciliogenesis *in vivo***

Scanning electron microscopy (SEM) images of tracheas from control or *Deup1<sup>-/-</sup>* mice.

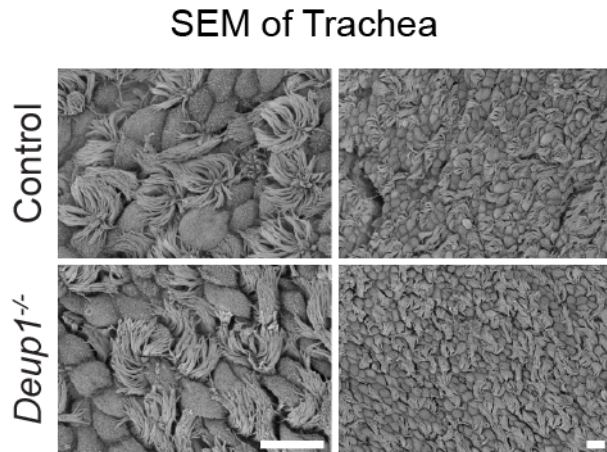




**Figure 17. Live-imaging of differentiating  $Deup1^{-/-}$  ependymal cells reveals deuterosome-independent centriole amplification.**

Still images from a time-lapse movie using a Centrin-GFP transgenic mouse, in a  $Deup1^{-/-}$  background, in order to track centriole biogenesis. Control movies show centrioles budding from the preexisting centrioles (data not shown). Centrin foci appear large and bright as they cluster around deuterosomes. Individual centrioles are hard to resolve when they are on the deuterosome, but during the disengagement stage individual centrioles can be seen detaching from deuterosomes. In the  $Deup1^{-/-}$  mouse (shown), centrioles form in singlets and doublets and never localize in large clusters, as they would if a deuterosome were present. Tens of centrioles disengage from the preexisting parental centrioles (green arrowheads), and join the singlets and doublets in the cytoplasm.

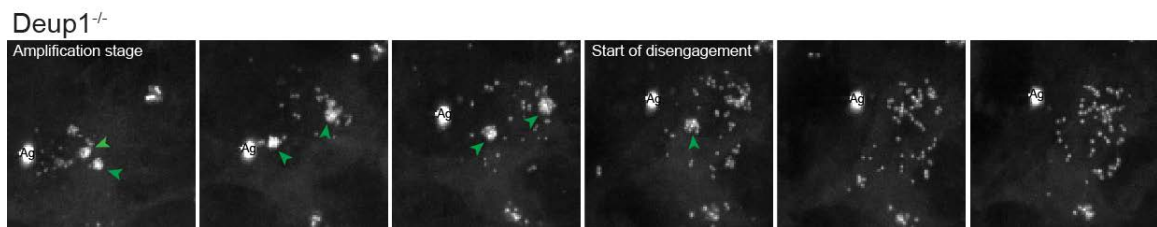


**Figure 18. Cep63 does not compensate for Deup1 loss.**

(A) Quantification of basal bodies in ependymal cells grown *in vitro* from *Cep63<sup>T/T</sup>*, *Deup1<sup>-/-</sup>*, *Deup1<sup>-/-</sup>;Cep63<sup>T/T</sup>* and control mice. Data from *Deup1<sup>-/-</sup>* mice is also shown in Figure 2. n=3 mice/genotype; >40 cells/mouse.

(B) Representative images of centrioles (Cep164) and tight junctions (ZO-1) from *Cep63<sup>T/T</sup>*, *Deup1<sup>-/-</sup>;Cep63<sup>T/T</sup>* or control mTECs.

(C) Quantification of basal bodies in mTECs from *Cep63<sup>T/T</sup>*, *Deup1<sup>-/-</sup>*, *Deup1<sup>-/-</sup>;Cep63<sup>T/T</sup>* and control mice. Data from *Deup1<sup>-/-</sup>* mice is also shown in Figure 2. n=3 mice/genotype; >40 cells/mouse.

(D) Representative images of mature centrioles and tight junctions using antibodies against acetylated-tubulin (AcTub) and ZO-1 from *Cep63<sup>T/T</sup>*, *Deup1<sup>-/-</sup>;Cep63<sup>T/T</sup>* or control mTECs. CEP164 marks the distal appendages on membrane docked basal bodies at the base of cilia.

(E) Quantification of centrioles in ependymal cells *in vivo* from *Cep63<sup>T/T</sup>*, *Deup1<sup>-/-</sup>*, *Deup1<sup>-/-</sup>;Cep63<sup>T/T</sup>* and control mice. Data from *Deup1<sup>-/-</sup>* mice is also shown in Figure 2. n=3 mice/genotype; >40 cells/mouse. (F) Representative images of centrioles (Cep164) in brain ependymal cells *in vivo*.

Scale bar represents 10µm. n.s.=not statistically significant (p>0.05)

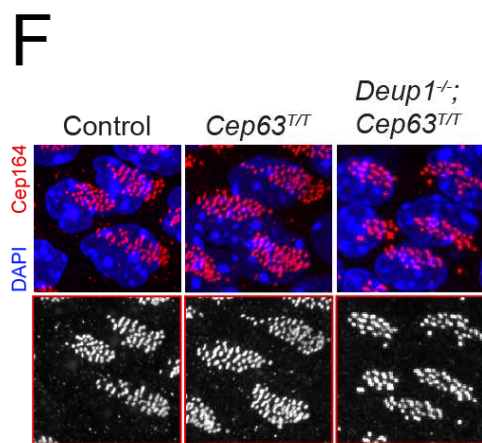
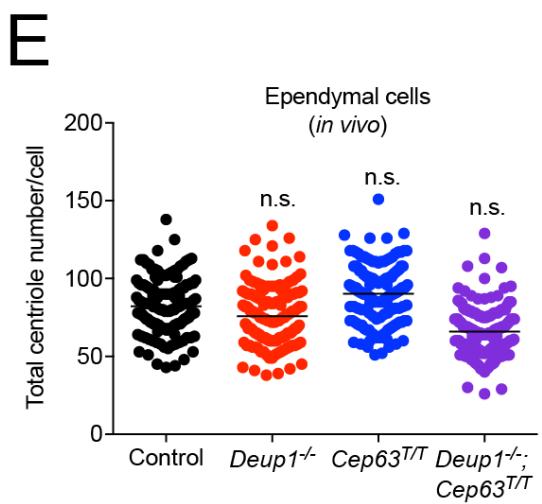
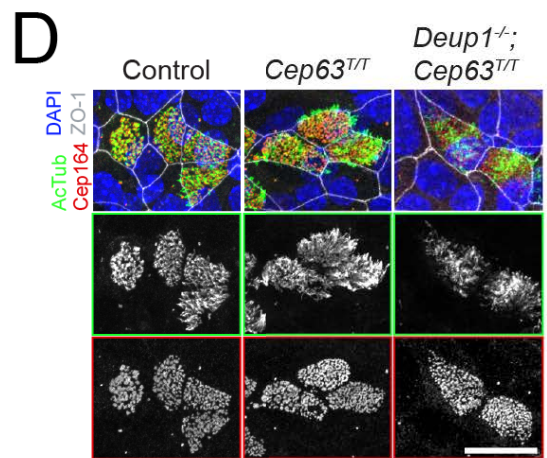
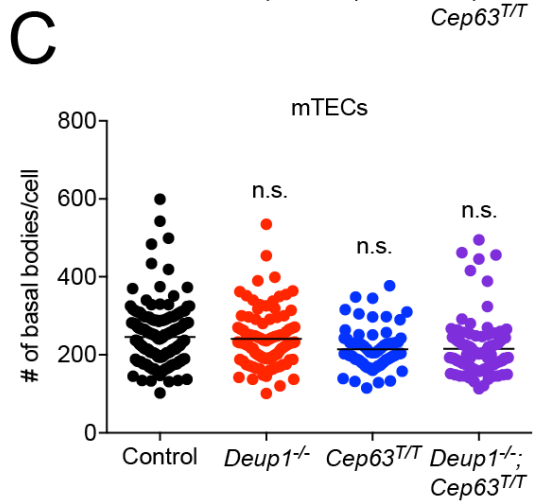
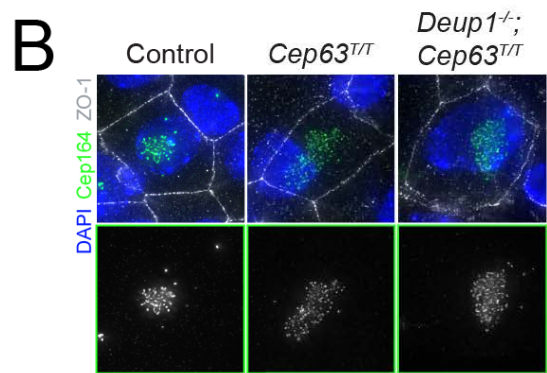
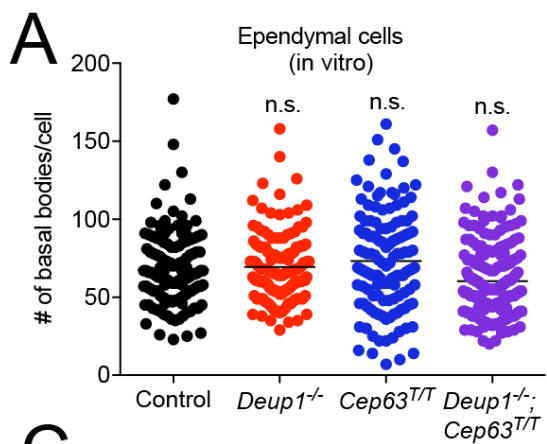


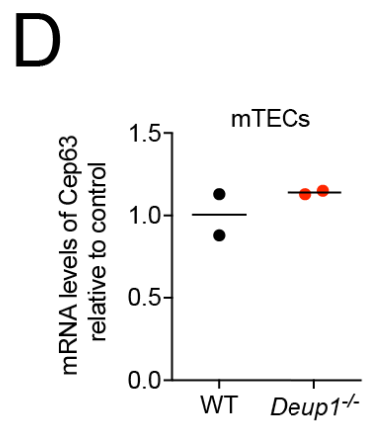
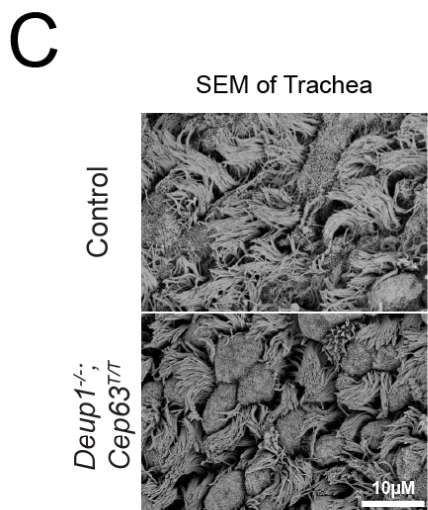
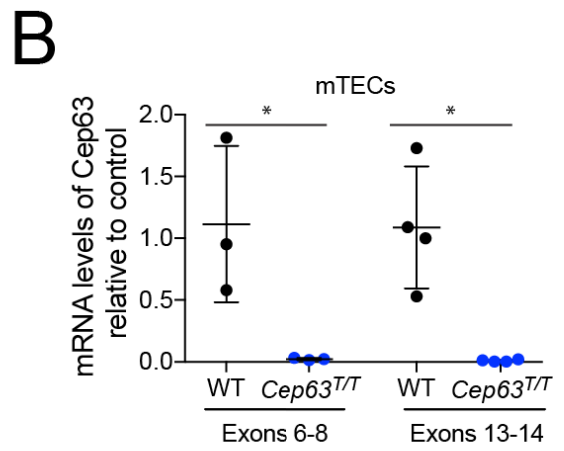
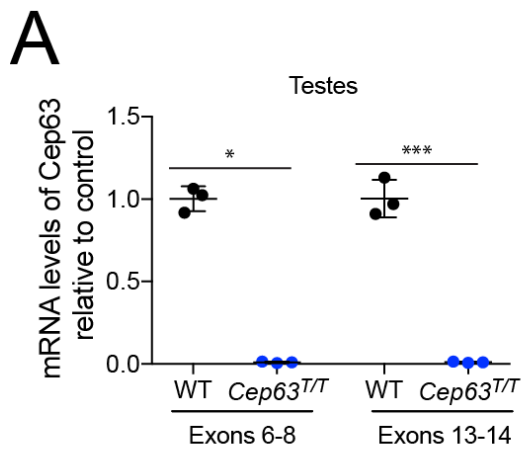
**Figure 19. Cep63 knockout animals and Deup1; Cep63 double-knockout animals do not exhibit defects in multiciliogenesis *in vitro* or *in vivo*.**

(A) qPCR analysis of *Cep63* expression levels in the testes of control and *Cep63*<sup>T/T</sup> mice. Analysis was performed with two different primer sets corresponding to mmCep63 mRNA.

(B) qPCR analysis of *Cep63* expression levels in mouse tracheal epithelial cells (mTECs) from control and *Cep63*<sup>T/T</sup> mice. Analysis was performed with two different primer sets corresponding to mmCep63 mRNA.

(C) Scanning electron micrographs (SEM) of trachea from control or *Deup1*<sup>-/-</sup>;*Cep63*<sup>T/T</sup> animals.

(D) qPCR analysis of *Cep63* expression levels in control and *Deup1*<sup>-/-</sup> mice. *Cep63* is not elevated in *Deup1*<sup>-/-</sup> mice.



## Chapter 4

# The Role of Extra Centrioles in Kidney Cystogenesis

**Data generated by Michelle Levine:** All data; ischemia-reperfusion injury surgery was performed by Dr. Sul Lee (Rabb laboratory, JHUSOM)

### 4.1 A mouse model to create extra centrosomes in the kidney

To test whether extra centrioles are sufficient to promote kidney cystogenesis, we overexpressed Plk4 specifically in the mouse kidney. We crossed our doxycycline-inducible Plk4 overexpression mouse to a Pax8 promoter-driven reverse tetracycline transactivator (rtTA) mouse, which drives expression in the renal tubule epithelial cells (Traykova-Brauch et al. 2008; Levine et al. 2017). These mice are hereafter referred to as Plk4<sup>Dox</sup>. First, to observe whether the Pax8-rtTA could drive expression of the Plk4 transgene at the Col1A1 locus, we crossed the Pax8-rtTA mice to a mCherry-H2B reporter mouse (Egli et al. 2007). We dosed mice throughout gestation with doxycycline,

and analyzed 1 week old mouse kidneys. Pax8-rtTA drives robust expression in the kidney as evidenced by red fluorescent nuclei throughout the kidney of Plk4<sup>Dox</sup> mice (Figure 20A).

## **4.2 Plk4 overexpression induces centrosome amplification but does not alter cilia number**

To determine the degree of centrosome amplification in the kidney, we examined cohorts of mice at E15.5, 1 week, 4 weeks, and 14 weeks of age. Robust centrosome amplification was observed at all time points examined, with an increasing trend over time (Figure 20B and 20C). To confirm that extra centrioles did not disrupt normal kidney development or homeostasis, we measured cell proliferation and death in these tissues. None of the Plk4<sup>Dox</sup> animals analyzed exhibited statistically significant differences in cell proliferation or cell death compared with controls (Figure 20D and 20E). The only phenotype observed was that 1 week old Plk4<sup>Dox</sup> kidneys were slightly smaller than controls, but the 4 week and 14 week old Plk4<sup>Dox</sup> kidneys no longer exhibit this effect. Furthermore, histology and weights of 14 week old kidneys revealed that Plk4<sup>Dox</sup> kidneys were indistinguishable from controls (Figure 21A-C). To understand whether extra centrosomes alter cilia number, we co-stained kidneys with centrosome and

cilia markers and quantified numbers of both structures. Despite increases in the number of extra centrosomes, cilia number remained unchanged (Figure 20F and 20G).

### **4.3 Extra centrosomes are not sufficient to promote kidney cystogenesis**

To address the role of extra centrosomes in the pathogenesis of polycystic kidney disease, we evaluated the impact of centrosome amplification on kidney cystogenesis. We aged a cohort of control and Plk4<sup>Dox</sup> animals, which had been dosed on dox throughout gestation and adulthood. Overall survival was unaffected in Plk4<sup>Dox</sup> animals, and they never developed cystic kidneys, showing that extra centrosomes are not sufficient to promote cystogenesis (Figure 22A-C). Previous work has shown that acute renal injury can promote cystogenesis (Kurbegovic and Trudel 2016). In collaboration with the Rabb laboratory (JHMI), we then asked whether extra centrosomes could cooperate with an injury model to promote increased cystogenesis. We used a unilateral ischemia-reperfusion injury system, in which 1 kidney was deprived of blood for 30 minutes, then the blood was allowed to perfuse back into the kidney and animals were sacrificed 6 weeks later for analysis (Figure 23A). While injured kidney weights were increased in Plk4<sup>Dox</sup> animals compared with controls, we did not observe increased cystogenesis



(Figure 23B-D). Taken together, extra centrosomes are neither sufficient nor cooperate with injury to promote cystogenesis.

**Figure 20. Centrosome amplification does not alter cilia number, cell death or proliferation in mouse kidneys.**

(A) Representative images from p7 kidneys of reporter mice, in which tet-on mCherry-H2B expression was induced by a Pax8 promoter-driven rtTA. Mice were dosed with doxycycline throughout gestation.

(B) Quantification of the level of centrosome amplification in Plk4<sup>Dox</sup> mouse kidneys compared with controls at multiple ages. 50 cells/mouse; n=3 mice/condition/age

(C) Representative images of mouse kidney tissue sections used for quantification, stained with the centrosome marker  $\gamma$ -Tubulin and the nuclear stain DAPI.

(D) Quantification of the fraction of Ki67+ cells per field of view.

(E) Quantification of the fraction of Cleaved Caspase 3+ cells per field of view.

(F) Quantification of cilia number in cells with normal and supernumerary centrosomes.

(G) Representative images of cilia in mouse kidneys stained with Acetylated tubulin (AcTub) to mark cilia,  $\gamma$ -Tubulin for centrosomes, and DAPI.

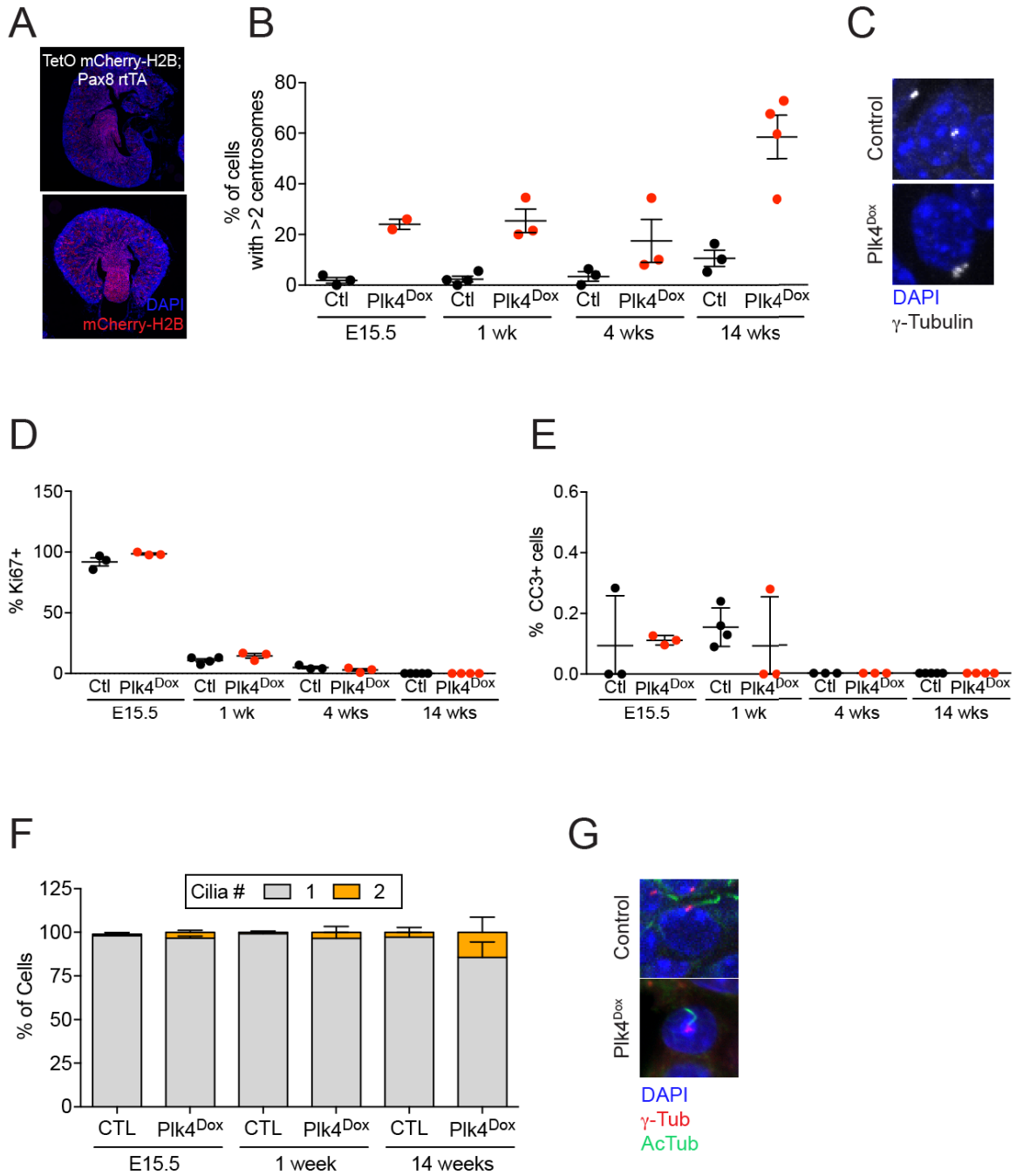


**Figure 21. Centrosome amplification in adult animals does not affect kidney histology or size**

(A) Representative Hematoxylin & Eosin stained images of kidneys from 14-week old animals.

(B) Average kidney weight/body weight ratios for control and Plk4<sup>Dox</sup> animals at different time points.

(C) Representative images of fixed kidneys used for weighing in (B).

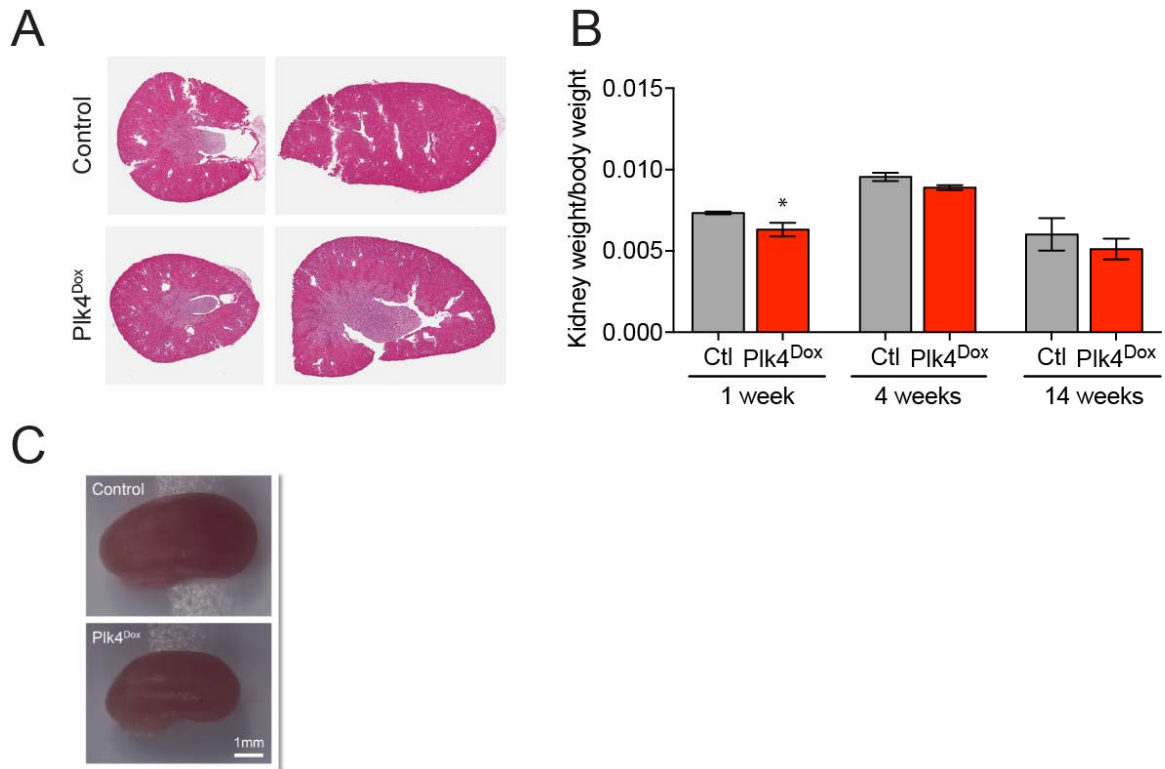


**Figure 22. Centrosome amplification is not sufficient to promote cystogenesis**

(A) Overall survival of aged cohort of control and Plk4<sup>Dox</sup> mice.

(B) Representative H&E images showing lack of cysts in control and Plk4<sup>Dox</sup> mice.

(C) Average kidney weight to body weight ratios for aged cohort.

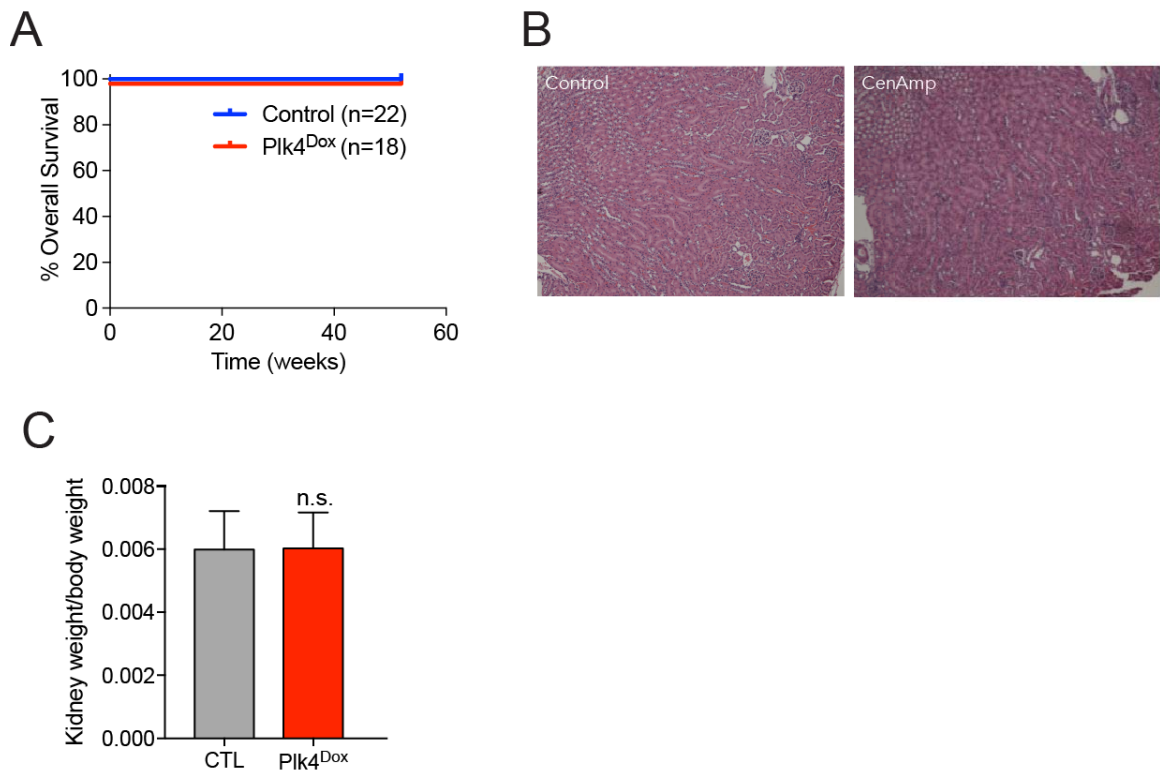


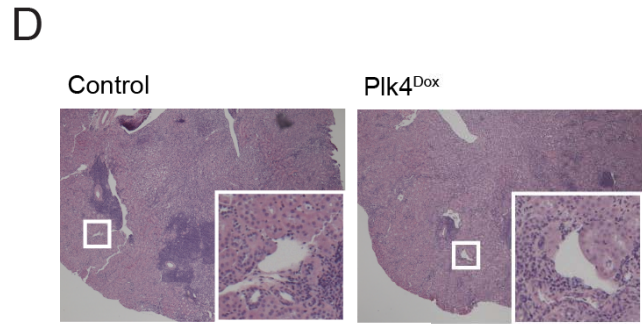
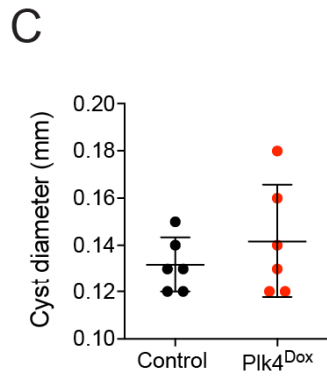
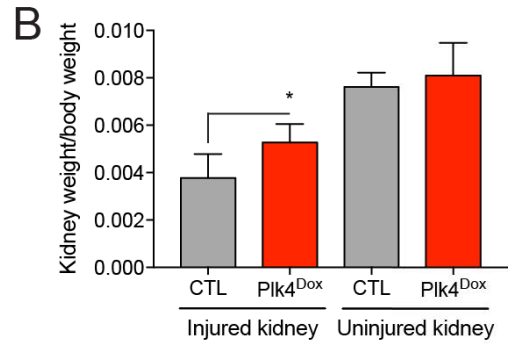
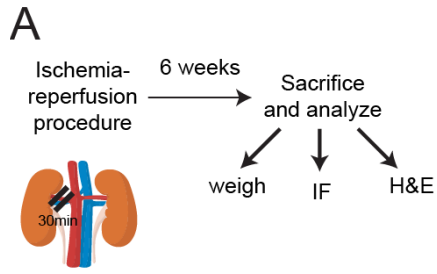
**Figure 23. Centrosome amplification does not cooperate with injury to promote kidney cystogenesis**

(A) Schematic of ischemia-reperfusion injury model system. Blood supply was clamped off to the kidney for 30 minutes then removed. Mice were euthanized 6 weeks later and kidneys were analyzed by weight, immunofluorescence (IF) microscopy, and hematoxylin & eosin (H&E) staining.

(B) Average kidney weight/body weight ratios for injured and uninjured kidneys of control and Plk4<sup>Dox</sup> animals.

(C) Quantification of cyst diameters in control and Plk4<sup>Dox</sup> animals.

(D) Representative images of H&E stained kidneys from control and Plk4<sup>Dox</sup> mice. White box indicates area zoomed in on for the inset image.



# Chapter 5

## Discussion

### **5.1 Centrosome amplification is sufficient to promote tumorigenesis**

A causal association between centrosome amplification and tumorigenesis was originally proposed by Boveri over a century ago, but has yet to be firmly established (Boveri 1914). Here, we have examined the long-term consequence of supernumerary centrosomes in mice. We demonstrate that centrosome amplification can increase tumor initiation events in a mouse model of intestinal cancer. Most importantly, we show that extra centrosomes cause aneuploidy and trigger spontaneous tumorigenesis in multiple tissues. We conclude that centrosome amplification is sufficient to promote tumorigenesis in mammals.

In our experiments, we used Plk4 overexpression as a tool to drive centrosome



amplification *in vivo*. While roles of Plk4 outside of centrosome biogenesis have been proposed (Martindill et al. 2007; Rosario et al. 2010; Rosario et al. 2015), multiple lines of evidence argue that centrosome amplification is responsible for triggering spontaneous tumorigenesis in mice that overexpress Plk4. First, modest increases in Plk4 protein are sufficient to promote persistent centrosome amplification and spontaneous tumor development. Second, centrosome number is elevated in all three tissues that exhibit a predisposition to tumor development; conversely, tissues with high levels of Plk4 expression, but no increase in centrosome amplification, do not show an increase in tumorigenesis. Third, tumors that develop in Plk4-overexpressing mice generally show higher levels of centrosome amplification than in the normal tissue from which they developed. Finally, even a transient increase in Plk4 promotes persistent centrosome amplification and tumorigenesis. Therefore, although we cannot formally exclude that the effects we observe reflect roles of Plk4 outside of centrosome duplication, our evidence firmly argues that increases in centrosome number drive the effects we observe *in vivo*.

To our knowledge, our study provides the first demonstration that centrosome amplification is sufficient to drive aneuploidy in tissues with wildtype p53. However, the role of centrosomes are not restricted to mitosis and extra copies of centrosomes have been shown to disrupt cilia signaling (Mahjoub and Stearns 2012) and promote

alterations in the interphase cytoskeleton that could facilitate invasion (Godinho et al. 2014). *Since* hematopoietic lineages lack primary cilia, alterations in ciliary signaling are unlikely to underlie lymphomagenesis in cells with supernumerary centrosomes (Finetti et al. 2011). Instead, our study demonstrates that tumors with extra centrosomes exhibit recurrent aneuploidies. In addition, we show that centrosome amplification increases tumor initiation in the APC<sup>Min/+</sup> mouse model. Since tumors in this model are proposed to be driven by loss of the wildtype allele of APC, we propose that centrosome amplification increases tumor initiation by facilitating the loss of the copy of chromosome 18 containing the wildtype APC allele (Luongo et al. 1994). Therefore, while further studies will be required to determine the precise mechanism by which extra centrosomes promote tumorigenesis, our data is consistent with a model in which centrosome amplification drives aneuploidy that promotes tumor development.

A central question that arises is why have other studies that employed Plk4 overexpression not reported spontaneous tumorigenesis (Marthiens et al. 2013; Coelho et al. 2015; Kulukian et al. 2015; Vitre et al. 2015; Sercin et al. 2016)? A key difference in the mouse model that we report here is that we use a single copy Plk4 transgene knocked into the Col1a1 locus to achieve a modest increase in Plk4 levels that typically leads to the creation of just one or two extra centrosomes per cell. This is similar to the extent of

centrosome amplification observed in human tumors (Kayser et al. 2005; Denu et al. 2016). We propose that small increases in centrosome number are permissive for tumor development. By contrast, large numbers of extra centrosomes are likely to be detrimental to cell viability because they are clustered inefficiently prior to division and lead to an increase in the frequency of lethal multipolar divisions. Mouse models that are created by the random integration of Cre-inducible, Plk4 transgenes may express the kinase at higher levels than achieved in our animal model (Kulukian et al. 2015; Vitre et al. 2015; Sercin et al. 2016). We predict that high levels of Plk4 overexpression, and thus larger increases in the number of centrosomes per cell, will be detrimental to long-term cell survival. This could explain silencing of Plk4 transgene expression that has been reported in the skin of one mouse model (Sercin et al. 2016), and also why global overexpression of Plk4 in another mouse model did not achieve centrosome amplification in the majority of tissues without the removal of p53 (Vitre et al. 2015). Finally, we note that a previous study that drove Plk4 overexpression using a single-copy transgene at the ROSA26 locus did not follow survival to the point at which we observe the development of spontaneous tumors in mice with centrosome amplification (Coelho et al. 2015).

In summary, we demonstrate that mice with extra centrosomes develop spontaneous tumors with high levels of genomic instability. We conclude that extra centrosomes are

not bystanders in tumor development, but actively promote tumorigenesis by provoking mitotic errors that facilitate the evolution of malignant karyotypes. These findings support the therapeutic targeting of cells with extra centrosomes in human tumors.

## **5.2 Deuterosomes are dispensable for multiciliogenesis**

Using a *Deup1*<sup>-/-</sup> mouse, we demonstrated that multiciliated cells do not require the deuterosome to amplify the correct number of basal bodies, contrary to what had been long proposed. Therefore, the dispensability of the deuterosome for producing proper numbers of centrioles in differentiating MCCs begs the question: what is the purpose of a deuterosome? One possibility is to allow the centriole amplification process to occur rapidly. Since *Deup1* arose in organisms transitioning to land, it is interesting to note that one of the early organisms to benefit from *Deup1* were frogs. *Xenopus* epidermal and tracheal cells undergo multiciliogenesis within 1-2 hours, whereas in higher order eukaryotes, such as chicken and mammals, the process occurs over several days (Steinman 1968; Kalnins and Porter 1969; Zhao et al. 2013). However, live-cell imaging revealed that the kinetics of centriole biogenesis without *Deup1* is unchanged (data not shown). We can then infer that there is likely to be another role for the deuterosome.

Another possible role is that the deuterosome ensures the correct assembly of centriolar proteins and centriole stability. Although the centrioles are formed, trafficked to the apical plasma membrane, and can nucleate cilia, it is possible that deuterosome help ensure the centrioles that are produced are free from structural defects (Garcia and Reiter 2016). We know that the cilia present (Figure 15-16) in *Deup1*<sup>-/-</sup> mice are not completely dysfunctional since the mice do not exhibit hydrocephaly (data not shown). However, it could be that the cilia beat more slowly, but not enough to cause an overt phenotype. It appears that *Deup1* may play a role in influencing, most likely indirectly, the cilia beat frequency since we observed a slightly slower beating in *Deup1*<sup>-/-</sup> cilia (data not shown). However, more replicates and quantification will have to be done to confirm these initial findings.

A third possibility is that *Deup1* loss is compensated for by its paralog, *Cep63*. These two proteins exhibit 37% sequence identity in mouse (Zhao et al. 2013). Expression of *Deup1* alone forms multiple ring structures surrounded by a key centriolar protein *Cep152*, which helps recruit procentriolar proteins. In addition, *Deup1* competes with *Cep63* for binding of *Cep152* (Zhao et al. 2013). So it is possible that in the absence of *Deup1*, naturally occurring elevated levels of *Cep63* could compensate for *Deup1* function by interacting with unoccupied molecules of *Cep152* and act as a procentriole nucleation

hub. However, knockout of both *Deup1* and *Cep63* in mice did not cause a defect in centriole amplification. Therefore, it is possible that there is a yet unidentified compensatory factor or that the parental centriolar pathway can compensate fully in a way that was not appreciated before.

It could be possible that pericentriolar satellites play a compensatory role in the face of deuterosome loss. It is interesting to note that pericentrin, a pericentriolar matrix protein, has been reported to recruit the critical centriolar protein SAS6 (Ito et al., BioRxiv, 2018). Also, without parental centrioles, procentrioles arise from a PCM cloud, comprising Pericentrin (Mercey et al., unpublished). Additionally, another pericentriolar protein, PCM1, forms granules in ciliating cells (Kubo et al. 1999; Vladar and Stearns 2007). Therefore, we speculate that pericentriolar material proteins could help provide nucleation centers and compensate for *Deup1* loss. Thus, it would be interesting to examine the effect of depleting pericentriolar components, such as PCM1 or pericentrin, on multiciliogenesis in *Deup1*<sup>-/-</sup> and *Deup1*<sup>-/-</sup>; *Cep63*<sup>T/T</sup> animals.

### **5.3 Extra centrioles do not play a role in kidney cystogenesis**

In this work, we have shown that extra centrioles are neither sufficient to induce kidney cystogenesis nor cooperate with an ischemia-reperfusion injury model of cystogenesis.

However, a recent report claims that extra centrosomes are sufficient to induce kidney cystogenesis (Dionne et al. 2018). Yet, the experimental model used by the authors induced massive cell death and caused defective kidney development, resulting in lethality around two weeks of age. This is unsurprising, as it has been shown that increased apoptosis is sufficient to cause polycystic kidneys in mice (Veis et al. 1993; Nagata et al. 1996; Sorenson et al. 1996; Moser et al. 1997). More specifically, in mice deficient in the antiapoptotic protein Bcl-2, kidneys exhibit a very similar phenotype to the mouse model of Plk4 overexpression (Veis et al. 1993; Dionne et al. 2018). In both models, kidneys are hypoplastic in the embryonic stage due to excessive apoptosis causing a reduction in nephron number and subsequently develop polycystic kidneys (Nagata et al. 1996). Here, we were able to create extra centrioles in mouse kidneys without increasing cell death in the kidney, and therefore able to test the role of centrioles in cystogenesis without this confounding variable.

Furthermore, we found that extra centrioles do not perturb cilia number in the kidney, despite conflicting reports previously that extra centrioles could increase cilia in cells or decrease cilia number in skin (Mahjoub and Stearns 2012; Coelho et al. 2015). This could be explained as a tissue-specific effect, however, our work directly contradicts the recent findings in the kidney that show that centrosome amplification causes increased numbers

of both aciliated and superciliated cells (Dionne et al. 2018). Disruption to proper tissue architecture and necrosis in the kidney has been shown to cause increased cilia length, so it is possible that the altered architecture and/or increased death causes alterations in cilia number as well (Verghese et al. 2009). We propose that future studies and potential therapeutic approaches for ADPKD should be focused on targeting cilia and not centrioles.



# Materials and Methods

## Generation and husbandry of mouse models

### *Plk4<sup>Dox</sup> and Rosa rtTA mice*

The Plk4<sup>Dox</sup> mouse line was created using previously described KH2 ES cells (Beard et al. 2006). KH2 ES cells possess the M2-rtTA gene targeted to the ROSA26 locus under the control of the ROSA promoter. In addition, an FRT-flanked PGK-neomycin-resistance gene followed by a promoterless, ATG-less hygromycin-resistance is targeted downstream of the Col1a1 locus to allow site-specific integration of a single copy transgene. To FLP-IN the tetracycline responsive Plk4-EYFP construct into KH2 ES cells, the mouse Plk4 ORF C-terminally tagged with EYFP was cloned downstream of the tetracycline operator and CMV minimal promoter in the pBS31 FLP-IN vector. KH2 ES cells were electroporated with pBS31-Plk4-EYFP and the pCAGGS-FLPe-puro plasmid encoding the FLP recombinase. Cells were selected with Hygromycin B and clones were amplified and checked by PCR for correct targeting. Blastocysts were injected with the targeted KH2 ES cells and chimeric mice identified. Germline transmission was detected by polymerase chain reaction analysis of tail DNA obtained at weaning. Plk4-EYFP

genotyping was performed with the following primers: ACT GTC GGG CGT ACA CAA AT, CAA CCT GGT CCT CCA TGT CT and TGC TCG CAC GTA CTT CAT TC. M2-rtTA genotyping was performed with the following primers: AAA GTC GCT CTG AGT TGT TAT, GCG AAG AGT TTG TCC TCA ACC and GGA GCG GGA GAA ATG GAT ATG. Plk4-EYFP; rtTA mice were maintained by mating with C57BL6/N mice. EGFP-Centrin mice were as previously described (Hirai et al. 2016). APCMin/+ mice were purchased from the Jackson Laboratory (stock 002020) and genotyped using the following primers: GCC ATC CCT TCA CGT TAG, TTC CAC TTT GGC ATA AGG C and TTC TGA GAA AGA CAG AAG TTA.

#### *Deup1<sup>-/-</sup> mouse*

Deup1 heterozygous sperm (Deup1<sup>tm1.1(KOMP)<sup>Vl</sup>cg</sup>) was obtained from the U.C.-Davis Knockout Mouse Phenotyping Consortium (project ID: VG11314). NIH grants to Velocigene at Regeneron Inc (U01HG004085) and the CSD Consortium (U01HG004080) funded the generation of gene-targeted ES cells for 8500 genes in the KOMP Program and archived and distributed by the KOMP Repository at UC Davis and CHORI (U42RR024244). Mice were rederived using C57B/L6 mice at the Johns Hopkins University, School of Medicine Transgenic Core Laboratory. These animals were maintained on a congenic C57BL/6 background. The following primers were used

for genotyping: Mut For 5'-ACT TGC TTT AAA AAA CCT CCC ACA-3', Mut Rev 5'-GGA AGT AGA CTA ACG TGG AGC AAG C-3', WT For 5'-TAG GGC ACT GTT GGG TAT ATT GG-3', WT Rev 5'-CCA CAC ATT TCT GCT TCT CC-3'.

#### *Cep63<sup>TT</sup> mouse*

*Cep63<sup>TT</sup>* mice were obtained from the laboratory of Travis Stracker from the Institute for Research in Biomedicine—Barcelona. The generation of these *Cep63* gene-trapped mice was described previously (Brown et al. 2013; Marjanovic et al. 2015). *Cep63<sup>TT</sup>* mice were maintained on a mixed 129/SvEv-C57Bl/6 background. The same following primers were used for genotyping: *Cep63-5P2* 5'-GTA GGA CCA GGC CTT AGC GTT AG-3', *Cep63-3P1a* 5'-TAA GTG TAA AAG CCG GGC GTG GT -3', and MutR (B32) 5'-CAA GGC GAT TAA GTT GGG TAA CG -3'.

#### *Pax8-rtTA and mCherry-H2B mice*

*Plk4<sup>Dox</sup>* and mCherry-Histone H2B mice were generated and genotyped as reported previously (Egli et al. 2007; Levine et al. 2017). *Pax8-rtTA* mice were obtained from the Baltimore PKD core center at University of Maryland Medical School (Traykova-Brauch et al. 2008). The following genotyping primers were used for *Pax8-rtTA*: CCA TGT CTA GAC TGG ACA AGA and CTC CAG GCC ACA TAT GAT TAG.

Embryos and adults from both genders were included in our analysis. Mice were housed and cared for in an AAALAC-accredited facility and all animal experiments were conducted in accordance with Institute Animal Care and Use Committee approved protocols.

### **Doxycycline Induction**

Mice were fed 1mg/mL doxycycline (RenYoung Pharma) in water supplemented with 25 mg/mL sucrose (Sigma). Water was changed twice per week for the duration of the treatment.

### **Spontaneous tumorigenesis studies**

Plk4<sup>Dox</sup> and C57BL6/J animals were dosed chronically with doxycycline from 1 or 2 months of age. Mice were monitored daily during the course of the study. Mice were euthanized when signs of distress or when visible tumors grew to > 2cm in size as per the Johns Hopkins University ACUC guidelines.

### **Kidney cystogenesis studies**

Plk4<sup>Dox</sup> and C57BL6/J animals were dosed chronically with doxycycline throughout gestation until time of euthanasia.

### **Ischemia-reperfusion injury system**

Mice were anesthetized with ketamine and surgery was performed on a heating pad. A vascular clamp was applied to the left renal pedicle for 30 minutes and then released and abdomens were sutured, and mice were analyzed 6 weeks later.

### **Histological Analysis**

A full necropsy was performed on every Plk4<sup>Dox</sup> mouse sacrificed. Mouse tissues were harvested and fixed overnight in 4% paraformaldehyde at 4°C and then stored in 10% Neutral Buffered Formalin. The Johns Hopkins University, School of Medicine phenotyping core or the Johns Hopkins Hospital pathology core performed tissue processing, paraffin embedding, and Hematoxylin & Eosin staining. All pathology and tumors were analyzed by Dr. Cory Brayton, a certified veterinary pathologist.

### **Intestinal sample collection, tumor counts, and measurements**

Mice were maintained in a C57BL6/J genetic background. Intestines from 90 day old mice were collected, opened lengthwise and laid flat on Whatman paper (GE Healthcare

Life Sciences). Intestines were imaged on a Zeiss dissecting microscope with Zen imaging software. Polyp number and size was quantified using FIJI. Intestines were fixed on Whatman paper in 4% PFA overnight. After fixation, polyps were cut in half and processed for histology or immunofluorescence.

#### **APC locus PCR-based assay**

Analysis of the loss of the wildtype APC locus was performed as described using a quantitative APC locus PCR assay (Luongo et al. 1994). Briefly, >15 intestinal polyps or areas of normal intestine from a single animal were pooled together and DNA extracted using the GenElute Mammalian Genomic DNA extraction kit (Sigma) following the manufacturer's instructions. Each DNA sample was amplified in two separate PCR reactions using the following primers: For: TCT CGT TCT GAG AAA GAC AGA AGC T and Rev: TGA TAC TTC TTC CAA AGC TTT GGC TAT. The PCR product digested overnight with HindIII and then separated on a 3% Agarose gel. The integrated intensity of the APC<sup>+</sup> and APC<sup>Min</sup> bands quantified using Fiji. Each band was background subtracted and the intensity of the APC<sup>+</sup> bands multiplied by 1.17 (144 bp/123 bp) to correct for the smaller size, and proportionally reduced incorporation of ethidium bromide, in the digested APC<sup>+</sup> allele. The mean ratio of the corrected APC<sup>+</sup>/APC<sup>Min</sup> band intensities was calculated for each sample.

## **Cell culture**

### *Cell lines*

DLD-1 and HEK293FT cells were grown in DMEM (Corning) containing 10% FB Essence (VWR Life Science Seradigm) and 100U/mL of penicillin and 100U/mL of streptomycin. All cells were maintained at 37°C in 5% CO<sub>2</sub> and atmospheric oxygen.

### *Primary cells*

Mouse embryonic fibroblasts (MEFs) were harvested as previously described (Xu 2005). Briefly, embryos were harvested at E13.5 and incubated in trypsin overnight at 4°C. The following day, the embryos incubated at 37°C for 30 minutes and cells dissociated by pipetting. Cells were plated in DMEM media (Corning Cellgro) supplemented with 10% fetal bovine serum (Sigma), 100 U/mL penicillin and 100 U/mL streptomycin. Cells were maintained at 37°C in an atmosphere with 5% CO<sub>2</sub> and 3% O<sub>2</sub>. For the growth assays, 2 x 10<sup>5</sup> cells/well were plated in 6 well dishes and cells counted every 3 days. Each condition was run in triplicate and each growth assay repeated at least 3 times. MEFs were passaged a maximum of 8 times before being discarded. Doxycycline (Sigma) was dissolved in H<sub>2</sub>O and used at a final concentration of 1 µg/ml and doxorubicin (Sigma) was dissolved in DMSO and used at 200 ng/ml unless otherwise stated.

Mouse tracheal epithelial cell (mTEC) cultures were harvested and grown as previously described (You and Brody 2013). Briefly, tracheas were harvested from mice from 3 weeks to 12 months of age. Tracheas were then incubated in Pronase (Roche) overnight at 4 degrees. The following day, tracheal cells were dissociated by enzymatic and mechanical digestion. Cells were plated onto 0.4  $\mu\text{m}$  Falcon transwell membranes (Transwell, Corning). Once cells were confluent ( $\sim$ proliferation day 5), media from the apical chamber was removed and basal media was replaced with low serum (NuSerum) media. This timepoint is considered Air-Liquid Interface (ALI) day 0. These cells were then allowed to differentiate until needed for analysis (ALI day 3 or day 5).

For mouse ependymal cell cultures, brains were dissected from p0 - p3 mice and dissociated and cultured as previously described (Delgehyr et al., 2015). Briefly, brains were harvested and digested with papain (Sigma-Aldrich) at 37°C for 1 hour. The enzymatic digestion reaction was stopped using a trypsin inhibitor solution. The cells were washed then resuspended in DMEM/Glutamax-10% FBS, 1% P/S and plated on poly-L-lysine-coated T25 flasks. Once cells became confluent, the T25 flask was left on a shaker overnight to remove weakly attached cells and enrich for ependymal progenitor cells. The next day, cells were trypsinized and plated onto coverslips in a 24-well plate.



The following day, the cells were washed and media was changed to DMEM/Glutamax, 1% P/S without FBS. Cells were allowed to differentiate on coverslips for 4-8 days and then analyzed.

### **Cloning and transfection**

#### *Deup1 full-length and exons 8-12*

The full-length mouse Deup1 ORF or Deup1 exons 8-12 were cloned into a pcDNA5 vector, containing an FRT site and tetO, using Gibson cloning. A myc tag was inserted on the 3' end of the cDNA sequence using the Gibson primers. The resulting constructs were sequence-verified (Genewiz) and transfected into either DLD-1 cells or HEK293FTs. The DLD-1 cells used contain an FRT site integrated into a single genomic site and stably express the tetracycline repressor protein. Therefore, using these plasmids allows for the single-site integration of these transgenes into DLD-1 cells. DLD-1 cells were seeded at  $2 \times 10^5$  cells per well in a 6-well plate. The next day a transfection mixture of 100 uL Opti-MEM (Thermo Fisher Scientific; Cat. # 31985070), 3 uL of X-tremeGene HP (Sigma-Aldrich, cat. no. 6366236001), 100 ng of pcDNA5 plasmid and 900 ng of POG44 (Flp recominase) was prepared and incubated at room temperature for 30 minutes and then added drop-wise to each well. Two days later, DLD-1 mmDeup1-myc full-length and exons 8-12 were selected with 50ug/mL of Hygromycin B (ThermoFisher, cat. no.

10687010). For the HEK293FT transfection, cells were seeded at  $6 \times 10^6$  cells in 15cm dishes.

*shRNAs targeting Puromycin and Deup1*

The GFP ORF from the pLKO.1 DEST GFP (Addgene 32684) was restriction enzyme cloned into the pLKO.1 Puro (Addgene 8453) plasmid using SpeI and KpnI restriction sites. The following sequences (Integrated DNA Technologies) were used to create 3 different shRNAs:

shRNA Deup1 Forward: CCG GAA GCT GAG ATT ACA CCA AAT GCT CGA GCA  
TTT GGT GTA ATC TCA GCT TTT TTT TG,

shRNA Deup1 Reverse: AAT TCA AAA AAA AGC TGA GAT TAC ACC AAA TGC  
TCG AGC ATT TGG TGT AAT CTC AGC TT,

shRNA Deup-2 Forward: CCG GGC ATT CAC AGT GCA CAT CAA TCT CGA GAT  
TGA TGT GCA CTG TGA ATG CTT TTT G,

shRNA Deup-2 Reverse: AAT TCA AAA AGC ATT CAC AGT GCA CAT CAA TCT  
CGA GAT TGA TGT GCA CTG TGA ATG C,

shRNA Puromycin Forward: CCG GTC CTA AGG TTA AGT CGC CCT CGC TCG  
AGC GAG GGC GAC TTA ACC TTA GGA TTT TTT G,

shRNA Puromycin Reverse: AAT TCA AAA AAT CCT AAG GTT AAG TCG CCC  
TCG CTC GAG CGA GGG CGA CTT AAC CTT AGG A.

Each oligonucleotide set was annealed together then ligated into the pLKO.1 GFP vector, which had been linearized using the AgeI and EcoRI sites. The ligation reaction was then transformed into competent STBL3 cells. The resulting clones were sequence-verified (Genewiz) and used for subsequent experiments.

### **Lentiviral production**

HEK293FT cells were plated onto poly-D-lysine-coated tissue culture treated dishes at a density of  $6 \times 10^6$  cells/15-cm dish. The next day, cells were transfected with for lentiviral production. For each 15-cm dish, the following DNA was diluted in Opti-MEM (Thermo Fisher Scientific): 9  $\mu$ g lentiviral vector, 12  $\mu$ g psPAX2, and 3  $\mu$ g pMD2.G (12260 and 12259; Addgene). Separately, 72  $\mu$ l of 1  $\mu$ g/ $\mu$ l 25-kD polyethylenimine (Sigma-Aldrich) was diluted into Opti-MEM, briefly vortexed, and incubated at room temperature for 5 min. After incubation, the DNA and polyethylenimine mixtures were combined, briefly vortexed, and incubated at room temperature for 20 min. During this incubation, the culture media was replaced with 17 ml pre-warmed DMEM with 1% FBS. The transfection mixture was then added drop-wise to the 15-cm dish. Viral particles were harvested 48 h and 72h after the media change, spun down for 5 minutes at 1500

RPM and filtered through a 0.45- $\mu$ m PVDF syringe filter (Denville Scientific). The viral supernatant was then spun down in an ultracentrifuge (Beckman Coulter) using a SW-28 rotor (Beckman Coulter) at 25,000 RPM for 2 hours at 4°C. The viral pellets were then resuspended in PBS overnight at 4°C at a volume equal to 1/500 the original volume.

### **Antibody production**

Fragments of  $\gamma$ -tubulin (CDEYHAATRDPYISWGTQEQ) or CEP192 (amino acids 1-211) were cloned into a pET-23b bacterial expression vector (EMD Millipore) containing a C-term 6-His tag. Recombinant protein was purified from *Escherichia coli* using Ni-NTA beads (QIAGEN) and used for immunization (ProSci Incorporated). Goat immune sera were affinity-purified using standard procedures. A custom made Plk4 peptide (aa 564-580) was synthesized and conjugated to KLH for immunization (ProSci Incorporated). Rabbit immune sera were affinity-purified using standard procedures. Affinity-purified antibodies were directly conjugated to DyLight 550 and DyLight 650 fluorophores (Thermo Fisher Scientific) for use in immunofluorescence. Full-length Deup1 was cloned into a pET-28 bacterial expression vector (EMD Millipore) containing a C-term 6-His tag. Recombinant protein was purified from *Escherichia coli* using Ni-NTA beads (QIAGEN) and used for immunization (ProSci Incorporated). Rabbit immune sera were affinity-purified using standard procedures. Purified antibodies were directly conjugated to

AlexaFluor 555 and AlexaFluor 650 fluorophores (Thermo Fisher Scientific) for use in immunofluorescence.

### **Immunofluorescence staining and microscopy**

#### *Mouse tissues*

For immunofluorescence in mouse tissues (with the exception of the brain sections for Figure S3A), samples were harvested and fixed overnight in 4% paraformaldehyde at 4°C. Tissues were washed 3 times for 30 minutes each with 1 x Phosphate Buffered Saline (PBS). Tissues were incubated in 30% sucrose overnight, embedded in OCT compound (Tissue-Tek) and frozen in a dry ice-ethanol bath cooled to -80°C. Tissues were cut in 12 µm sections using a Leica cryostat (Leica Biosystems, CM3050) and placed on Superfrost Plus treated microscope slides (Fisher Scientific). For staining, slides were rehydrated with PBS supplemented with 0.5% Triton X-10 (PBST), and incubated in primary antibody diluted in blocking solution (10% donkey serum in PBST) for 2 hours at room temperature or overnight at 4°C. Slides were washed 3 times with PBST and incubated for 1 hour at room temperature in secondary antibody with 1 µg/ml 4',6-diamidino-2-phenylindole (DAPI) diluted in blocking solution. Slides were washed 3 more times with PBST and mounted in ProLong Gold Antifade (Invitrogen). For brain sections (for quantification of cortical thickness in Figure S3A), brains were harvested

from 4 month old mice, fixed in 1% PFA overnight and 4°C, washed three times in PBS for 30 minutes each, then dehydrated in methanol overnight at -20°C. The next day, brains were rehydrated in PBS and embedded in 3% agarose. Once set, brains were cut in 120 µm sections using a Leica vibratome (Leica Biosystems) and kept in 1x PBS until staining. Sections were stained with 1 µg/ml DAPI diluted in PBS for 1 hour at room temperature and mounted in Fluoromount-G (SouthernBiotech).

*Brains for in vivo imaging of ependymal cells*

Mice were perfused with 1% paraformaldehyde (PFA) and dissected brains were post-fixed in 1% PFA overnight at 4°C. The next day, brains were washed 3x in PBS for 1 hour at room temperature, then embedded in 3% low-melting point agarose. Brains were cut coronally into 100 µm sections, using a vibratome (Leica Biosystems). Brain sections were stained overnight at 4°C in primary antibodies diluted in 10% donkey serum (in PBST; 1x PBS, 0.5% Triton X-100). The next day sections were washed 3 x with PBST at room temperature then incubated in secondary antibodies and 1 µg/ml 4,6-diamidino-2-phenylindole (DAPI) diluted in 10% donkey serum at 4°C. The following day sections were washed 3 x with PBST at room temperature then mounted onto slides with Fluoromount G mounting media. (SouthernBiotech).

### *MEFs*

For immunofluorescence, primary MEFs were grown on 18-mm glass coverslips and fixed for 10 minutes in 100% ice cold methanol at -20°C for 10 minutes. Cells were blocked in 2.5% FBS, 200 mM glycine, and 0.1% Triton X-100 in PBS for 1 hour. Primary and secondary antibodies were incubated in the blocking solution for 1 hour at room temperature. DNA was stained with DAPI for 1 minute and cells were mounted in ProLong Gold Antifade (Invitrogen).

### *mTEC cultures*

Membranes were incubated in microtubule stabilization buffer (30% glycerol, 100mM PIPES, 1mM EGTA, 1mM MgSO<sub>4</sub>) for 60 seconds, followed by fixation in 4% PFA for 10 minutes at room temperature. Membranes were washed with PBST (1x PBS, 0.1% Triton X-100) 3 x for 5 minutes each. Membranes were then blocked at room temperature for an hour. Membranes were then cut into quarters and cut membranes were incubated with primary antibodies diluted in blocking buffer for an hour at room temperature. Membranes were then washed 3 x in PBST for 5 minutes each. Membranes were then incubated with secondary antibodies diluted in blocking buffer for 45 minutes at room temperature. Membranes were then incubated with DAPI diluted in PBS for 1 minute at

room temperature. Membranes were mounted onto slides with ProLong Gold Antifade (Invitrogen) and covered with 18-mm glass coverslips.

#### *Ependymal cells*

Cells were grown on 12-mm glass coverslips and fixed for 10 minutes in either 4% PFA at room temperature or 100% ice-cold methanol at -20°C. Coverslips were then stained and mounted as noted above.

#### **Cilia beat frequency**

Cells were seeded onto a 4 well glass bottom slide (Ibidi), and serum-starved for 7 days before imaging. Cells were imaged on a 3i Live-Cell Spinning Disk Confocal (Zeiss), using at 32x Air objective with 1.6x magnification using widefield light with a 3ms exposure time at 330 frames/second for 10 seconds. Number of beats per second were measured using previous methods (Mahuzier et al. 2018). Briefly, a 16x16pixel region of interest was selected containing a beating cilium, and changes in intensity over time was counted using the ImageJ z-axis profile tool. The average beats per second over a 3-5 second interval were measured for each cell.



## **Antibodies**

Staining was performed with the following primary antibodies: Pericentrin (rabbit, Abcam 1:1000), Cleaved Caspase 3 (rabbit, Cell Signaling Technologies, 1:500), p-Histone H2A.X (Ser139) (rabbit, Cell Signaling Technologies, 1:1000), Centrin (mouse, Millipore, 1:1000), CEP192 (rabbit, raised against CEP192 a.a. 1-211, a kind gift from Karen Oegema, Ludwig Institute for Cancer Research, 1:1000), Rabbit polyclonal anti-Cep164 (EMD Millipore, ABE2621, 1:1000), Mouse monoclonal Acetylated-alpha tubulin (Cell Signaling Technologies, 12152, 1:1000), and Rat polyclonal anti-ZO-1 (ThermoFisher Scientific, 14-9776-82, 1:1000). Secondary donkey antibodies were conjugated to Alexa Fluor 488, 555 or 650 (Life Technologies). TUNEL staining was performed using the *in situ* cell death detection kit (Sigma) following the manufacturer's instructions. Secondary donkey antibodies were conjugated to Alexa Fluor® 488, 555 or 650 (Life Technologies).

## *Microscopy*

Immunofluorescence images of MEFs, DLD-1s, and ependymal cells were collected using a Deltavision Elite system (GE Healthcare) controlling a Scientific CMOS camera (pco.edge 5.5). Acquisition parameters were controlled by SoftWoRx suite (GE Healthcare). Images were collected at room temperature (25°C) using an Olympus 40x

1.35 NA, 60x 1.42 NA or Olympus 100x 1.4 NA oil objective at 0.2  $\mu\text{m}$  z-sections.

Images were acquired using Applied Precision immersion oil (N=1.516).

Immunofluorescence images of tissues and mTECs were collected using a Zeiss LSM700 confocal microscope. Acquisition parameters were controlled by ZEN (Zeiss). Images were collected at room temperature (25°C) using a Zeiss 63x 1.4 NA oil objective at 0.3  $\mu\text{m}$  z-sections. Images were acquired using Zeiss immersion oil (N=1.518).

### **Image Analysis**

Quantification of Plk4 levels at the centrosome was performed as previously described (Lambrus et al. 2015). Imaris software (Bitplane) was used to quantify of total number of nuclei per field of view in the tissues stained with CC3 or Ki67.

### *Scanning electron microscopy*

Scanning electron microscopy was performed by the Johns Hopkins microscopy facility. Briefly, tracheas were cut open lengthwise and fixed in 2.5% glutaraldehyde, 100 mM sodium cacodylate, 3 mM  $\text{MgCl}_2$  pH 7.2 overnight at 4°C. Following a buffer rinse containing 3% sucrose, samples were post-fixed with 2% osmium tetroxide in 100 mM cacodylate buffer containing 3 mM  $\text{MgCl}_2$  for 1.5 hours on ice in the dark. Samples were

rinsed in dH<sub>2</sub>O and dehydrated through a graded series of ethanol to 90%. Dehydration was continued through 100% ethanol, then passed through ethanol:HMDS (Hexamethyldisiloxane Polysciences) 1:1 solution followed by pure HMDS. Samples were then placed in a desiccator overnight to dry. Tracheal pieces were attached to aluminum stubs via carbon sticky tabs (Pella), and coated with 40 nm of AuPd with a Denton Vacuum Desk III sputter coater. Stubs were viewed on a Leo 1530 FESEM operating at 1 kV and digital images captured with Smart SEM version 5.

#### Transmission electron microscopy

Cells on coverslips were washed twice with 1x PBS, and fixed for 2 hours with 2.5% glutaraldehyde. They were then washed 3x with 1x PBS and post-fixed with 1% osmium tetroxide in PBS for 30 minutes at 4°C in the dark with gentle shaking. Samples were then washed twice with PBS for 5 minutes each then dehydrated through a graded series of ethanol to 100%. Samples were impregnated with an ethanol/resin mix containing Epon, dodecenylsuccinic anhydride, and methyl nadic anhydride.

#### **Western blotting**

For immunoblot analyses, protein samples were collected using 2x sample buffer (125mM Tris-HCl, pH 6.8, 20% glycerol, 4% SDS, 0.1% bromophenol blue, 4% β-

mercaptoethanol). Samples were then separated by SDS-PAGE, transferred onto nitrocellulose membranes with a Trans-Blot Turbo Transfer System (Bio-Rad Laboratories) and then blocked in 5% milk for one hour at room temperature, followed by 1 hour incubation at room temperature with primary antibodies diluted in 5% milk, washed 3 x with TBST (1x TBS/1% Tween-20) then incubated in secondary antibody diluted in 5% milk. Blots were washed 3 x in TBST for 5 minutes each. Blots were incubated with either SuperSignal West Pico PLUS or Femto enhanced chemiluminescent substrate (ThermoFisher Scientific) for 1 minute then imaged using a G:Box (SynGene). The following primary antibodies were used: YL1/2 (rat anti- $\alpha$ -tubulin, 1:3,000; Pierce Antibodies), rabbit anti-Deup1 #38 (custom made against full-length mmDeup1, ProSci Incorporated). The following secondary antibodies were used: anti-rat or anti-rabbit IgG linked to HRP (Cell Signaling Technologies).

### **Quantitative real time PCR**

Total RNA was isolated from cells or homogenized tissue using Trizol Reagent (Thermo Fisher Scientific) and prepared for reverse transcription using SuperScript III/IV Reverse transcriptase (Thermo Fisher Scientific). Quantitative real time PCR was performed using SYBRGreen qPCR Master Mix (Thermo Fisher Scientific) on iQ5 multicolor real time PCR detection system (Bio-Rad). Analysis was performed using iQ5 optical system

software (Bio-Rad). Reactions were carried out in triplicate using the following primers:

Plk4 Fow: 5'-GAA ACA CCC CTC TGT CTT GG-3' and Rev: 5'-GCA TGA AGT GCC TAG CTT CC-3'; p53 Fow: 5'- CCC GAG TAT CTG GAA GAC AG-3' and Rev: 5'-ATA GGT CGG CGG TTC ATG CC-3'; FAS Fow: 5'- GGA AAA GGA GAC AGG ATG ACC-3' and Rev: 5'-CTT CAG CAA TTC TCG GGA TG-3'; BCL2 Fow: 5'-TTC GCA GCG ATG TCC AGT CAG CT-3' and Rev: 5'-TGA AGA GTT CTT CCA CCA CCG T-3'; BAX Fow: 5'-ATG CGT CCA CCA AGA AGC TGA-3' and Rev: 5'-AGC AAT CAT CCT CTG CAG CTC C-3'; PUMA Fow: 5'-GCA GCA CTT AGA GTC GCC-3' and Rev: 5'-GTC GAT GCT GCT CTT CTT GT-3', Deup1 (deleted exons) For: 5'- GCC AGA TGT AGA CAT TTC TTG GCA TGG -3', Rev: 5'- CCC ACC TCC TGG CCT TT -3', Deup1 (exons 10-12): For: 5'- TAC GTC TTC CAG AGC CAG C -3', Rev: 5'- CAG GAA GTG CTG TGC AGC -3', Deup1 (exons 9-10): For: 5'- GAA TTA AGC AAG GCT GTG GAC T -3' Rev: 5'- CTC TGG AAG ACG TAT GCC CC -3', Cep63 (exons 6-8): For: 5'- ATC AGA CCT ACA GTT CTG CC -3', Rev: 5'- CTG ACT TAG AAT CTC CTT ATG CTC -3', Cep63 (exons 13-14): For: 5'- GCA GGA GGA ATT AAG CAG ACT -3', Rev: 5'- CTG TCG GAA TTC CTC TAT TTT TCC AG -3' and GAPDH For: 5'- AAT GTG TCC GTC GTG GAT CTG A -3' and Rev: 5'- GAT GCC TGC TTC ACC ACC TTC T -3'. Expression values for p53 target genes (Figure S5C) were normalized to GAPDH, amplified with GAPDH Fow: 5'-AAT GTG

TCC GTC GTG GAT CTG A-3' and Rev: 5'-GAT GCC TGC TTC ACC ACC TTC T-3'. Plk4 overexpression values in MEFs and tissues (Figure 2A and S1A and S2A) were normalized to  $\beta$ -actin, amplified with  $\beta$ -actin Fow: 5'-GGC TGT ATT CCC CTC CAT CG-3' and  $\beta$ -actin Rev: 5'-CCA GTT GGT AAC AAT GCC ATG T-3' primers, with the exception of the APC<sup>min/+</sup> MEF experiment in Figure S4D, which were normalized to HPRT, amplified with HPRT Fow: 5'-TGA TCA GTC AAC GGG GGA CA-3' and HPRT Rev: 5'-TTC GAG AGG TCC TTT TCA CCA-3'. The fold changes in mRNA expression were calculated using the  $2^{-\Delta\Delta Ct}$  method, and expression values were expressed as fold increase in the average expression compared with non-transgenic tissues.

### **Metaphase spreads and FISH analysis**

To harvest splenocytes, freshly harvested spleens were minced and filtered through a 40  $\mu$ m cell strainer. Cells were resuspended in RPMI media (Corning Cellgro) supplemented with 10% fetal bovine serum (Sigma), 100 U/mL penicillin, 100 U/mL streptomycin, 1% HEPES (Sigma), 1% Sodium Pyruvate (Corning Cellgro), 1% Nonessential amino acids (Sigma), 10 U/mL Interleukin-2 (Roche), 5  $\mu$ g/mL Concanavalin A (Sigma), 10  $\mu$ g/mL Lipopolysaccharides (Sigma) and grown overnight at 37°C in an atmosphere of 5% CO<sub>2</sub> and 3% O<sub>2</sub>. Cells were treated with 100 ng/ml Colcemid (Sigma) for 4 hours, trypsinized

and resuspended in 75 mM KCl for 15 minutes at room temperature. Five drops of freshly prepared Carnoy's fixative (75% Methanol: 25% Acetic Acid) was added, the cells pelleted and resuspended in fixative overnight at 4°C. Cells were dropped onto slides pretreated with acetic acid. Dried slides were incubated with DAPI for 1 minute and imaged using a Deltavision Elite system.

Mouse FISH probes for 10 cM loci on chromosome 15 or 16 were purchased from Empire Genomics. Cells were fixed with Carnoy's fixative (75% Methanol: 25% Acetic Acid) for 15 minutes at room temperature and stored at -20°C until needed. DNA and probes were denatured at 69°C for 2 minutes, and hybridization was performed at 37°C overnight. The next day, cells were washed with 0.4x SSC buffer (Sigma) for 2 minutes at 72°C, then washed with 2x SSC (0.05% Tween-20) at room temperature for 30 seconds. Cells were briefly washed with dH<sub>2</sub>O, air dried and mounted with VectaShield containing 150 ng/mL DAPI.

### **Flow cytometry**

Cell pellets were fixed in cold 70% EtOH for 24 hours, washed once in PBS and resuspended in PBS supplemented with 10 µg/ml RNase A and 50 µg/ml Propidium

Iodide (PI). Samples were incubated at room temperature for 30 minutes and analyzed on a flow cytometer (FACSCalibur; Becton Dickinson).

### **Single cell sequencing**

Single cells were isolated from thymic or B-cell lymphomas by dissecting the tumor and mincing the tissue through a 70  $\mu\text{m}$  cell strainer. To isolate single epidermal cells, the skin was removed and floated on 0.25% trypsin with 1 mM EDTA in DMEM (Gibco) overnight at 4°C. The epidermis was scraped off using a scalpel and tissue was dissociated into single cells by pipetting. Trypsin was neutralized by addition of 7% FBS diluted in PBS. This suspension was then passed through a 70  $\mu\text{m}$  (BD Biosciences) filter followed by a 40  $\mu\text{m}$  (BD Biosciences) filter. Isolated single cells from the thymus, spleen and epidermis were washed twice in PBS and stored in FBS with 10% DMSO at -80 °C until sorted. Single cell karyotype analysis was performed and analyzed as previously described (Bakker et al. 2016).

### **Whole genome sequencing**

Genomic DNA was extracted from tissue samples using the GenElute Mammalian Genomic DNA extraction kit (Sigma) following the manufacturer's instructions. Shallow Whole Genome Sequencing (WGS) was performed as previously described (Nassar et al.



2015). Briefly, whole-genome DNA libraries were created using the Illumina TruSeq DNA sample preparation kit V2 according to the manufacturer's instructions, and resulting whole-genome libraries were sequenced at low coverage on a HiSeq2500 (Illumina) using a V3 flow cell generating 50-bp reads. Raw sequencing reads were mapped to the mouse reference genome (GRCm38/mm10) using Burrows-Wheeler Aligner (Li and Durbin 2009). We removed PCR duplicates with Picard (v1.32 and v1.43) and obtained an average of 7,788,246 unique mapped reads per sample. The number of reads was counted in windows of 50 Kb and corrected for the genomic wave. Segmentation was performed by the Ascat algorithm (Van Loo et al. 2010). GISTIC 2.0 (Genomic Identification of Significant Targets in Cancer) (Beroukhi et al. 2007) was used to identify recurrent Copy Number Alterations in Figure 4d,e.

### **Quantification and statistical analysis**

Statistical analysis was performed using GraphPad Prism software. Differences between samples were tested using a two-tailed Student's *t*-test or a Log-rank test for survival analysis. Error bars represent SEM unless otherwise indicated. Please refer to figures and figure legends for number of cells or animals used per experiment.

# References

- Al Jord A, Lemaitre AI, Delgehyr N, Faucourt M, Spassky N, Meunier A. 2014. Centriole amplification by mother and daughter centrioles differs in multiciliated cells. *Nature* **516**: 104-107.
- Anderson RG, Brenner RM. 1971. The formation of basal bodies (centrioles) in the Rhesus monkey oviduct. *J Cell Biol* **50**: 10-34.
- Arquint C, Gabryjonczyk AM, Nigg EA. 2014. Centrosomes as signalling centres. *Philos Trans R Soc Lond B Biol Sci* **369**.
- Bakker B, Taudt A, Belderbos ME, Porubsky D, Spierings DC, de Jong TV, Halsema N, Kazemier HG, Hoekstra-Wakker K, Bradley A et al. 2016. Single-cell sequencing reveals karyotype heterogeneity in murine and human malignancies. *Genome Biol* **17**: 115.
- Basto R, Brunk K, Vinadogrova T, Peel N, Franz A, Khodjakov A, Raff JW. 2008. Centrosome amplification can initiate tumorigenesis in flies. *Cell* **133**: 1032-1042.
- Battini L, Macip S, Fedorova E, Dikman S, Somlo S, Montagna C, Gusella GL. 2008. Loss of polycystin-1 causes centrosome amplification and genomic instability. *Hum Mol Genet* **17**: 2819-2833.
- Beard C, Hochedlinger K, Plath K, Wutz A, Jaenisch R. 2006. Efficient method to generate single-copy transgenic mice by site-specific integration in embryonic stem cells. *Genesis* **44**: 23-28.
- Beroukchim R, Getz G, Nghiemphu L, Barretina J, Hsueh T, Linhart D, Vivanco I, Lee JC, Huang JH, Alexander S et al. 2007. Assessing the significance of chromosomal

- aberrations in cancer: methodology and application to glioma. *Proc Natl Acad Sci U S A* **104**: 20007-20012.
- Bettencourt-Dias M, Rodrigues-Martins A, Carpenter L, Riparbelli M, Lehmann L, Gatt MK, Carmo N, Balloux F, Callaini G, Glover DM. 2005. SAK/PLK4 is required for centriole duplication and flagella development. *Curr Biol* **15**: 2199-2207.
- Boon M, Wallmeier J, Ma L, Loges NT, Jaspers M, Olbrich H, Dougherty GW, Raidt J, Werner C, Amirav I et al. 2014. MCIDAS mutations result in a mucociliary clearance disorder with reduced generation of multiple motile cilia. *Nat Commun* **5**: 4418.
- Boveri T. 1914. Zur Frage der Entstehung maligner Tumoren. *Fischer, Jena*.
- Brenner RM. 1969. Renewal of oviduct cilia during the menstrual cycle of the rhesus monkey. *Fertil Steril* **20**: 599-611.
- Brown NJ, Marjanovic M, Luders J, Stracker TH, Costanzo V. 2013. Cep63 and cep152 cooperate to ensure centriole duplication. *PLoS One* **8**: e69986.
- Castellanos E, Dominguez P, Gonzalez C. 2008. Centrosome dysfunction in Drosophila neural stem cells causes tumors that are not due to genome instability. *Curr Biol* **18**: 1209-1214.
- Chan JY. 2011a. A clinical overview of centrosome amplification in human cancers. *Int J Biol Sci* **7**: 1122-1144.
- . 2011b. A clinical overview of centrosome amplification in human cancers. *International journal of biological sciences* **7**: 1122-1144.
- Cimini D, Howell B, Maddox P, Khodjakov A, Degraffi F, Salmon ED. 2001. Merotelic kinetochore orientation is a major mechanism of aneuploidy in mitotic mammalian tissue cells. *J Cell Biol* **153**: 517-527.
- Cimini D, Moree B, Canman JC, Salmon ED. 2003. Merotelic kinetochore orientation occurs frequently during early mitosis in mammalian tissue cells and error correction is achieved by two different mechanisms. *Journal of cell science* **116**: 4213-4225.

- Coelho PA, Bury L, Shahbazi MN, Liakath-Ali K, Tate PH, Wormald S, Hindley CJ, Huch M, Archer J, Skarnes WC et al. 2015. Over-expression of Plk4 induces centrosome amplification, loss of primary cilia and associated tissue hyperplasia in the mouse. *Open Biol* **5**: 150209.
- Conduit PT, Wainman A, Raff JW. 2015. Centrosome function and assembly in animal cells. *Nat Rev Mol Cell Biol* **16**: 611-624.
- Crasta K, Ganem NJ, Dagher R, Lantermann AB, Ivanova EV, Pan Y, Nezi L, Protopopov A, Chowdhury D, Pellman D. 2012. DNA breaks and chromosome pulverization from errors in mitosis. *Nature* **482**: 53-58.
- Denu RA, Zasadil LM, Kanugh C, Laffin J, Weaver BA, Burkard ME. 2016. Centrosome amplification induces high grade features and is prognostic of worse outcomes in breast cancer. *BMC Cancer* **16**: 47.
- Dionne LK, Shim K, Hoshi M, Cheng T, Wang J, Marthiens V, Knoten A, Basto R, Jain S, Mahjoub MR. 2018. Centrosome amplification disrupts renal development and causes cystogenesis. *J Cell Biol* **217**: 2485-2501.
- Egli D, Rosains J, Birkhoff G, Eggan K. 2007. Developmental reprogramming after chromosome transfer into mitotic mouse zygotes. *Nature* **447**: 679-685.
- Finetti F, Paccani SR, Rosenbaum J, Baldari CT. 2011. Intraflagellar transport: a new player at the immune synapse. *Trends Immunol* **32**: 139-145.
- Fukasawa K, Choi T, Kuriyama R, Rulong S, Vande Woude GF. 1996. Abnormal centrosome amplification in the absence of p53. *Science* **271**: 1744-1747.
- Funk MC, Bera AN, Menchen T, Kualess G, Thriene K, Lienkamp SS, Dengjel J, Omran H, Frank M, Arnold SJ. 2015. Cyclin O (Ccn0) functions during deuterosome-mediated centriole amplification of multiciliated cells. *EMBO J* **34**: 1078-1089.
- Ganem NJ, Godinho SA, Pellman D. 2009. A mechanism linking extra centrosomes to chromosomal instability. *Nature* **460**: 278-282.
- Ganem NJ, Pellman D. 2012. Linking abnormal mitosis to the acquisition of DNA damage. *The Journal of cell biology* **199**: 871-881.
- Garcia G, 3rd, Reiter JF. 2016. A primer on the mouse basal body. *Cilia* **5**: 17.

- Godinho SA, Pellman D. 2014. Causes and consequences of centrosome abnormalities in cancer. *Philos Trans R Soc Lond B Biol Sci* **369**.
- Godinho SA, Picone R, Burute M, Dagher R, Su Y, Leung CT, Polyak K, Brugge JS, Thery M, Pellman D. 2014. Oncogene-like induction of cellular invasion from centrosome amplification. *Nature* **510**: 167-171.
- Habedanck R, Stierhof YD, Wilkinson CJ, Nigg EA. 2005. The Polo kinase Plk4 functions in centriole duplication. *Nat Cell Biol* **7**: 1140-1146.
- Hao LY, Greider CW. 2004. Genomic instability in both wild-type and telomerase null MEFs. *Chromosoma* **113**: 62-68.
- Hirai M, Chen J, Evans SM. 2016. Generation and Characterization of a Tissue-Specific Centrosome Indicator Mouse Line. *Genesis* **54**: 286-296.
- Hochedlinger K, Yamada Y, Beard C, Jaenisch R. 2005. Ectopic expression of Oct-4 blocks progenitor-cell differentiation and causes dysplasia in epithelial tissues. *Cell* **121**: 465-477.
- Holland AJ, Fachinetti D, Zhu Q, Bauer M, Verma IM, Nigg EA, Cleveland DW. 2012a. The autoregulated instability of Polo-like kinase 4 limits centrosome duplication to once per cell cycle. *Genes & development* **26**: 2684-2689.
- . 2012b. The autoregulated instability of Polo-like kinase 4 limits centrosome duplication to once per cell cycle. *Genes Dev* **26**: 2684-2689.
- Holland AJ, Lan W, Cleveland DW. 2010a. Centriole duplication: A lesson in self-control. *Cell cycle* **9**: 2731-2736.
- Holland AJ, Lan W, Niessen S, Hoover H, Cleveland DW. 2010b. Polo-like kinase 4 kinase activity limits centrosome overduplication by autoregulating its own stability. *The Journal of cell biology* **188**: 191-198.
- Janssen A, van der Burg M, Szuhai K, Kops GJ, Medema RH. 2011. Chromosome segregation errors as a cause of DNA damage and structural chromosome aberrations. *Science* **333**: 1895-1898.

- Kalnins VI, Porter KR. 1969. Centriole replication during ciliogenesis in the chick tracheal epithelium. *Zeitschrift für Zellforschung und mikroskopische Anatomie* **100**: 1-30.
- Kayser G, Gerlach U, Walch A, Nitschke R, Haxelmans S, Kayser K, Hopt U, Werner M, Lassmann S. 2005. Numerical and structural centrosome aberrations are an early and stable event in the adenoma-carcinoma sequence of colorectal carcinomas. *Virchows Arch* **447**: 61-65.
- Kubo A, Sasaki H, Yuba-Kubo A, Tsukita S, Shiina N. 1999. Centriolar satellites: molecular characterization, ATP-dependent movement toward centrioles and possible involvement in ciliogenesis. *J Cell Biol* **147**: 969-980.
- Kulukian A, Holland AJ, Vitre B, Naik S, Cleveland DW, Fuchs E. 2015. Epidermal development, growth control, and homeostasis in the face of centrosome amplification. *Proc Natl Acad Sci U S A* **112**: E6311-6320.
- Kurbegovic A, Trudel M. 2016. Acute kidney injury induces hallmarks of polycystic kidney disease. *Am J Physiol Renal Physiol* **311**: F740-F751.
- Kwon M, Godinho SA, Chandhok NS, Ganem NJ, Azioune A, They M, Pellman D. 2008. Mechanisms to suppress multipolar divisions in cancer cells with extra centrosomes. *Genes & Development* **22**: 2189-2203.
- Lambrus BG, Uetake Y, Clutario KM, Daggubati V, Snyder M, Sluder G, Holland AJ. 2015. p53 protects against genome instability following centriole duplication failure. *J Cell Biol* **210**: 63-77.
- Leber B, Maier B, Fuchs F, Chi J, Riffel P, Anderhub S, Wagner L, Ho AD, Salisbury JL, Boutros M et al. 2010. Proteins required for centrosome clustering in cancer cells. *Sci Transl Med* **2**: 33ra38.
- Levine MS, Bakker B, Boeckx B, Moyett J, Lu J, Vitre B, Spierings DC, Lansdorp PM, Cleveland DW, Lambrechts D et al. 2017. Centrosome Amplification Is Sufficient to Promote Spontaneous Tumorigenesis in Mammals. *Dev Cell* **40**: 313-322 e315.
- Levine MS, Holland AJ. 2018. The impact of mitotic errors on cell proliferation and tumorigenesis. *Genes Dev* **32**: 620-638.

- Li H, Durbin R. 2009. Fast and accurate short read alignment with Burrows-Wheeler transform. *Bioinformatics* **25**: 1754-1760.
- Liu Y, Pathak N, Kramer-Zucker A, Drummond IA. 2007. Notch signaling controls the differentiation of transporting epithelia and multiciliated cells in the zebrafish pronephros. *Development* **134**: 1111-1122.
- Luongo C, Moser AR, Gledhill S, Dove WF. 1994. Loss of Apc<sup>+</sup> in intestinal adenomas from Min mice. *Cancer Res* **54**: 5947-5952.
- Mahjoub MR, Stearns T. 2012. Supernumerary centrosomes nucleate extra cilia and compromise primary cilium signaling. *Curr Biol* **22**: 1628-1634.
- Mahuzier A, Shihavuddin A, Fournier C, Lansade P, Faucourt M, Menezes N, Meunier A, Garfa-Traore M, Carlier MF, Voituriez R et al. 2018. Ependymal cilia beating induces an actin network to protect centrioles against shear stress. *Nat Commun* **9**: 2279.
- Marjanovic M, Sanchez-Huertas C, Terre B, Gomez R, Scheel JF, Pacheco S, Knobel PA, Martinez-Marchal A, Aivio S, Palenzuela L et al. 2015. CEP63 deficiency promotes p53-dependent microcephaly and reveals a role for the centrosome in meiotic recombination. *Nat Commun* **6**: 7676.
- Marthiens V, Rujano MA, Penner C, Tessier S, Paul-Gilloteaux P, Basto R. 2013. Centrosome amplification causes microcephaly. *Nat Cell Biol* **15**: 731-740.
- Martindill DM, Risebro CA, Smart N, Franco-Viseras Mdel M, Rosario CO, Swallow CJ, Dennis JW, Riley PR. 2007. Nucleolar release of Hand1 acts as a molecular switch to determine cell fate. *Nat Cell Biol* **9**: 1131-1141.
- Moser AR, Pitot HC, Dove WF. 1990. A dominant mutation that predisposes to multiple intestinal neoplasia in the mouse. *Science* **247**: 322-324.
- Moser M, Pscherer A, Roth C, Becker J, Mucher G, Zerres K, Dixkens C, Weis J, Guay-Woodford L, Buettner R et al. 1997. Enhanced apoptotic cell death of renal epithelial cells in mice lacking transcription factor AP-2beta. *Genes Dev* **11**: 1938-1948.

- Moyer TC, Clutario KM, Lambrus BG, Daggubati V, Holland AJ. 2015. Binding of STIL to Plk4 activates kinase activity to promote centriole assembly. *J Cell Biol* **209**: 863-878.
- Nagata M, Nakauchi H, Nakayama K, Nakayama K, Loh D, Watanabe T. 1996. Apoptosis during an early stage of nephrogenesis induces renal hypoplasia in bcl-2-deficient mice. *Am J Pathol* **148**: 1601-1611.
- Nassar D, Latil M, Boeckx B, Lambrechts D, Blanpain C. 2015. Genomic landscape of carcinogen-induced and genetically induced mouse skin squamous cell carcinoma. *Nat Med* **21**: 946-954.
- Nemajerova A, Kramer D, Siller SS, Herr C, Shomroni O, Pena T, Gallinas Suazo C, Glaser K, Wildung M, Steffen H et al. 2016. TAp73 is a central transcriptional regulator of airway multiciliogenesis. *Genes Dev* **30**: 1300-1312.
- Nigg EA. 2006. Origins and consequences of centrosome aberrations in human cancers. *Int J Cancer* **119**: 2717-2723.
- Nigg EA, Holland AJ. 2018. Once and only once: mechanisms of centriole duplication and their deregulation in disease. *Nat Rev Mol Cell Biol*.
- Nigg EA, Raff JW. 2009. Centrioles, centrosomes, and cilia in health and disease. *Cell* **139**: 663-678.
- Ong AC, Devuyst O, Knebelmann B, Walz G, Diseases E-EWGfIK. 2015. Autosomal dominant polycystic kidney disease: the changing face of clinical management. *Lancet* **385**: 1993-2002.
- Park JH, Woo YM, Ko JY, Kim DY. 2015. Autosomal Dominant Polycystic Kidney Disease Induced by Ciliary Defects. in *Polycystic Kidney Disease* (ed. X Li), Brisbane (AU).
- Quintyne NJ, Reing JE, Hoffelder DR, Gollin SM, Saunders WS. 2005. Spindle multipolarity is prevented by centrosomal clustering. *Science* **307**: 127-129.
- Ring D, Hubble R, Kirschner M. 1982. Mitosis in a cell with multiple centrioles. *J Cell Biol* **94**: 549-556.



- Rosario CO, Kazazian K, Zih FS, Brashavitskaya O, Haffani Y, Xu RS, George A, Dennis JW, Swallow CJ. 2015. A novel role for Plk4 in regulating cell spreading and motility. *Oncogene* **34**: 3441-3451.
- Rosario CO, Ko MA, Haffani YZ, Gladdy RA, Paderova J, Pollett A, Squire JA, Dennis JW, Swallow CJ. 2010. Plk4 is required for cytokinesis and maintenance of chromosomal stability. *Proc Natl Acad Sci U S A* **107**: 6888-6893.
- Sabino D, Gogendeau D, Gambarotto D, Nano M, Penetier C, Dingli F, Arras G, Loew D, Basto R. 2015. Moesin is a major regulator of centrosome behavior in epithelial cells with extra centrosomes. *Curr Biol* **25**: 879-889.
- Sercin O, Larsimont JC, Karambelas AE, Marthiens V, Moers V, Boeckx B, Le Mercier M, Lambrechts D, Basto R, Blanpain C. 2016. Transient PLK4 overexpression accelerates tumorigenesis in p53-deficient epidermis. *Nat Cell Biol* **18**: 100-110.
- Silkworth WT, Nardi IK, Scholl LM, Cimini D. 2009. Multipolar spindle pole coalescence is a major source of kinetochore mis-attachment and chromosome mis-segregation in cancer cells. *PLoS ONE* **4**: e6564.
- Siller SS, Sharma H, Li S, Yang J, Zhang Y, Holtzman MJ, Winuthayanon W, Colognato H, Holdener BC, Li FQ et al. 2017. Conditional knockout mice for the distal appendage protein CEP164 reveal its essential roles in airway multiciliated cell differentiation. *PLoS Genet* **13**: e1007128.
- Song R, Walentek P, Sponer N, Klimke A, Lee JS, Dixon G, Harland R, Wan Y, Lishko P, Lize M et al. 2014. miR-34/449 miRNAs are required for motile ciliogenesis by repressing cp110. *Nature* **510**: 115-120.
- Sorenson CM, Padanilam BJ, Hammerman MR. 1996. Abnormal postpartum renal development and cystogenesis in the bcl-2 (-/-) mouse. *Am J Physiol* **271**: F184-193.
- Sorokin SP. 1968. Reconstructions of centriole formation and ciliogenesis in mammalian lungs. *J Cell Sci* **3**: 207-230.
- Steinman RM. 1968. An electron microscopic study of ciliogenesis in developing epidermis and trachea in the embryo of *Xenopus laevis*. *Am J Anat* **122**: 19-55.

- Su LK, Kinzler KW, Vogelstein B, Preisinger AC, Moser AR, Luongo C, Gould KA, Dove WF. 1992. Multiple intestinal neoplasia caused by a mutation in the murine homolog of the APC gene. *Science* **256**: 668-670.
- Terre B, Piergiovanni G, Segura-Bayona S, Gil-Gomez G, Youssef SA, Attolini CS, Wilsch-Brauninger M, Jung C, Rojas AM, Marjanovic M et al. 2016. GEMC1 is a critical regulator of multiciliated cell differentiation. *EMBO J* **35**: 942-960.
- Thompson SL, Compton DA. 2011. Chromosome missegregation in human cells arises through specific types of kinetochore-microtubule attachment errors. *Proc Natl Acad Sci U S A* **108**: 17974-17978.
- Traykova-Brauch M, Schonig K, Greiner O, Miloud T, Jauch A, Bode M, Felsner DW, Glick AB, Kwiatkowski DJ, Bujard H et al. 2008. An efficient and versatile system for acute and chronic modulation of renal tubular function in transgenic mice. *Nat Med* **14**: 979-984.
- Van Loo P, Nordgard SH, Lingjaerde OC, Russnes HG, Rye IH, Sun W, Weigman VJ, Marynen P, Zetterberg A, Naume B et al. 2010. Allele-specific copy number analysis of tumors. *Proc Natl Acad Sci U S A* **107**: 16910-16915.
- Veis DJ, Sorenson CM, Shutter JR, Korsmeyer SJ. 1993. Bcl-2-deficient mice demonstrate fulminant lymphoid apoptosis, polycystic kidneys, and hypopigmented hair. *Cell* **75**: 229-240.
- Vergheze E, Ricardo SD, Weidenfeld R, Zhuang J, Hill PA, Langham RG, Deane JA. 2009. Renal primary cilia lengthen after acute tubular necrosis. *Journal of the American Society of Nephrology : JASN* **20**: 2147-2153.
- Vitre B, Holland AJ, Kulukian A, Shoshani O, Hirai M, Wang Y, Maldonado M, Cho T, Boubaker J, Swing DA et al. 2015. Chronic centrosome amplification without tumorigenesis. *Proc Natl Acad Sci U S A* **112**: E6321-6330.
- Vladar EK, Stearns T. 2007. Molecular characterization of centriole assembly in ciliated epithelial cells. *J Cell Biol* **178**: 31-42.
- Wallmeier J, Al-Mutairi DA, Chen CT, Loges NT, Pennekamp P, Menchen T, Ma L, Shamseldin HE, Olbrich H, Dougherty GW et al. 2014. Mutations in CCNO result

- in congenital mucociliary clearance disorder with reduced generation of multiple motile cilia. *Nat Genet* **46**: 646-651.
- Weaver BA, Silk AD, Montagna C, Verdier-Pinard P, Cleveland DW. 2007. Aneuploidy Acts Both Oncogenically and as a Tumor Suppressor. *Cancer Cell* **11**: 25-36.
- Xu J. 2005. Preparation, culture, and immortalization of mouse embryonic fibroblasts. *Curr Protoc Mol Biol* **Chapter 28**: Unit 28 21.
- You Y, Brody SL. 2013. Culture and differentiation of mouse tracheal epithelial cells. *Methods in molecular biology* **945**: 123-143.
- Zhang CZ, Spektor A, Cornils H, Francis JM, Jackson EK, Liu S, Meyerson M, Pellman D. 2015. Chromothripsis from DNA damage in micronuclei. *Nature* **522**: 179-184.
- Zhao H, Chen Q, Huang Q, Yan X, Zhu X. 2018. Mother centrioles are dispensable for deuterosome formation and function during basal body amplification. *bioRxiv*.
- Zhao H, Zhu L, Zhu Y, Cao J, Li S, Huang Q, Xu T, Huang X, Yan X, Zhu X. 2013. The Cep63 paralogue Deup1 enables massive de novo centriole biogenesis for vertebrate multiciliogenesis. *Nat Cell Biol* **15**: 1434-1444.
- Zhou JX, Li X. 2015. Apoptosis in Polycystic Kidney Disease: From Pathogenesis to Treatment. in *Polycystic Kidney Disease* (ed. X Li), Brisbane (AU).

# Curriculum Vitae

## MICHELLE LEVINE

915 S Wolfe St., Unit 261 | Baltimore, MD 21231  
Levine.michelle.s@gmail.com, 305-790-2200

### EDUCATION

**Johns Hopkins, School of Medicine**, Baltimore, MD..... PhD expected Jan. 2019  
PhD program: Biochemistry, Cellular, and Molecular Biology  
Mentor: Andrew Holland, PhD

**Boston College**, Chestnut Hill, MA ..... B.A. 2010  
Major: Biology

**Universidad Pablo de Olavide**, Seville, Spain..... Spring Semester 2009

### PROFESSIONAL EXPERIENCE

**Johns Hopkins, School of Medicine**, Baltimore, MD..... June 2014 – Present  
*PhD Student, Laboratory of Dr. Andrew Holland, PhD*

- Characterizing the structure proposed to be essential for multiciliogenesis: the process by which cells produce motile cilia, or hairlike projections from cells, for fluid flow of mucus in the respiratory tract and cerebrospinal fluid in the brain
- Studying the role of extra centrosomes, structures that help coordinate cell division, in polycystic kidney disease, which affects 1 in 750 people
- Determined that supernumerary centrosomes play a causative role in tumorigenesis

**Acidophil, LLC.**, Lutherville-Timonium, MD..... Oct. 2017 – April 2018  
*Intern Analyst*

- Performed scientific due diligence for Chalante, an animal health startup company
- Assisted in market and competitive analysis in preparation of Series A funding

**Brigham and Women’s Hospital, Boston, MA**

*Technical Research Assistant II, Dr. Nancy Berliner, MD*..... Sept. 2011 – May 2013

*Technical Research Assistant I, Dr. Nancy Berliner, MD*..... Sept. 2010 – Sept. 2011

*Undergraduate Intern, Dr. Nancy Berliner, MD*..... Oct. 2009 – April 2010

- Investigated the positive effect of the thrombopoietin receptor agonist, eltrombopag, on platelet production in hematopoietic stem cells (HSCs) from patients with multiple myeloma
- Interrogated the specificity and efficacy of a JAK2 inhibitor in suppressing the proliferation of HSCs isolated from Polycythemia vera patients
- Determined the therapeutic benefit of vitamin D on inflammation-induced suppression of red blood cell production, which resulted in funding to study the role of vitamin D in patients with anemia of inflammation
- Defined a novel interaction between a transcriptional and translational regulatory factor in myelodysplastic syndrome

**AWARDS AND FELLOWSHIPS**

NIH Ruth L. Kirschstein NRSA (F31) fellow ..... Jan. 2017 – Aug. 2018

JHU Graduate Student Association poster award – 2<sup>nd</sup> place ..... June 2017

Hans Joaquim Prochaska JHU Young Investigators award ..... May 2017

American Society for Cell Biology travel award ..... Dec. 2016

American Society for Cell Biology poster award – 1<sup>st</sup> place..... Dec. 2016

JHU BCMB Colloquium presentation award – 2<sup>nd</sup> place ..... June 2016

American Society for Cell Biology travel award ..... Dec. 2014

**PUBLICATIONS**

1. **Levine MS** and Holland AJ. The impact of mitotic errors on cell proliferation and tumorigenesis. *Genes Dev.* 2018 May 1; 32(9-10): 620–638. doi: 10.1101/gad.314351.118 (PMC6004076).

2. **Levine M** and Holland AJ. Mitotic machinery moonlights in multiciliogenesis. *Science.* 2017 Nov 10;358(6364):716-718. doi: 10.1126/science.aag0770. (PMC5749915).

3. **Levine MS**, Bakker B, Boeckx B, Moyett J, Lu J, Vitre B, Spierings DC, Lansdorp PM, Cleveland DW, Lambrechts D, Foijer F and Holland AJ. Centrosome amplification is sufficient to promote spontaneous tumorigenesis in mammals. *Developmental Cell.* **2017** Feb 6;40(3):313-322.e5. doi: 10.1016/j.devcel.2016.12.022. (PMC5296221).

4. Jeong JY, **Levine MS**, Abayasekara N, Berliner N, Laubach J, Vanasse GJ. The non-peptide thrombopoietin receptor agonist eltrombopag stimulates megakaryopoiesis in bone marrow cells from patients with relapsed multiple myeloma. *Journal of Hematology & Oncology*. 2015 Apr 16;8(1):37. doi: 10.1186/s13045-015-0136-2 (PMC4405817).
5. **Levine MS** and Holland AJ. Plk4 Shapes Up. *Structure*, 2014 Aug 5; 22(8):1071-3. doi: 10.1016/j.str.2014.07.004 (PMID: 25099950; does not have PMID).
6. Payne E, Virgilio M, Narla A, Sun H, **Levine M**, Paw BH, Berliner N, Look AT, Ebert B, Khanna-Gupta A. L-Leucine improves anemia and developmental defects associated with Diamond-Blackfan anemia and del(5q)MDS by activating the mTOR pathway. *Blood*, 2012 Sep 13; 120(11): 2214-24 (PMC3447780).
7. Khanna-Gupta, A, Abayasekara N, **Levine M**, Bolli N, Sun H, Silver M, Virgilio M, Halene S, Sportoletti P, Pandolfi PP, Berliner N. Upregulation of eIF4E in Nucleophosmin 1 (NPM1) haploinsufficient cells results in changes in CCAAT enhancer binding protein alpha (C/EBPα) activity: implications in MDS and AML. *Journal of Biological Chemistry*, 2012 Jul 31 (PMC3463350).

#### **ABSTRACTS AND PRESENTATIONS**

1. **Michelle Levine**, Bjorn Bakker, Bram Boeckx, Julia Moyett, James Lu, Benjamin Vitre, Diana C. Spierings, Peter M. Lansdorp, Don W. Cleveland, Diether Lambrechts, Floris Foijer and Andrew J. Holland. *Determining the role of centrosome amplification in tumorigenesis*. (American Society of Cell Biology Annual Meeting, 2016, Abstract, Poster, and Microsymposium talk).
2. **Michelle Levine** and Andrew Holland. *Elucidating the Role of Centrosome Amplification in Tumorigenesis*. (American Society of Cell Biology/International Forum for Cell Biology Annual Meeting, 2014, Abstract and Poster).
3. Jee-Yeong Jeong, **Michelle S. Levine**, Bertal H. Aktas, Michael Chorev, Nirmalee Abayasekara, Matthew Silver, Nancy Berliner, Jose A. Halperin and Gary J. Vanasse. *A N,N'-diaryllurea inhibitor of protein translation initiation selectively suppresses the proliferation of CD34+ cells isolated from Polycythemia Vera patients via activation of the HRI-eIF2α pathway*. (European Hematology Association, 17<sup>th</sup> Congress meeting, 2012, Poster).
4. **Michelle Levine, BA**, Jee-Yeong Jeong, PhD, Nancy Berliner, MD and K. Gary J. Vanasse, MD. *1, 25-Dihydroxyvitamin D Suppresses TNFα-Mediated NF-κB Activation in K562 and Human CD34+ Cells and Promotes Recovery of Erythroid Colony Formation in Human CD34+ Cells* (American Society of Hematology, 53<sup>rd</sup> Annual

Meeting, 2011, Abstract and Poster).

5. Nirmalee Abayasekara, MS, **Michelle Levine, BA**, Niccolo Bolli, MD, Hong Sun, MD, Matthew Silver, BS, Navid Nia, Paolo Sportoletti, MD, Pier Paolo Pandolfi, MD, PhD, Nancy Berliner, MD and Arati Khanna-Gupta, PhD. *Upregulation of eIF4E in Nucleophosmin 1 (NPM1) Haploinsufficient Cells Alters CCAAT Enhancer Binding Protein Alpha (C/EBP $\alpha$ ) Activity: Implications for MDS and AML* (American Society of Hematology, 53<sup>rd</sup> Annual Meeting, 2011, Abstract and Poster).

### **VOLUNTEER EXPERIENCE**

**Project Bridge**, Baltimore, MD ..... April 2017 – April 2018

*Community outreach leader*

- Lead a group of 40 volunteers in brainstorming and organizing monthly scientific demonstrations at a local farmer's market to engage the public in different scientific topics

**Project Bridge**, Baltimore, MD ..... October 2015 – Present

*Community outreach volunteer*

- Demonstrate different scientific topics and experiments at a local farmer's market

**BCMB Colloquium**, Baltimore, MD ..... August 2016 – May 2017

*Organizer*

- Coordinated student speakers to present at monthly colloquia
- Designed surveys in order for the audience to provide helpful feedback to the speakers

**Thread**, Baltimore, MD ..... Oct. 2013 – Oct. 2014

*Mentor*

- Engaged weekly with an at-risk, underperforming high school student to help improve scholastic performance

**Brigham and Women's Hospital Science Club**, Boston, MA.. Nov. 2012 – Dec. 2012

*Teacher*

- Led science classes at Tobin Elementary School